MICRO-SITING OF WIND TURBINES USING NAVIER-STOKES
SOLUTIONS COUPLED WITH A NUMERICAL WEATHER PREDICTION
MODEL

A THESIS SUBMITTED TO
THE GRADUATE SCHOOL OF NATURAL AND APPLIED SCIENCES
OF
MIDDLE EAST TECHNICAL UNIVERSITY

BY

GÖKHAN AHMET

IN PARTIAL FULFILLMENT OF THE REQUIREMENTS
FOR
THE DEGREE OF DOCTOR OF PHILOSOPHY
IN
AEROSPACE ENGINEERING

SEPTEMBER 2014

Approval of the thesis:

MICRO-SITING OF WIND TURBINES USING NAVIER-STOKES SOLUTIONS COUPLED WITH A NUMERICAL WEATHER PREDICTION MODEL

submitted by **GÖKHAN AHMET** in partial fulfillment of the requirements for the degree of **Doctor of Philosophy in Aerospace Engineering Department, Middle East Technical University** by,

Prof. Dr. Canan Özgen
Dean, Graduate School of **Natural and Applied Sciences**

_____

Prof. Dr. Ozan Tekinalp
Head of Department, **Aerospace Engineering**

_____

Prof. Dr. İsmail Hakkı Tuncer
Supervisor, **Aerospace Eng. Dept., METU**

_____

Examining Committee Members:

Prof. Dr. Ünver Kaynak
Mechanical Engineering Department, TOBB-ETU

_____

Prof. Dr. İsmail Hakkı Tuncer
Aerospace Engineering Department, METU

_____

Assoc. Prof. Dr. Oğuz Uzol
Aerospace Engineering Department, METU

_____

Assoc. Prof. Dr. Sinan Eyi
Aerospace Engineering Department, METU

_____

Assist. Prof. Dr. Mustafa Kaya
Department of Flight Training, UTAA

_____

Date: _____

I hereby declare that all information in this document has been obtained and presented in accordance with academic rules and ethical conduct. I also declare that, as required by these rules and conduct, I have fully cited and referenced all material and results that are not original to this work.

Name, Last Name: GÖKHAN AHMET

Signature   :

ABSTRACT

MICRO-SITING OF WIND TURBINES USING NAVIER-STOKES SOLUTIONS COUPLED WITH A NUMERICAL WEATHER PREDICTION MODEL

AHMET, Gökhan

Ph.D., Department of Aerospace Engineering

Supervisor   : Prof. Dr. İsmail Hakkı Tuncer

September 2014, 86 pages

High resolution atmospheric flow solutions are obtained with an in-house, parallelized 3 dimensional Navier-Stokes solver, HYP3D coupled with a meso-scale meteorological weather prediction software, WRF, and the wind potential of a specified terrain is assessed based on long term atmospheric flow solutions. Body-fitted grids are employed to discretize the complex terrain of interest in HYP3D. In the study, high resolution (1.5 arcsec) topographical data is used to discretize the specified terrain. In HYP3D solver, the flow field is initialized and the unsteady and spatially varying boundary conditions are continuously updated at the domain boundaries using the data extracted from the WRF solutions in 5 minute time intervals. The unsteady flow solutions and the implementation of the boundary conditions on HYP3D are achieved in a parallel computing environment. The difficulties in coupling the WRF and HYP3D solutions due to the mesh structure and the resolution differences are resolved

through two different algorithms. The results are presented as contour plots of velocity fields in time series, and as the Weibull distributions along with wind roses based on integrated data. The velocity fields computed are compared against the met-mast observation data for validation. In the study unsteady Navier-Stokes solutions closely coupled with the WRF solutions on high resolution, terrain fitted grids are successfully obtained, the performance of the in-house solver developed is assessed, and several tools are developed for the micro-siting of wind turbines.

Keywords: WRF-CFD Coupling, Wind Assessment, Wind Energy Forecasting, Long/Short Term Energy Production Estimation, Wind Energy, Numerical Weather Forecast, Computational Fluid Dynamics, Parallel Computing

ÖZ

METEOROLOJİK TAHMİN MODELİ VE NAVIER-STOKES ÇÖZÜMLERİ KULLANILARAK RÜZGAR TÜRBİNLERİNİN MİKRO-KONUMLANDIRILMASI

AHMET, Gökhan

Doktora, Havacılık ve Uzay Mühendisliği Bölümü

Tez Yöneticisi   : Prof. Dr. İsmail Hakkı Tuncer

Eylül 2014 , 86 sayfa

Bu çalışmada türbülanslı atmosferik akış çözümlerinin elde edilmesi amacıyla kurum içinde geliştirilen paralel çalışabilen 3 boyutlu Navier-Stokes çözücü HYP3D, mezo ölçekli meteorolojik tahmin yazılımı WRF ile akuple edilerek 1 yıl süre için çalıştırılmış, bölgenin rüzgar güç potansiyeli hesaplanmıştır. Atmosferik gözlem verileri temin edilen araştırma bölgesi için detaylı topografya bilgisi temin edilmiş, yüksek çözünürlüklü (1.5 arcsec) hesaplamalı akışkanlar dinamiği çözüm ağı oluşturulmuştur. HYP3D ile çözülecek alan için zamana bağlı başlangıç ve sınır koşulları, yaygın olarak kullanılan meteorolojik tahmin yazılımı WRF'dan 5 dakikalık zaman aralıkları için elde edilmiştir. WRF yazılımından elde edilen zamana bağlı başlangıç ve sınır koşulları, kurum içinde geliştirilen hesaplamalı akışkanlar dinamiği yazılımı HYP3D'nin sınır koşulu uygulama rutinlerinde yapılan değişiklikler yardımıyla sürekli güncellenerek uygulanmış atmosferik akış dağılımları paralel hesaplama ortamında elde edilmiştir. Bu çalışmada düşük

çözünürlüklü WRF çözüm ağındaki yer yüzeyinin yüksek çözünürlüklü Navier-Stokes çözüm ağıyla eşleştirilebilmesi için elde edilen sınır koşulları iki farklı yaklaşımla modifiye edilmiştir. Elde edilen sonuçlar kontur grafikleri, zaman serileri, weibull dağılımları ve rüzgar gülü grafikleri ile sunulmuş, akış değişkenleri, gerçek gözlem verileri ve WRF sonuçları ile kıyaslanmıştır. Bu çalışmada, WRF ile akuple edilmiş yüksek çözünürlüklü Navier-Stokes çözümleri başarıyla elde edilmiş, geliştirilen mikro konumlandırma araçlarının ve kurum içi çözücünün performansı değerlendirilmiş ve modelin kabiliyetleri sunulmuştur.

Anahtar Kelimeler: WRF-CFD Akuple Edilmesi, Rüzgar potansiyeli belirleme, Rüzgar Enerji Üretim Tahmini, Uzun/Kısa Vadeli Enerji Üretim Tahmini, Rüzgar enerjisi, Nümerik Hava Tahmini, Hesaplamalı akışkanlar dinamiği, Paralel hesaplama

Nothing is impossible for a determined mind

ACKNOWLEDGEMENTS

First and foremost, I would like to express my deep gratitude to my supervisor, Prof.Dr. İsmail H. Tuncer for his patient guidance and useful critiques throughout my academical experiences. I would like to offer my special thanks to Dr. Oğuz Uzol who encouraged me always, Dr. Ömer Emre Orhan who is my invaluable guide on wind industry, Dr. Mustafa Kaya who has been a role-model as an academician.

This thesis would not have been possible without the supports of my team mate Engin Leblebici, my brother Bayram Mercan, my buddy Seyfullah Aktaşoğlu, and the fellows Başak Zeka, Anas Abdulrahim, Ozan Gözcü, Sinan Körpe and Serpil Selvi.

I would like to express my eternal gratitude to my caring, deepless loving, and supportive life partner Zeynep Zerey.

In particular, I want to heartfelt thank to my whole family, who has always stood by me and supported all of my decisions.

I wish to express my endless love to my niece Cansın Miray Sarıkaya. Yet, I owe her my earnest apologies for not being around enough during the most beautiful first years of her life.

TABLE OF CONTENTS

LIST OF TABLES

TABLES

LIST OF FIGURES

FIGURES

LIST OF SYMBOLS

z	Height
z_{ref}	Reference height
V	Wind velocity
V_{ref}	Wind velocity at z_{ref}
α	Wind shear exponent
z_0	Roughness length
L	Monin-Obukov length
u_*	Friction velocity
T_v	Virtual temperature
κ	Von Karman constant
g	Gravitational acceleration
$Q_{\nu 0}$	Virtual temperature flux.
η	Non-dimensional independent vertical coordinate
$\bar{p_s}$	Pressure at the ground level
R	Gas constant for dry air,
$\bar{\rho}$	Density
$\bar{p}$	Pressure
T	Virtual temperature
s	Spatial derivative,
PHB	Geopotential
PH	Geopotential perturbation
W_s	Weighting function
D	Distance between source point and destination point
E	Exponent of the weighting function
ψ_i	Variable at destination point
P	Power
A	Area
ρ	Density
λ	Scale factor,
k	Shape factor
Re	Reynolds number
y^+	Dimensionless wall coordinate
u^+	Dimensionless velocity
u^*	Friction velocity
C_f	Skin friction coefficient

RANS   Reynolds-Averaged Navier–Stokes
LES   Large Eddy Simulation
DNS   Direct Numerical Simulation
WAsP   the Wind Atlas Analysis and Application Program
CFD   Computational Fluid Dynamics
WRF   Weather Research and Forecasting Model
AEP   Annual Energy Production
NCAR   National Center for Atmospheric Research
NOAA   the National Oceanic and Atmospheric Administration
NCEP   the National Centers for Environmental Prediction
FSL   the Forecast Systems Laboratory
AFWA   the Air Force Weather Agency
FAA   Naval Research Laboratory, the University of Oklahoma, and the
            Federal Aviation Administration
NetCDF   Network Common Data Form
RMS   Root Mean Square
METIS   Serial Graph Partitioning and Fill-reducing Matrix Ordering
PVM   Parallel Virtual Machine
ASTER   Advanced Spaceborne Thermal Emission and Reflection Radiometer
GDEM   Global Digital Elevation Map
METI   The Ministry of Economy, Trade, and Industry of Japan
NASA   The United States National Aeronautics and Space Administration
FEM   Finite Element applications
CPU   Central Processing Unit

CHAPTER 1

INTRODUCTION

For the ever growing need for energy in both our country and the world, carbon based fuels such as coal, petroleum and natural gas yield to environmental friendly, renewable energy sources. Wind and Solar energy have the most potential and are the most efficient among these resources.

Wind Energy is extracted via wind turbines installed at the locations where the wind energy potential is high. Various wind energy potential atlases have been developed based on atmospheric observational data and simulations done by using numerical weather prediction software.

As wind farms consisting of several wind turbines have a high initial investment cost, the siting of wind turbines in a wind farm has significant importance. Over a complex terrain, a misplacement of 30 m may cut the power output of a wind turbine to half. Low-resolution wind energy potential atlases have the necessary statistical information for macro-siting of wind farms but they lack the precision for the micro-siting of the wind turbines. For a successful micro-siting, high resolution, accurate and time dependent wind field information may be needed.

Consumption and production of the electricity change in time. This undesirable fluctuations may cause serious problems at electricity grids. Therefore smart grid solutions and co-generation alternatives are very recent research areas. Because

of being wind speed is directly proportional to energy production of the wind turbines, fluctuation in electricity production is inevitable for the wind farms. With the help of power production forecasts for the wind farms, balancing the energy production with the other base power plants is a feasible solution for the protection of grid and meeting the demand. Therefore any improvement on the wind forecast and the power production estimation is of utmost importance.

1.1 Nature of Wind

A good understanding of the atmospheric flowfield is quite important in order to efficiently use the most significant green energy source; the wind energy. Worldwide wind circulation Figure 1.1. involves large-scale wind patterns, affecting prevailing near surface winds, that cover the entire planet.[25] There are four basic forces that should be considered in the analysis of atmospheric flows. These are pressure forces, the Coriolis force caused by the rotation of the earth, inertial forces due to large-scale circular motion of air in the atmosphere, and friction forces at the earth's surface.
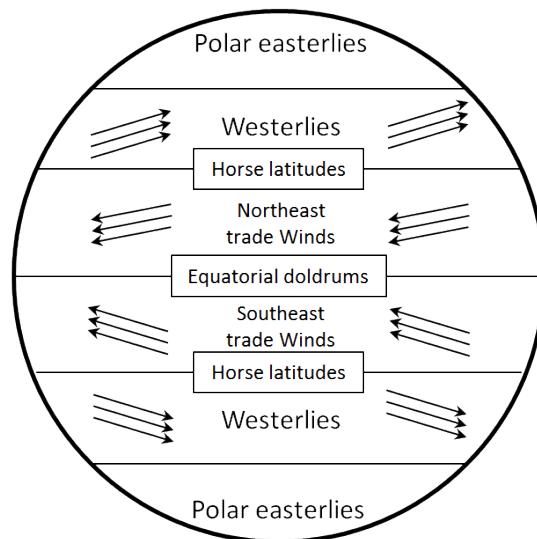
Figure 1.1: Winds of worldwide circulation pattern (Re-illustrated)[13]

Large scale atmospheric flows also create boundary layer type flow over the earth surface. Boundary layer thickness is considered about 2 km. In the atmospheric

boundary layer flow; viscousity, turbulence, gusts, and the non-linear interactions occur. But the mean velocity profile may be expressed by two components; Power exponent function and Logarithmic function.[36]
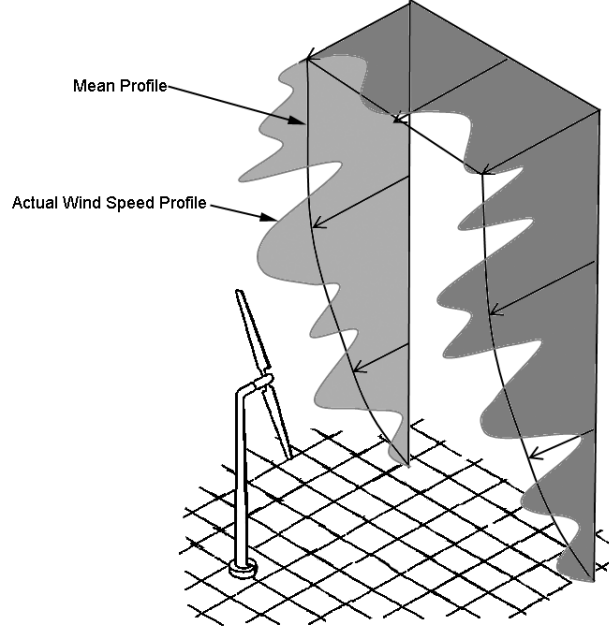
Figure 1.2: Planetary boundary layer profile (Re-illustrated)[36]

Power exponent function can be defined as;

$$V(z) = V_{ref} \left(\frac{z}{z_{ref}} \right)^{\alpha} \qquad (1.1)$$

here $V(z)$ is the velocity at a height of z, V_{ref} is the velocity at z_{ref}, and the variable α is the wind shear exponent and it depends on surface roughness. The logarithmic function is given by;

$$\frac{V(z)}{V(10)} = \frac{ln\dfrac{z}{z_0}}{ln\dfrac{10}{z_0}} \qquad (1.2)$$

$V(z)$ is the velocity at a height of z, $V(10)$ is velocity at $z = 10m$ and z_0 is the roughness length. Both z_0 and α values which depend on terrain roughness are based on empirical data and given in Table 1.1. In numerical simulations

3

of atmospheric flows; high rise buildings and rugged terrains are usually modelled and small structures and trees are modelled by surface roughness. Open water and ocean surfaces are usually taken into consideration with slip condition.

Table 1.1: Surface Roughness Lengths and the Wind Shear Exponent[11]

Terrain	Surface Roughness Length z_0 (m)	Wind Shear Exponent α
Ice	0.00001	0.07
Snow on flat ground	0.0001	0.09
Calm Sea	0.0001	0.09
Coast with onshore winds	0.001	0.11
Snow-covered crop stubble	0.002	0.12
Cut grass	0.007	0.14
Short-grass prairie	0.02	0.16
Crops, tall-grass prairie	0.05	0.19
Hedges	0.085	0.21
Scattered trees and hedges	0.15	0.24
Trees,hedges, a few buildings	0.3	0.29
Suburbs	0.4	0.31
Woodlands	1	0.43

Note: Relative to a reference height of 10 m

Adapted from characteristics of the Wind by Walter Frost and Carl Aspliden in Wind Turbine Technology, and Wind energy, Anwendung,Messung by Jens-Peter Molly
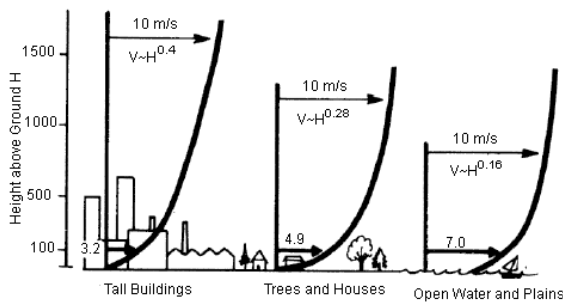
Figure 1.3: Effect of ground roughness on vertical distribution of wind speeds [10]
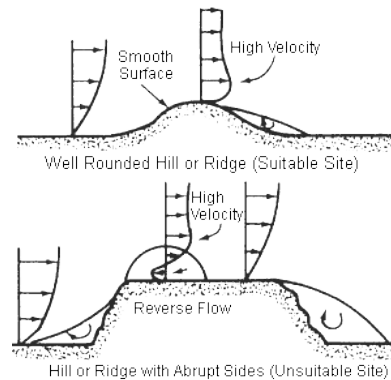
Figure 1.4: Effect of topography on wind profile [10]

4

Topography of wind farm sites plays an important role in micro-siting. Figure 1.3 and Figure 1.4 show the effects of topography and buildings on vertical distributions of wind speeds. The simulation of wind fields without the consideration of the high resolution topography may not be accurate. Therefore it is quite important that in the numerical simulations, topographical characteristics of wind farms is taken into account properly.

1.2 Atmospheric Stability

For the lower regions of atmosphere, vertical movement of the air due to buoyancy and gravitational force is a function of Monin-Obukov Length.

Monin-Obukhov Length also known as Obukhov Length is a parameter that defines the stability condition of lower atmosphere. It is first introduced in 1946 and later on improved for several atmospheric conditions. Monin-Obukov Length L is given by;

$$L = \frac{-u_*^3 T_v}{\kappa g Q_{\nu 0}} \tag{1.3}$$

Here u_* is friction velocity, T_v is virtual temperature, κ is von Karman constant, g is gravitational acceleration and $Q_{\nu 0}$ is virtual temperature flux.[1] Atmospheric stability conditions are classified[33] in Table 1.2.

Table 1.2: Classification of stability according to Obukhov lengths [33]

Very stable	0<L<200 m
Stable	200<L<1000 m
Near-neutral	|L|>1000 m
Unstable	-1000<L<-200 m
Very Unstable	-200<L<0 m

In the numerical simulation of atmospheric flows, atmospheric stability conditions due to buoyancy and gravitational force should be modelled.

1.3 Background

Micro-siting is about deciding the best location of an individual wind turbine for the maximum power production. For a successful micro-siting based on numerical simulations, a high resolution flowfield analysis; with the proper topographical modelling and surface roughness information is needed.

In addition, such a study significantly makes it possible to forecast the power generation of an operative wind farm. This ability is financially very important for the wind farm investors. Therefore numerical solutions become very important at this point. Accurate predictions of unsteady rural and urban atmospheric flow fields have a wide range of usage such as micro-site selection for wind farms and pollution tracking, each of which are of current research topics with several examples in literature[8],[31]. Due to high initial investment cost, wind farm siting is an active research field.[9]

Bowen(2004)[6] in a Risø-R Report states that Botta et al (1992)[5], Bowen and Saba (1995)[7], Reid (1995)[32] and Sempreviva et al (1986)[34] experience in the operation of commercial wind farms (Lindley et al., 1993[23]) have confirmed that effects from the local complex terrain on the site characteristics of each turbine have a significant influence on the output (and perhaps even the viability) of a wind energy project.

Low resolution wind energy potential atlases have the necessary statistical information for macro-siting of wind farms but lack the precision for the micro-siting. Therefore; high resolution, more accurate wind field information may be needed for micro-siting in order to improve the power output of a wind-farm and fore-

cast the power production of installed turbines.

F.J.Zajackowski et.al.[38] compares Numerical Weather Prediction Models (NWP) and Computational Fluid Dynamics (CFD) simulations. They conclude that NWP can take radiation, moist convection physics, land surface parametrization, atmospheric boundary layer physics into account, but wind flow features finer than 1 km are not captured by the turbulence physics of such models. CFD simulations, however, have proved to be useful at capturing the details of smaller scales due to a finer scale topography, and details around urban features such as high-rise buildings.

In the our previous studies [19],[4],[22],[20],[21],[18], atmospheric flow solutions with spatially and time varying boundary conditions obtained from a numerical weather prediction model is performed with the commercial Navier-Stokes Solver, FLUENT. However FLUENT can not carry out computations in parallel if the unsteady boundary conditions are provided with UDF (User Defined Function). The CPU time required for one day atmospheric flow simulation is, in general, in the order of days.

1.4 Motivation

As wind farms consisting of several wind turbines have a high initial investment cost, wind farm siting must be given a significant importance. A misplacement of a turbine by 30 meters may cut the power output of a wind turbine to half. Low-resolution Wind Energy Potential Atlases have the necessary statistical information for macro-siting of wind farms but they lack the precision for the micro-siting of the wind turbines. For the micro-siting, high resolution, precise and time dependent wind field information is needed.

Widely used numerical models can be divided into 4 groups;

- Linearized Models

- RANS Reynolds Average modelling

- LES Large eddy simulation

- DNS Direct numerical simulation

Some of the mostly used commercial wind-farm design packages are WAsP, Windfarm, WindPRO, Openwind etc... All these software are developed in order to estimate the power production and increase the maximum energy output of the wind farm.

WAsP (Wind Atlas Analysis and Application Program) from Risø based on the concept of linearized flow models is the most popular model among the above[15]. It is a PC-program for horizontal and vertical extrapolation of wind data. The program contains a complete set of models to calculate the effects on the wind of sheltering obstacles, surface roughness changes and terrain height variations. The analysis part consists of a transformation of an observed wind climate (speed and direction distributions) to a wind atlas data set. The wind atlas data set can subsequently be applied for estimation of the wind climate and wind power potential, as well as for siting of specific wind turbines.[27]

- "Developed initially for neutrally stable flow over hilly terrain

- Contains simple models for turbulence and surface roughness

- Best suited to more simple geometries

- Quick and accurate for mean wind flows

- Poorly predict flow separation and recirculation

- Limitations in more complex terrain regions due to the linearity of the equation set" [12]

Mostly used wind assessment tools use linearized models. Although these mod-

els are very powerful for smooth terrains, CFD based tools are needed for the complex terrains such as wind energy plant projects in Turkey. Therefore CFD based wind assessment tools (like WindSim, Meteodyne, WAsP-CFD) are getting more and more popular all over the world. On the other hand most of CFD software use fictitious flowfields. These flowfields are created just by using different constant boundary conditions. Starting from the zero degree, this software rotates inlet and outlet boundary conditions till 360 degrees. For each case, boundary conditions are defined as follows.
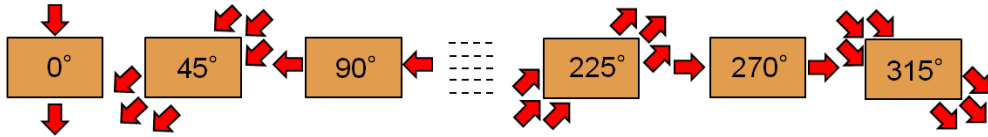
Figure 1.5: Sector-wise simulations of commercial wind assessment tools

Each sector means a different simulation. Therefore this process may take a long time depending on the grid resolution. Using these fictitious flowfields they correlate whole domain with the observation data. Therefore, observation is a must. For the projects which cannot provide observation data, meteorological data serie, so called virtual met-mast data, can be used in these commercial software. This "one point serie" can be purchased from the market.

Unlike other methodologies, in this study, observation data is significantly not a must. Spatially varying boundary conditions taken from WRF can be defined in the CFD code, not only at one point like commercial tools but also whole flow domain boundaries. This creates a competitive advantage because wind assessment and power production forecast can be performed with any high cost investments such as measurement masts.

9

Table 1.3: Comparison of current tools and present approach

Current Commercial Tools	Present Approach
✳ Wind Atlas Methodology (CFD is newly introduced)	✓ 3D Navier-Stokes Solver with turbulence model
✳ Constant/Steady Boundary Conditions	✓ Unsteady Boundary Conditions from NWP solutions
✳ Azimuthal-Sector-wise simulations (at least 16)	✓ Unsteady flow simulation over extended time range
✳ Correlation between steady simulations and time series data	✓ AEP & Short term energy production forecast
✳ Met-mast data is a must	✓ High resolution terrain
✳ Only annual energy production estimation (AEP)	✓ Hybrid grid capability

1.5 Objective of the Study

For wind assessment studies, there are two important statistical parameters: Weibull distribution and wind power density, namely. Weibull probability distribution function is a widely known statistical distribution function which is used for wind velocity distributions among other things such as reliability engineering, manufacturing-delivery times in industrial engineering and so on. Wind power density is basically the kinetic energy of the wind passing through a unit area per unit time. It is a useful parameter for the micro-siting of wind turbines.

Wind assessment tools mostly uses linearized models along with steady and uniform boundary conditions in order to correlate whole domain of interest to observation data taken for that location for a given time period. But this approach, as less time consuming computationally, may prove to be inaccurate and needs yearly observation data. Also, daily power predictions are out of question as the simulations from wind assessment tools are steady.

For this, coupling atmospheric weather prediction models with CFD are becoming an important research topic. As the simulations must be done unsteadily and with spatially varying boundary conditions, interpolation from the weather

prediction data to CFD domain is needed in both time and space. But the resolution of the weather prediction data and CFD domain may differ causing interpolation errors. So, interpolation errors due to difference in the resolution of WRF (low resolution) and CFD (high resolution) must be minimized. This is achieved by shifting/stretching the ground level in WRF solution to the same level of the CFD domain, which is explained in detail in the following section.

The objective of this study is to simulate atmospheric flows in a parallel computational environment using unsteady in-house code HYP3D to decrease the computational time required and also to test and assess the performance of the in-house code HYP3D in terms of accuracy and the computation time. In addition, average wind power potential density at a specific height above the ground level is obtained for the region of interest using CFD simulation results. Also, Weibull distributions and wind rose patterns are obtained at regions of interest.

CHAPTER 2

NUMERICAL METHOD

In this study, a coupled flow solution methodology with an atmospheric weather forecast software, WRF, and the in-house 3D Navier-Stokes solver HYP3D, is developed. WRF produces a low resolution, unsteady atmospheric weather forecast data, which provides the unsteady boundary conditions for the atmospheric flow solutions obtained with HYP3D on terrain fitted, high resolution grids.

2.1 Weather Research and Forecast Model: WRF

"Weather Research & Forecasting Model" (WRF) is a fully compressible, Eulerian, eta-coordinate based, nest-able, non-hydrostatic, freely available for community use, numerical weather prediction model with a large suite of options for numerical schemes and parametrization of physical processes.[37][35]

WRF has been a collaborative partnership;
- National Center for Atmospheric Research (NCAR),
- the National Oceanic and Atmospheric Administration (NOAA)
- the National Centers for Environmental Prediction (NCEP)
- the Forecast Systems Laboratory (FSL),
- the Air Force Weather Agency (AFWA),
- Naval Research Laboratory, the University of Oklahoma, and the Federal Aviation Administration (FAA).
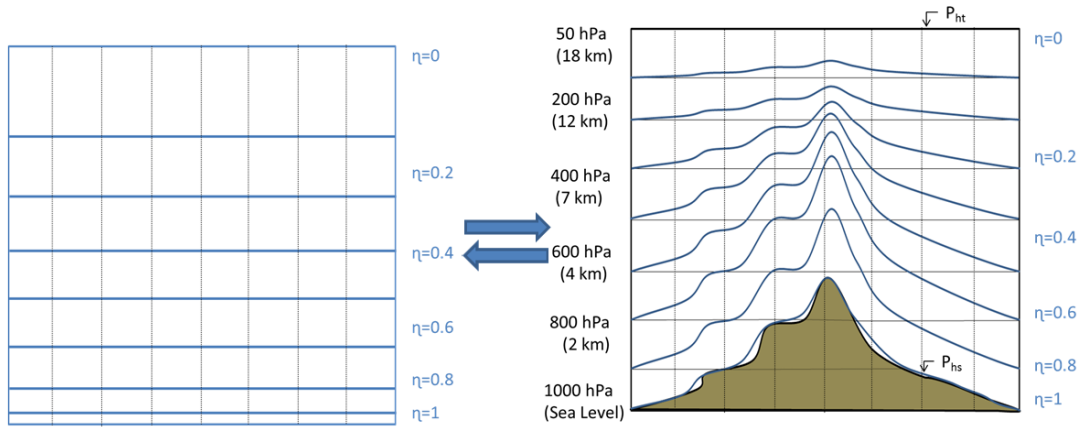
Figure 2.1: Vertical η-based coordinate system

The vertical η-based coordinate system used in WRF can be seen in Figure 2.1. It is defined as Equation 2.1;

$$\eta = \frac{\bar{p}}{\bar{p}_s} \tag{2.1}$$

Where $\bar{p}_s$ is the pressure at the ground level. Therefore, η is a non-dimensional independent vertical coordinate that decreases upward from a value of 1 at the ground to 0 at the top of the atmosphere. (Generally; 5000Pa $\sim$ 13km) (e.g. If surface pressure 1013hPa, $\eta = 0.87$ corresponds about 880hPa)

The definition of hydrostatic relation, used for the coordinate transformation[16] from z-height to η coordinate is given by;

$$\frac{\partial \bar{p}}{\partial z} = -\bar{\rho} g \tag{2.2}$$

where $\bar{\rho}$ satisfies the equation of state in hydrostatic system as

$$\bar{p} = \bar{\rho} R T \tag{2.3}$$

14

and g is gravitational constant, R is gas constant for dry air, z is physical height, $\bar{\rho}, \bar{p}$ and T are density, pressure and virtual temperature in hydrostatic system.

Then hydrostatic relation of Equation 2.2. can be rewritten as;

$$\frac{\partial z}{\partial \eta} = -\frac{R\bar{T}}{g\eta} \tag{2.4}$$

for the coordination transformation. This definition is detailed by Philips (1957) [29] for the hydrostatic system in σ coordinates, but it is used to define the coordinate for the non-hydrostatic system here.

Using the above definition for the coordinate transformations can be given as;

$$\frac{\partial}{\partial z} = -\frac{g\eta}{R\bar{T}}\frac{\partial}{\partial \eta} \tag{2.5}$$

for vertical transformation, and

$$\frac{\partial}{\partial s}|_z = \frac{\partial}{\partial s}|_\eta + \frac{1}{R\bar{T}}\frac{\partial}{\partial \ln \eta}\frac{\partial \bar{\Phi}}{\partial s}|_\eta \tag{2.6}$$

for others, where s can be either x or y for spatial derivative (can be found Equation 5. in Juang(1992)[16]) and $\bar{\Phi} = gz$ is geopotential. Using Equations 2.5 and 2.6. the fully compressible non-hydrostatic system in z coordinate can be directly transformed into the η coordinate without any assumption. It is important to note that usage of η coordinate system may not take into account the complex terrain effects as can be seen from Figure2.1.

In Figure 2.1. note that η changes from 1 at the surface to 0 at the upper boundary of the solution domain. Figure 2.2. shows an example of grid distribution of WRF. In this plot, z-axis is assigned as elevation from the sea level. Eta value of any point is affected from the altitude and surface elevation.

15
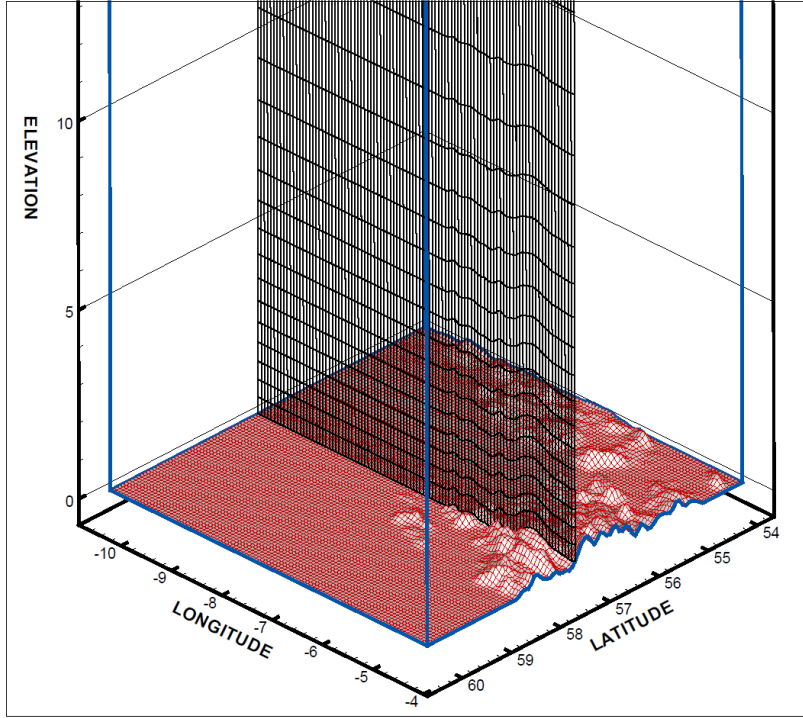
Figure 2.2: Mesh Distribution

In the WRF data structure, which is stored in "NetCDF" format, some variables are defined at grid nodes and some are at cell centers in a staggered grid fashion. (This staggered grid convention is explained in following section.) In order to express all the variables at the cell centers, the quantities defined at the nodes are to be carried to the cell centers. In addition, in WRF vertical elevation of a point is expressed as a geopotential height rather than as a vertical distance. The geopotential ϕ is defined as [14];

$$d\phi = gdh$$

and Geopotential Height is;

$$z = \phi(h)/g$$

In the WRF data structure "PHB+PH" is geopotential height, PHB is calculated at the beginning of the simulation and stays constant in time. PH is the geopotential perturbation, starts with zero and changes with time.

16

$$z = \frac{PHB + PH}{g}$$

Here g is Gravitational Constant and equal to 9.81.

From another point of view; terrain height can also be calculated from;

$$Terrain\_Height = \frac{PHB}{g}$$
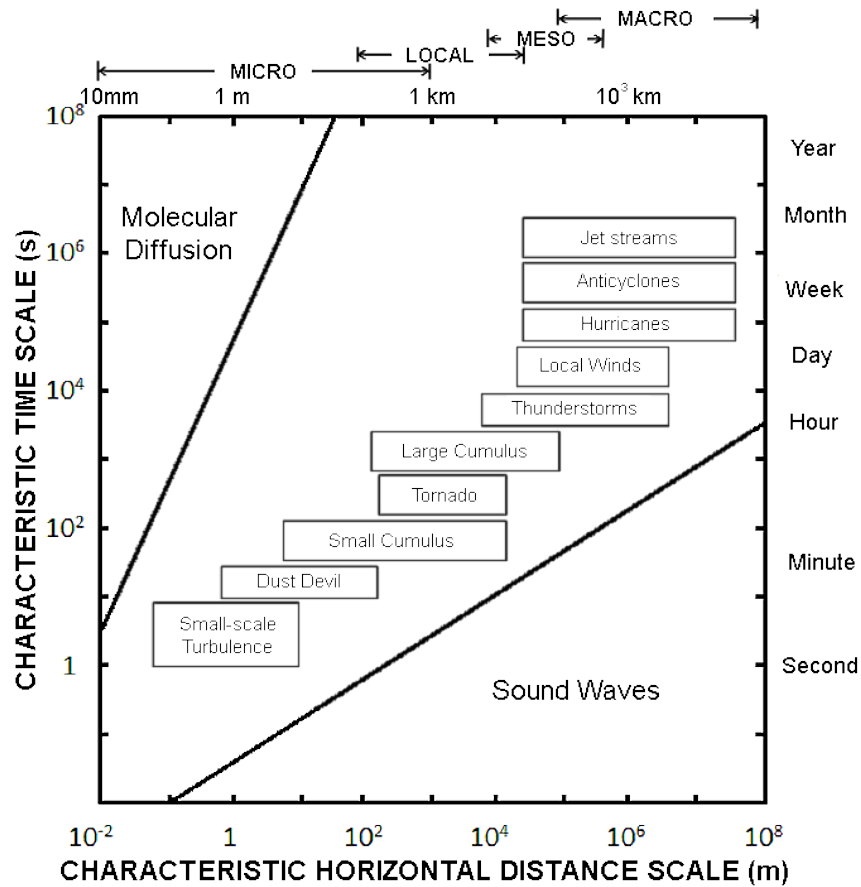
Figure 2.3: Time and space scales of various atmospheric phenomena.(Re-illustrated) Oke (1987)[30] (modified after Smagorinsky, 1974)

The Micro, Meso, and Macro scales of various atmospheric phenomena are given in Figure 2.3. The Meso-scale ranges approximately from 2 kilometres to 2000 km. In general, WRF simulations are carried out in a few kilometres horizontal and tens of meters vertical resolutions at the lowest level. These studies are

called high-resolution mesoscale simulations. However resolution may further be increased using several nests in the solution domain. [38]

Figure 2.4: Nested grid configuration for model runs of the WRF-ARW

The nesting in WRF is only allowed in latitudinal and longitudinal directions and is limited by 3:1 grid nesting ratio. That is, a nested grid can have 1/3 spatial grid resolution of its parent. It should be noted that defining the resolution by a factor of 3; increases number of grid points by a factor of 9 and requires 3 times as many time steps. Going from 9 km to 3 km spatial resolution increases the work load by at least 27 times, and the memory and storage requirements by 9 times.

Similarly in the case of increasing the resolution from 9 km to a 1 km; a numerical solution that takes 1 hour CPU time, 4 Gbytes of memory and 100 Gbytes of disc storage will now take at least 729 hours (a month), 324 Gbytes of memory and 8,100 Gbytes (8.1 Tbytes) of disc storage.[28]

Although such a study can not be performed for large domains, for a small domain, in a high performance computing environment with parallel processing high resolution simulation may be possible.

The standard topographical data set for the WRF simulation is available at a resolution of 30 arc seconds (about 900 meters).[37] WRF simulations at such low resolutions may provide inaccurate flowfields, close to the terrain surface. In order to simulate wind flows in a wind farm and micro-site of a wind turbine, high resolution simulations are needed.[24]

Table 2.1: Selected WRF options in simulations

Physics	Model
Microphysics	WRF Single-Moment 6-class scheme
Longwave Radiation	RRTM scheme
Shortwave Radiation	Dudhia scheme
Land Surface	Noah Land Surface Model
Planetary Boundary layer	Yonsei University scheme
Cumulus Parameterization	Kain-Fritsch scheme

2.1.1 Resolution Effect of Number of Eta Levels in WRF

To further analyse the effect of the number of Eta levels, 20-35-50-100 numbers of Eta Level solutions are produced for a selected region and depicted in Figure 2.5 and 2.6. Assuming the most accurate solution is the finest mesh, which has 100 Eta levels, is expected to provide more accurate solutions. On the other hand, the computational time increases linearly as shown in Table 2.2. The WRF solutions are obtained with 3 nested grids (100x100, 65X66, 57X57) and the minimum surface grid resolution in the third nest is 900 meters.

Table 2.2: Effect of Number of Eta Levels to Calculation Time

Number of Eta Levels	Cell Number of Mesh	Calculation Time [Minutes]
20	200K	29:43
35	350K	51:45
50	500K	70:50
100	1M	140:55
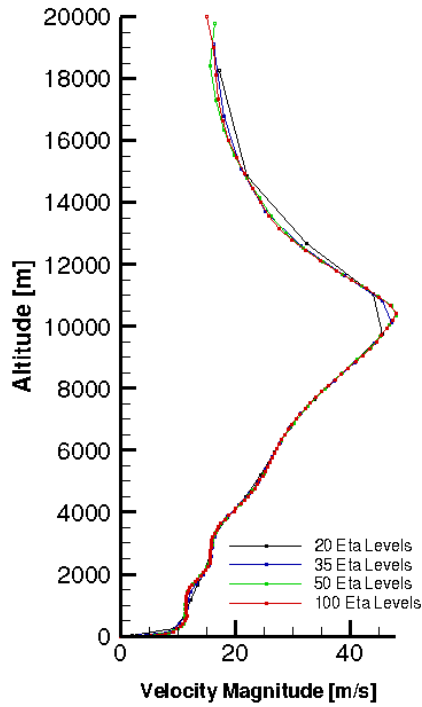
Figure 2.5: Wind profile for various Eta levels
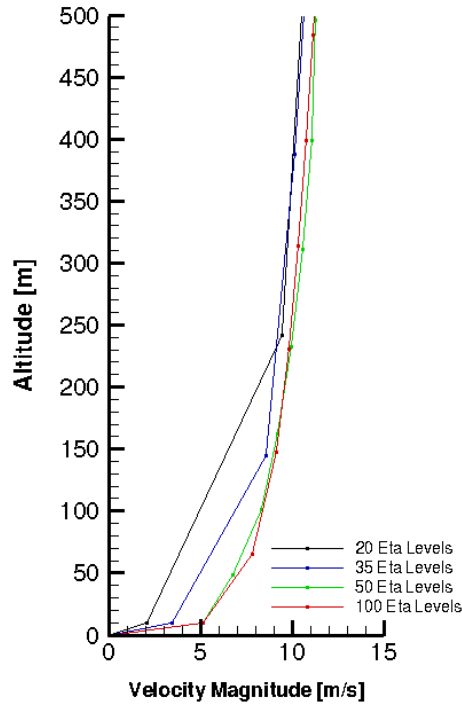
Figure 2.6: Wind profile for various Eta levels - First 500 meters

Considering the results presented in Figure 2.6. and the CPU time, the number of eta levels for the simulations is chosen as 50 in the remaining simulations.

2.2 In-House Navier-Stokes Solver HYP3D

HYP3D is a 3-Dimensional, finite volume method based, hybrid grid capable, parallel Navier-Stokes Solver with a Spalart Allmaras turbulence model. It employs an explicit three stage Runge Kutta time integration. HYP3D uses PVM for interprocess communications in parallel computations. It is based on master-worker algorithm. The unstructured solution domain is partitioned using METIS (Serial Graph Partitioning and Fill-reducing Matrix Ordering) [17] and the flow solutions of each partition is carried out in the worker process. The worker processes apply physical boundary conditions if needed and exchange intergrid boundary conditions among themselves at each time step of the solu-

tion. The master process performs input/output of data and synchronizes the solution among worker processes.
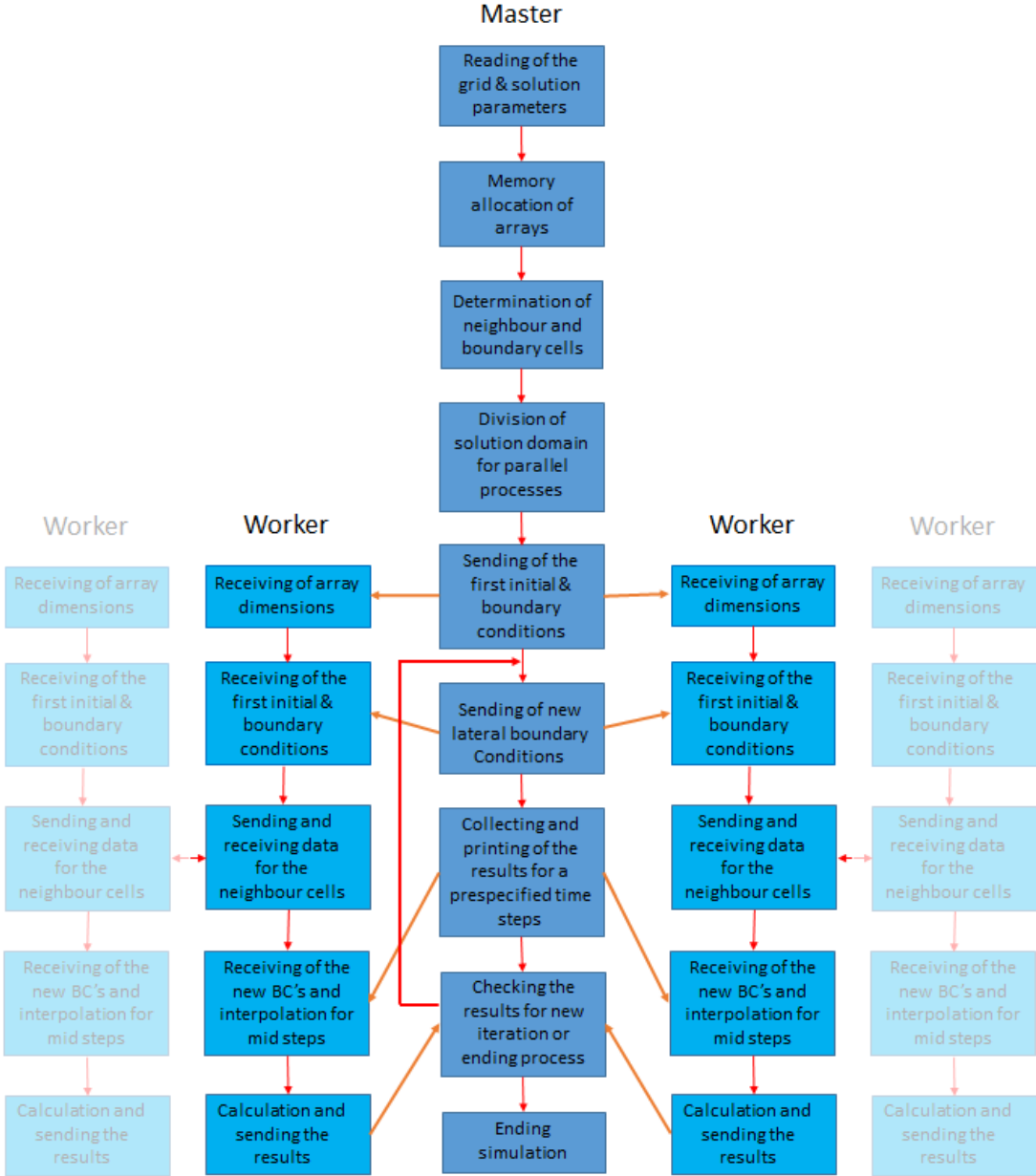
Figure 2.7: HYP3D algorithm

In this study physical unsteady boundary conditions are taken from WRF solution and applied in parallel HYP3D solutions. The parallel implementation of physical boundary conditions now requires master process to read the proper boundary conditions from files prepared a priory and sharing of these conditions

with the worker processes at the proper time levels along the unsteady computations. The physical boundary conditions in a worker process is then interpolated in space and in time from the two sets of proper boundary conditions received in a timely manner from the master process.

The parallel solution algorithm is depicted in flow chart in the Figure 2.7. In the very beginning of the solution process, master process reads solution parameters (laminar, turbulent, iteration count, Reynolds number, worker count and meshfile etc.) and computational grid, allocates the memory for calculation of the flow variables. It establishes the neighbour connectivity. The computational grid is partitioned using METIS. A worker process is then created for each partition and proper partition data are sent to the worker processes. The parallel computations initiate the worker processes. Along the computations worker processes exchange intergrid boundary conditions among themselves and receive unsteady physical boundary conditions from the master process at proper time steps. Fortran code pieces for master and worker processes are shown in Figure 2.8.

2.3 Generation of Computational Grids

In computational grids for CFD solutions, the high resolution terrain topography is generated using the data obtained from ASTER GDEM, which is a product of METI (The Ministry of Economy, Trade, and Industry of Japan) and NASA (The United States National Aeronautics and Space Administration). The topographic data has a worldwide elevation at 1.5 arc-sec horizontal resolution($\approx$ 30 meters). The computational grid is then generated using GAMBIT software. The horizontal resolution of terrain fitted grid is about 30 meters. The vertical resolution of the domain can be set as low as 7.5 meters for the first cell off the terrain surface and then stretches up to about 2000 meters altitude to resolve the atmospheric boundary layers.

```
                    MASTER                              WORKER
...                                          ...
...                                          ...
       time=0.                                   time=0.
       time_bcfar=dt_bcfar                       time_bcfar=dt_bcfar
    do i=1,npar
      call SENDWRFBC(bcfar) ──────────────────> call RECVWRFBC(bcfar)
    enddo
  DO ns = ns1,nslast                          DO ns = ns1,nslast
    do j=1,3
      ress(j,1) = 0.                             if (ns .eq. ns1)then
    enddo                                          do j=1,5
    do k=1,8                                         do k=1,ncbc
      Coef(k) = 0.                                     bcfar(2,j,k)=bcfar(1,j,k)
    enddo                                            enddo
    dtmin = 10.                                    enddo
    If (mod(ns,100) .eq. 1) then                 endif
      do nr=1,npar
      call RECVQ(nr,np,isend,ilocal, q,qt)       do i=1,3
        if(isend .gt. 10) then                     ress(i) = 0.
        print*, 'Error partition:',np, isend      enddo
        call SHUTDOWN
        endif
      enddo                                      if (mod(ns,100).eq.1) call
    CALL SENDDT ───────────────────────────> >CALDT(q,press,dxmin,dt)
    Endif
       time=time+dtming                           time=time+dtming
       IF (time .gt. time_bcfar) then          IF (time .gt. time_bcfar) then
       CALL SENDWRFBC(bcfar) ─────────────────> call RECVWRFBC(bcfar)
       time_bcfar=time_bcfar+dt_bcfar            print*,'Calling WRFBC',time,time_bcfar
       ENDIF                                     time_bcfar=time_bcfar+dt_bcfar
 IF( mod(ns,nsres).eq.0.or.ns.eq.ns1.or.ns.eq. ENDIF
 >nslast) then
      do nr=1,npar                               call RK3(tids,ilocal,libc,ibcs,ibcps,ibcrec,
        call RECVQ(nr,np,isend,ilocal,q,qt) <── >neigh,ntype,q,press,dq,qn,flux,vgrad,qt,tnu,
        if(isend .gt. 10) then                 >dt,wdist,area,volume,cosn,cost)
          print*, 'Error partition ',np , isend   if( mod(ns,nsres) .eq. 0 .or. ns .eq. ns1
          call SHUTDOWN                         >.or. ns .eq. nslast) then
        endif                                       do n=1,ncell
      enddo                                           ress(1) =  ress(1) + dq(1,n)**2 +
                                               >dq(2,n)**2 + dq(3,n)**2 + dq(4,n)**2+
      do j =1,3                                >dq(5,n)**2
        ress(j,1) = sqrt(ress(j,1)/ncell)          enddo
        if(ress(j,2).eq. 0.) ress(j,2) =      ──if(ns .ne. nslast) call SENDQ(2,q,qt)
 ress(j,1)                                        endif
        if(ress(j,1).ne. 0.) ress(j,1) =
 >ALOG10(ress(j,1)/ress(j,2))                  ENDDO
      enddo                                    ── call SENDQ(3,q,qt)
                                                    call PVMFEXIT(info)
      write(*,'(" LogRes-Cd-Cl : ",i6,2x,f6.3, stop
 >1x,f6.3,4x,3E11.3)')                         end...
 >ns,ress(1,1),ress(2,1),Coef(1),Coef(2)       ...
      write(21,'(i6,2x,3e12.4)')               ...
 >ns,(ress(j,1),j=1,2)                         ...
      write(22,'(i6,2x,8e12.4)')               ...
 ns,(Coef(k),k=1,8)                            ...
      if(MAX(ress(1,1),ress(2,1)) .gt. 2. ) then  ...
        print*, '   Residuals hit the roof...'    ...
        call SHUTDOWN                           ...
      endif                                     ...
    ENDIF                                       ...
 ENDDO                                          ...
 ...                                            ...
```

Figure 2.8: Master and worker routines of HYP3D

2.4 Coupling the CFD Solver HYP3D with WRF

HYP3D is coupled with WRF through the application of the initial and unsteady
boundary conditions as shown in Figure 2.9. The unsteady WRF solution is first
obtained in the low resolution WRF domain for the duration of interest. The
flow variables computed are saved at 5 minute intervals. HYP3D solution starts
with the initialization of the solution with the first instance of the unsteady
solutions of the WRF. It is achieved by interpolating the flow variables at the

cell centers of the HYP3D grid from the WRF solution properly. Flow variables at the boundary cells of the CFD domain are also interpolated in space and in time from the WRF solution. Time interpolation is performed between two datasets saved consecutively with 5 minute intervals. As the unsteady solution progresses proper datasets for the boundary conditions are sent from the master process to the worker processes.

It should be noted that WRF has a horizontal resolution of 1 km and a vertical resolution of about 30 m on the ground which stretches rapidly. In addition, as shown in Figure 2.11, the surface boundaries in the WRF and HYP3D domains differ significantly mainly due to the high resolution topographic data used in the generation of the HYP3D domain, and due to the η coordinate system employed in WRF.
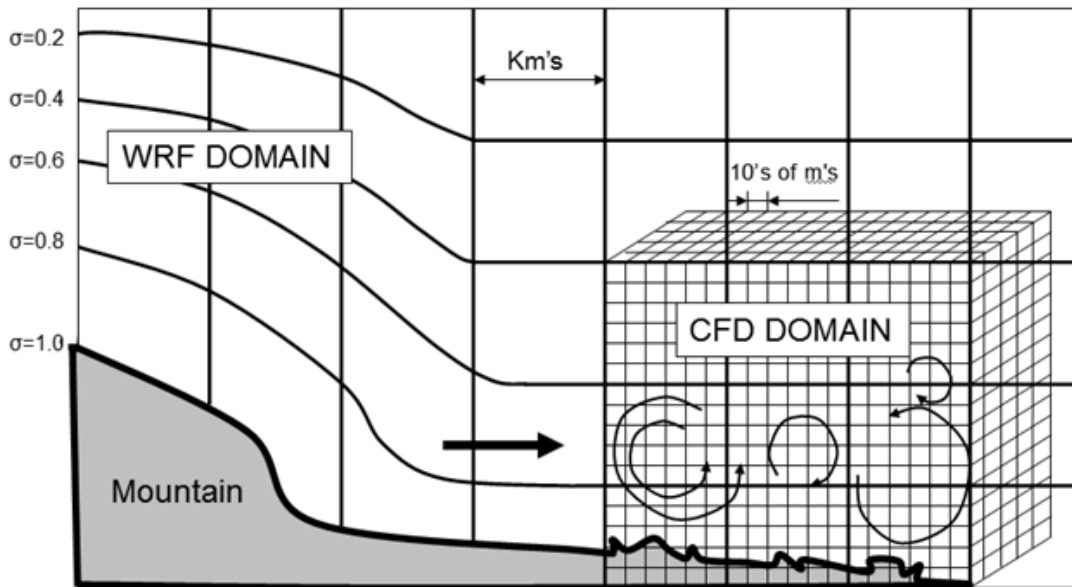
Figure 2.9: Coupling WRF with CFD Solver.

Due to the differences in grid and ground surface resolution in WRF and HYP3D solution domains, failures in the interpolation of flow variables may be observed in the application of initial and boundary conditions for HYP3D solutions. In order to overcome this problem, two approaches are tested. In the first approach; the vertical distances of the cell centers of boundary cells from the ground are evaluated. And the velocities at these distances above the ground level of WRF domain are interpolated as the boundary conditions. In other words; the ground
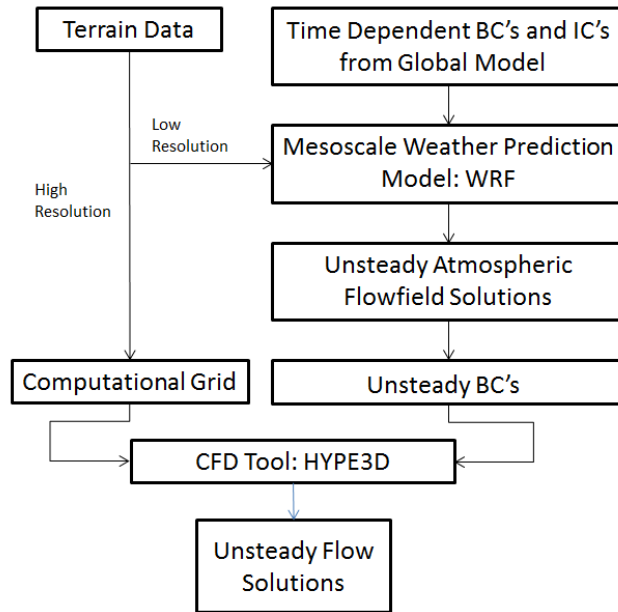
Figure 2.10: Flowchart.

level of WRF domain is locally shifted to the same level of the HYP3D domain and the interpolation in the vertical direction is performed[18]. This approach which is called the "shifting approach" is depicted at Figure 2.12.

In the second approach, a limited stretching of the WRF domain is implemented. In this approach the grid nodes located within the 200 meter vertical distance
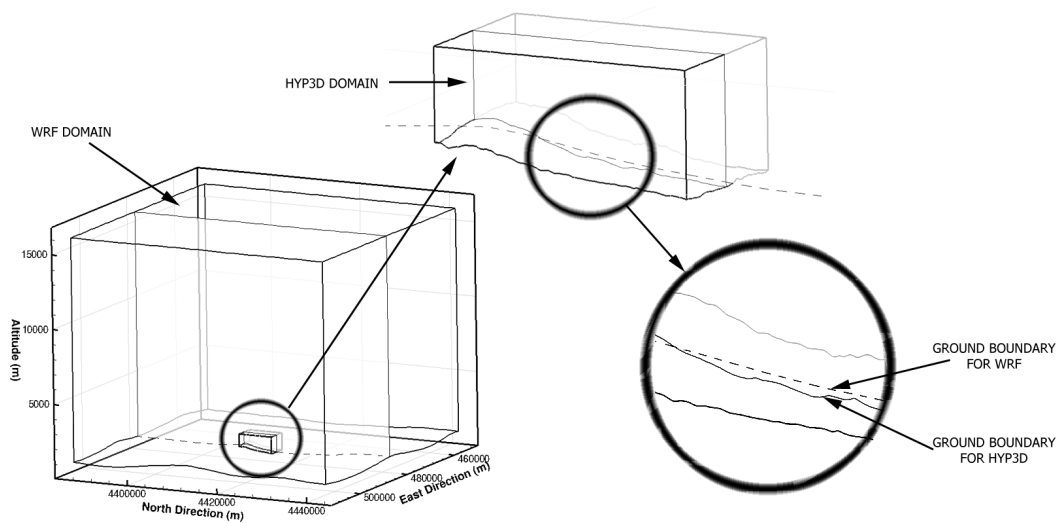
Figure 2.11: WRF and HYP3D solution domains and close-up views

in the WRF domain are stretched, so that the WRF surface boundary over-
lapse with the HYP3D surface boundary. The computed quantities are not
shifted/stretched above the limiting vertical distance when the boundary condi-
tions are extracted from the WRF solution.
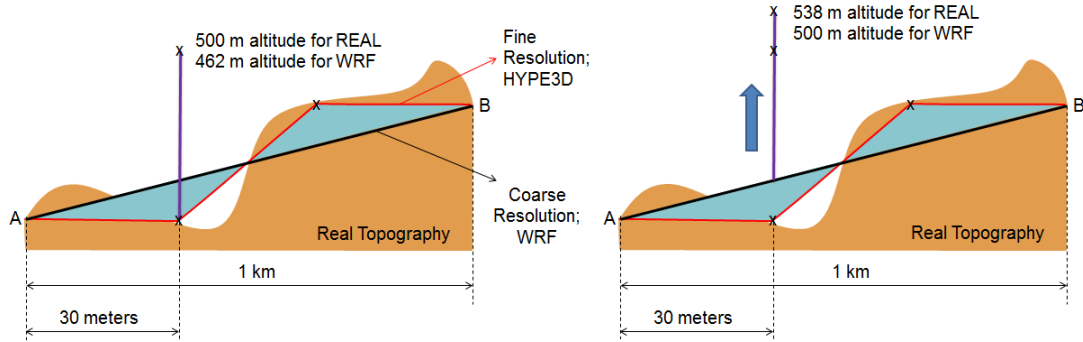
Figure 2.12: Shifting Method
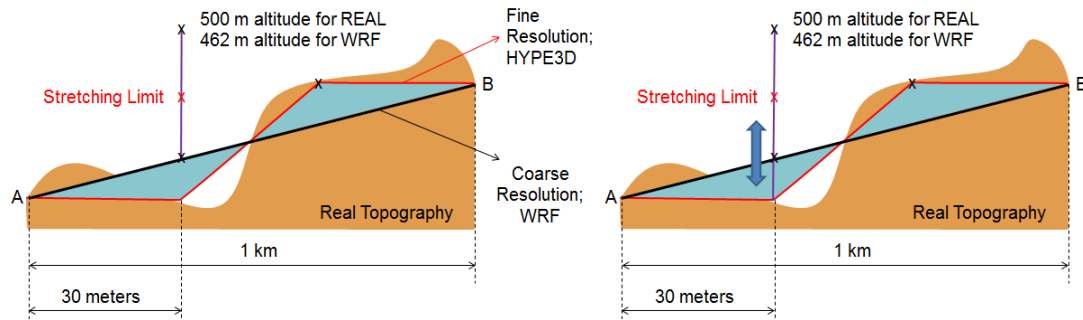
Figure 2.13: Stretching Method

2.5 Extraction of Initial and Boundary Conditions from WRF Solutions

As stated earlier the coupling between WRF and HYP3D solutions is achieved
by the application of initial and boundary conditions on the HYP3D solution
domain. The flow variables at the outer boundaries of the HYP3D domain at
each time step are extracted from the unsteady WRF solution. The following
steps are performed in the extraction and interpolation processes.

Preparation of WRF data: The grid coordinates and the flow variables in the
WRF solution domain such as latitude, longitude, elevation, velocity compo-

nents and pressure perturbation are first extracted. The geographic latitudinal and longitudinal coordinates are converted into Universal Transverse Mercator (UTM) coordinates. Additionally, in the WRF solution, some variables which are defined at the grid nodes are carried over to the cell centers. (Figure 2.14. and Figure 2.15.).[35]
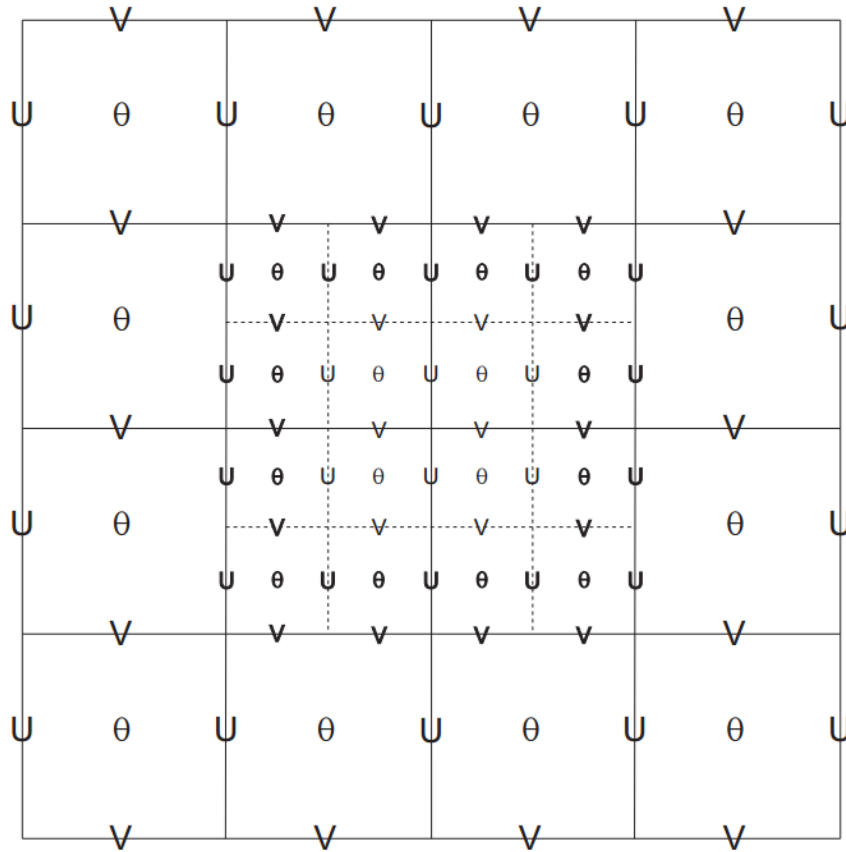
Figure 2.14: Staggered grid structure with nest[35]

Localization of a point in the WRF domain: For the interpolation of the flow variables at the cell center of a boundary cells in the HYP3D domain the coordinates of the cell center have to be localized in the WRF domain through a search process. The computational grid in the WRF domain is equally distributed in latitudinal and longitudinal directions and stretched in the altitudinal direction. Therefore the search process is easily performed in the latitudinal and longitudinal direction. Once the projection of the point is localized on the surface, it is localized in the vertical direction within a cartesian cell of the WRF domain.
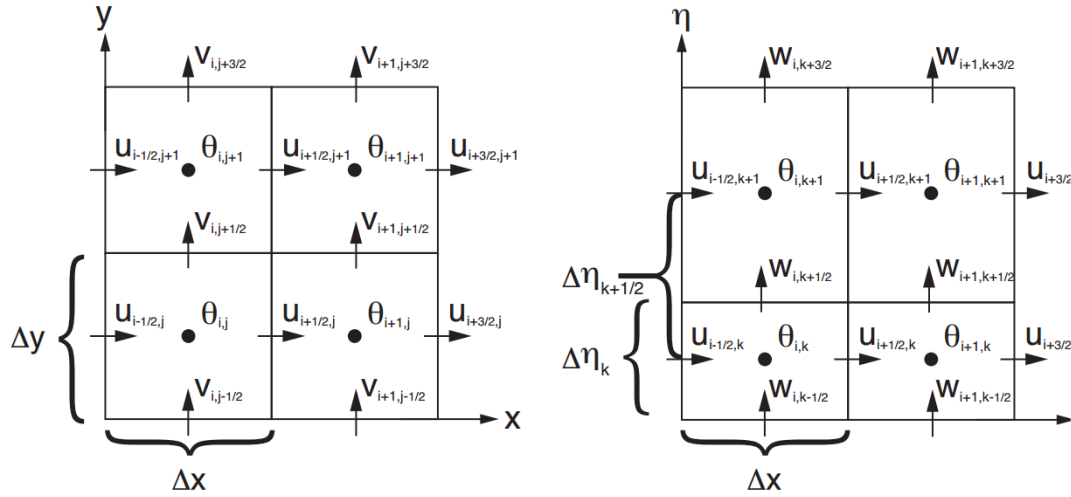
Figure 2.15: Horizontal(left) and Vertical (right) staggered grid structure[35]

Interpolation: Once a point is localized within a cubical cell, interpolation is performed. Trilinear Interpolation is assessed for the linear distribution in a cell.

Trilinear interpolation is widely used in the Finite Element applications (FEM). Its implementation for a cubical cell is shown in Figure 2.16.

$$\psi_i = \psi_{0,0,0}(1-x)(1-y)(1-z)$$
$$+\psi_{0,0,1}(1-x)(1-y)(\ z\ )$$
$$+\psi_{0,1,0}(1-x)(\ y\ )(1-z)$$
$$+\psi_{0,1,1}(1-x)(\ y\ )(\ z\ )$$
$$+\psi_{1,0,0}(\ x\ )(1-y)(1-z)$$
$$+\psi_{1,0,1}(\ x\ )(1-y)(\ z\ )$$
$$+\psi_{1,1,0}(\ x\ )(\ y\ )(1-z)$$
$$+\psi_{1,1,1}(\ x\ )(\ y\ )(\ z\ )$$
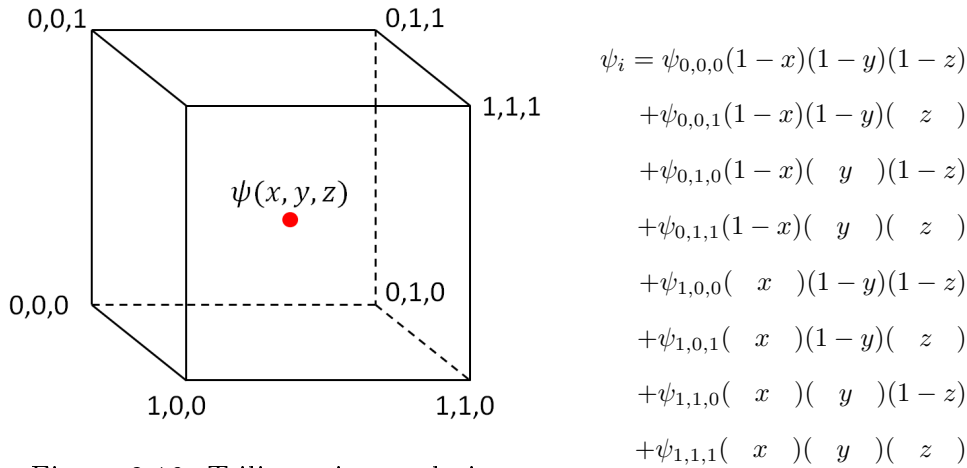
Figure 2.16: Trilinear interpolation

In order to assess the performance of the interpolation algorithms a test case is created and each corner is assigned with a different value. Creating 10X10 points on each direction interpolation method is implemented for these points. Distributions for this imaginary cell trilinear interpolation is drawn in Figure

28

2.17. In the Figure 2.18. distributions are also plotted for trapezoidal octagons. And defining 3 different lines, variation along these paths are drawn.
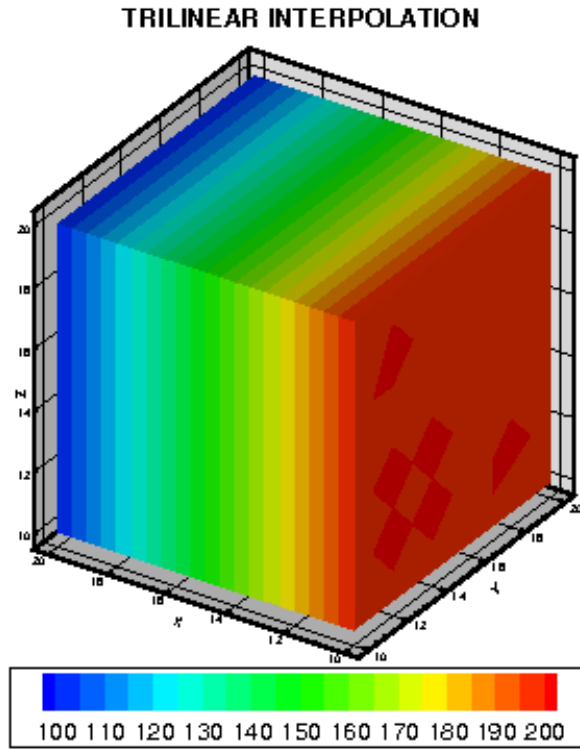
Figure 2.17: Trilinear Interpolation

Developed code is capable of extracting any property for any point in the solution domain. This capability is needed for the nodes that are on the boundaries of Navier-Stokes solver. By using this tool, virtual met-mast time series data is produced and results in several aspects are researched. [26].
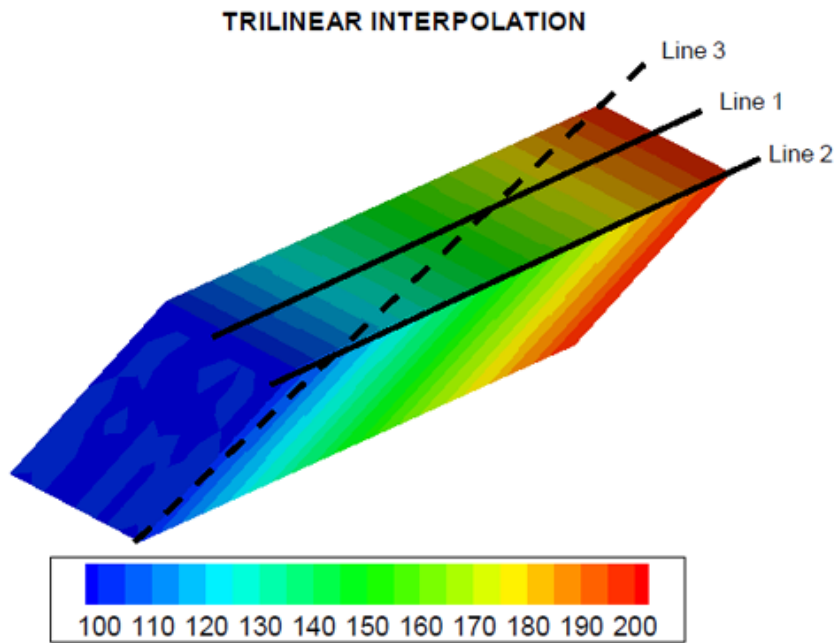
Figure 2.18: Variation along paths for trilinear interpolation

Within the solution domain of WRF, an imaginary diagonal plane is created. Then, interpolation with the developed code and Tecplot[3] interpolation are implemented for the points on this plane. Figure 2.19. shows these interpolation results. It can be commented that results are very close each other. Insignificant differences due to numerical errors can be realized, though.
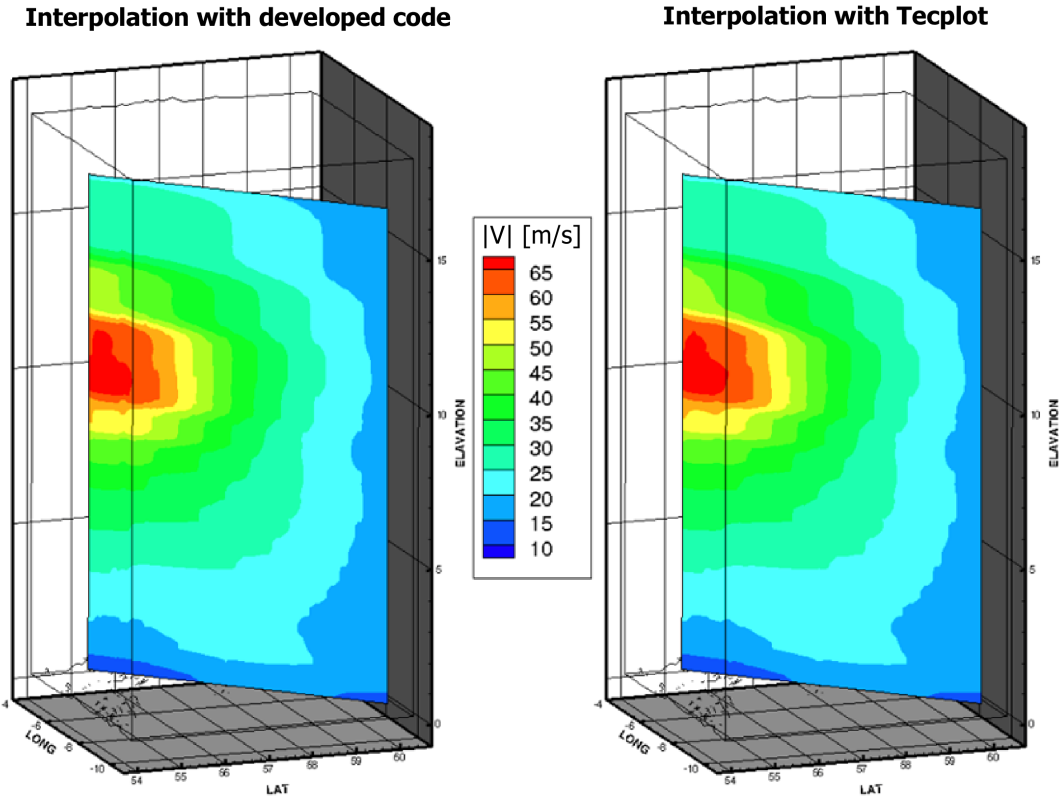
Figure 2.19: Comparison of Interpolation Results with Tecplot

2.6 Wind Assessment

In order to assess the wind potential and statistical analysis of the region, specialized output and data collection routines are implemented to the HYP3D.

For the time series analysis, the flow variables of the selected points are written during the simulations. Also to make a statistical analysis of the whole domain, the classification of the variables is performed at each cell in the solution domain. The velocity magnitude is divided 24 equally spaced bins between 0 and 24 m/s. Whereas the wind direction is divided into 12 wind directions with 30 degree intervals.

Along the computations frequency of occurrences of the wind magnitude and the directions are cumulated for the each time steps. In the end of the simulations frequency of occurrences obtained for each cell is saved for further statistical analyses.

Weibull probability function is a widely known statistical distribution function which is used for wind speed distributions. For the wind speed distribution, Weibull function represents the probability (or frequency) of wind speed. Weibull distribution function can be given as:

$$f(v, \lambda, k) = \frac{k}{\lambda}(\frac{v}{\lambda})^{k-1} e^{(\frac{v}{\lambda})^k} \tag{2.7}$$

where λ is the scale factor, k is the shape factor and v is the wind speed for the case which will be examined in this study. For the interpretation of these parameters it can be said that λ is related to the most probable average wind speed and; k is related to the shape and width of the distribution. Low values of k indicate a scattered distribution whereas high values of k indicate clustered distribution around λ value. Figures 2.20 and 2.21. are show Weibull probability functions for different shape and scale parameters.
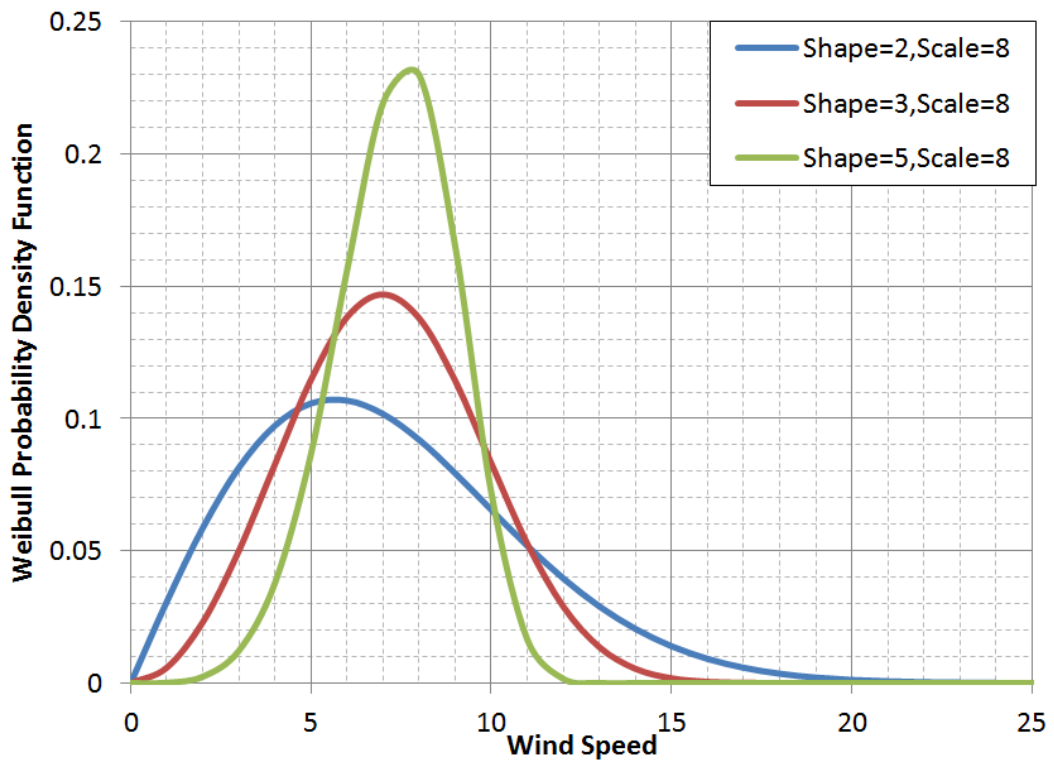
Figure 2.20: Different shape parameters for constant scale parameter
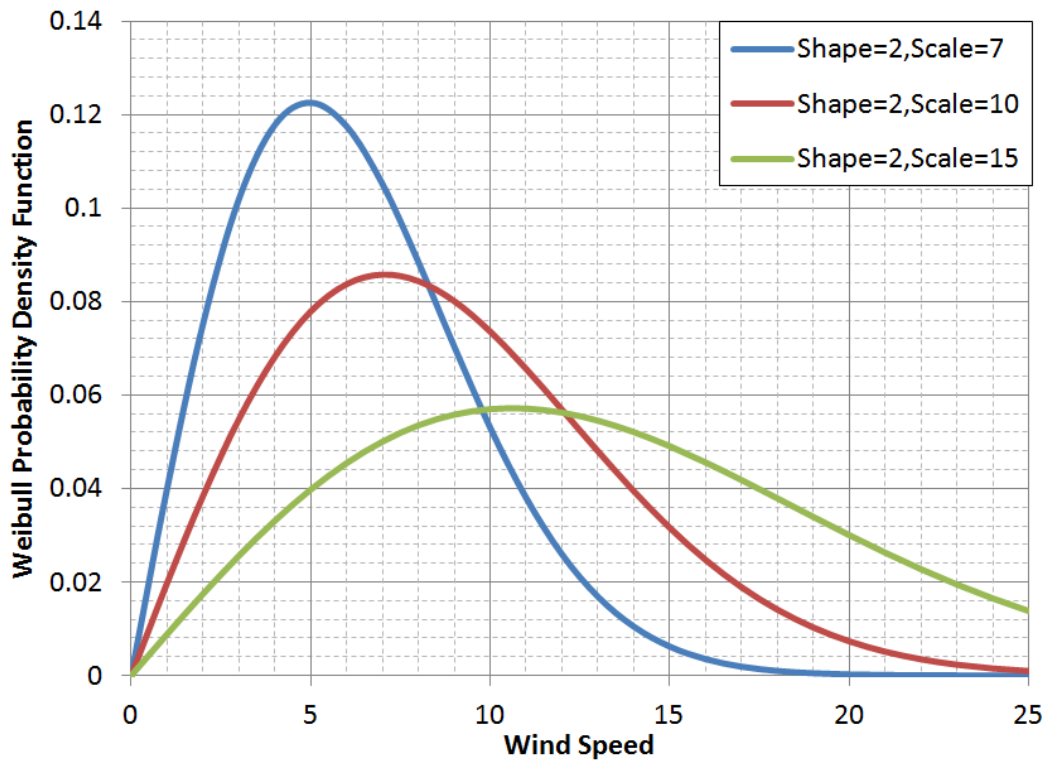
Figure 2.21: Different scale parameters for constant shape parameter

Figure 2.22. shows example of wind probability distributions, Weibull function fit curve and wind rose distributions. In wind probability distribution blue bars show the percentage of different wind speed occurrences. First bar which represents probability of 1 [m/s] wind speed, has a probability of 2 % of all wind speed variations. From the plot, it can also be commented that most frequent wind speeds are 7 and 8 [m/s] which of each are 12 % of all wind speed distributions. The red line shows the Weibull function fit to this distribution. For this function, calculated shape and scale parameters are 1.9790 and 8.0707 respectively. When the wind rose plot is considered, wind directions and the speed probabilities of this distribution can be examined. In this example it can be concluded that, around 30 % of the wind blow from the North direction. 25 % of the north blowing winds have the speeds of less than 10 [m/s]. And also it can be concluded that 5 % of these north blowing winds have a speeds of between 10 and 13 [m/s].
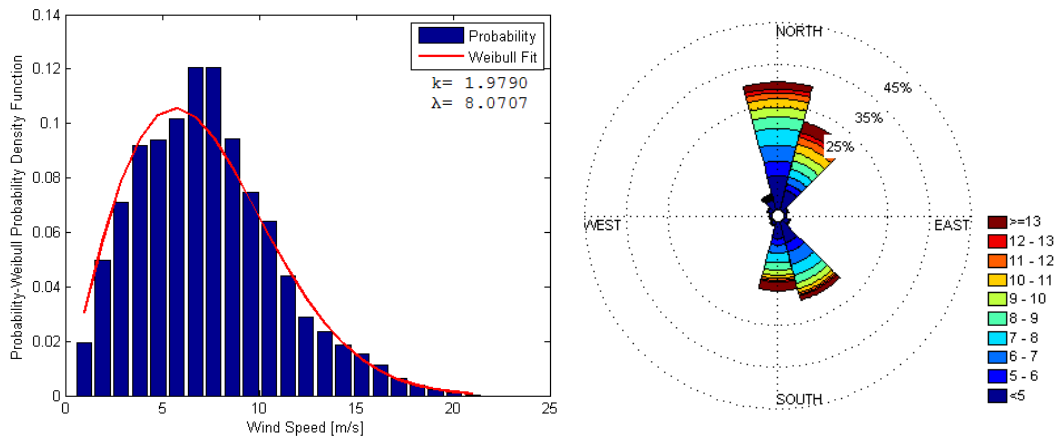
Figure 2.22: Example of Weibull probability function and wind rose plot

Wind power density is simply wind power distribution that can be calculated per unit area such as;

$$PowerDensity = \frac{P}{A} = \frac{1}{2}\rho v^3 \qquad (2.8)$$

For getting the average power density for a year, velocity magnitude data taken at 1 hour time intervals are integrated and divided by simulation duration (1

34

year). Using wind power density distribution maps most windy areas can be choose for wind turbine. Also it is easy to estimate approximate annual energy production for a turbine. For the Weibull distribution and wind roses, wind field data is stored at each iteration in the categories of 24 wind speed bins and 12 wind directions. Using these wind field information, Weibull bar charts and wind rose distributions are plotted.

CHAPTER 3

RESULTS AND DISCUSSION

In this study, unsteady coupled atmospheric flow simulations is performed for one year period for the Mut/Mersin region in Turkey where a wind farm is being constructed and met-mast data for year 2010 are available. The terrain data for the WRF simulations are automatically downloaded from UCAR (University Corporation of Atmospheric Research) server. Initial and time dependent boundary conditions for the WRF simulations are obtained from NCEP (National Centers for Environmental Prediction) Final Analysis (FNL from GFS) (ds083.2 dataset). It should be noted that this dataset has globally 1 degree resolution data for every 6 hours.

Nested WRF solutions are first performed for a 1 year period, within a parent domain of 3 km horizontal resolution and a nest of 1 km resolution where the wind farm is located. The computations are performed from the date 01.01.2010 to 15.12.2010. The parent and the nested solution domains are of the size 100x79 (horizontal) x 50 (vertical), and 88x67 (horizontal) x 50 (vertical) respectively.

WRF solutions for the nested domain are saved for each 5 minute interval. The parent and nested domains used for the WRF simulations are shown in Figure 3.1.

WRF solutions saved store certain variables at nodes and remaining ones at cell centers. In order to facilitate the interpolation process for the HYP3D boundary conditions, the flow variables defined at the nodes are carried to the cell centers prior to the HYP3D solutions.

Figure 3.1: Parent and nested WRF domains

The Navier Stokes solver employed in the study, HYP3D, is first validated against the flat plate solutions. Then a grid resolution and a validation study are performed with WRF coupled solutions. The numerical solutions are also compared with the met-mast data. In addition performance of the parallel HYP3D computations are assessed in terms of speed-up and efficiency figures. Following the validation studies, unsteady flow solutions are performed for a year period with 12 monthly solutions in parallel. Each WRF solution starts at the first day of the each month and continues till the end of the month as the boundary conditions are updated at every 6 hours. And flow solutions are saved at 5 minutes intervals.

HYP3D solutions are similarly performed for a period of a month in parallel using 16 processors. The unsteady boundary conditions are extracted from the WRF solutions with 5 minute intervals are applied along the unsteady parallel flow solutions. In addition the statistical wind data in terms of wind direction and magnitude are accumulated along the unsteady flow solutions.

38

In the end of the simulations all the statistical data stored are data-mined and power density, Weibull distributions, wind rose figures are generated and evaluated for maximum power generation. In the wind assessment process a new indicator for micro-siting which is based on the Weibull function parameters is introduced.

Finally, using the statistical data constructed and power production curves for 2 different wind turbine models, the annual energy production estimations are evaluated in the solution domain. and the best locations for the maximum power production are identified. It is shown that the new indicator introduced helps to identify the best locations for turbines with different power production characteristics. Turbine specific annual energy production estimations are also performed for various altitudes above the ground.

3.1 Validation of HYP3D

The validation of the 3-D, parallel Navier-Stokes solver with the Spalart All-
maras turbulence model, HYP3D, is performed in this section. For a case study
flow over flat plate is computed for laminar and turbulent flows. In the simu-
lations a structured grid with 94736 nodes, 70110 cubic cells are employed and
shown Figure 3.2. and 3.3.
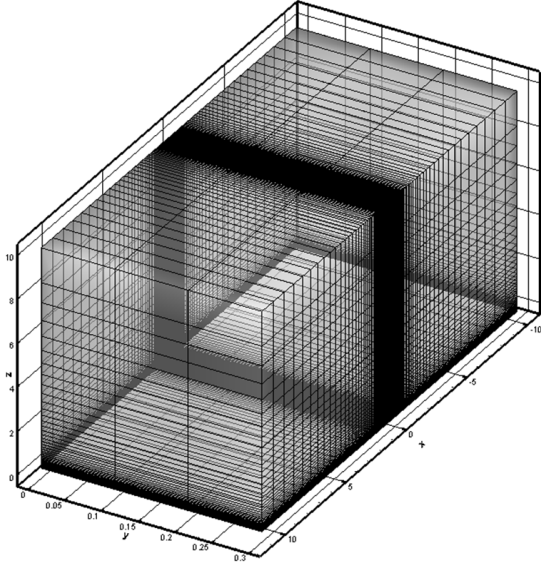
Figure 3.2: Computational Grid   Figure 3.3: Boundary Conditions
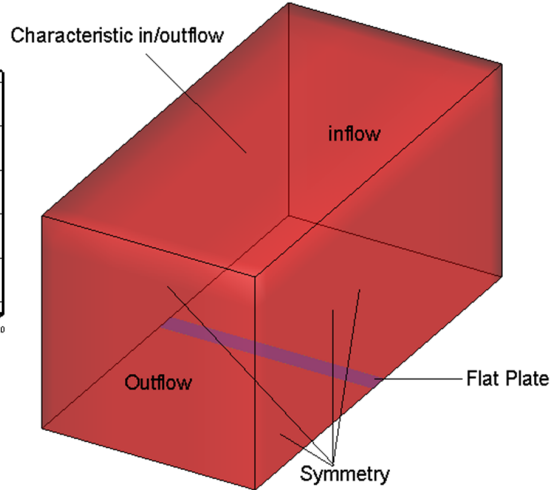
For the viscous laminar flow case, The Reynolds number an the Mach number
is 50000 and 0.2 respectively. As shown in Figure 3.4 after 50000 time steps
solution is converged for laminar case. For the turbulent case (Figure 3.5) con-
vergence is achieved after 210000 iterations. Case parameters are summarized
in Table 3.1.

Table 3.1: Flat plate case for Validation

Case	Laminar	Turbulent
Reynolds Number	50000	5000000
Mach Number	0.2	0.2
Iteration	100000	250000
Partition	8	8
Residue	E-4.5	E-3.5

40
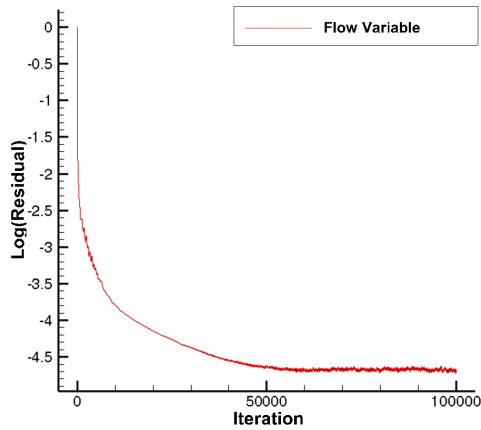
Figure 3.4: Residual history of laminar case
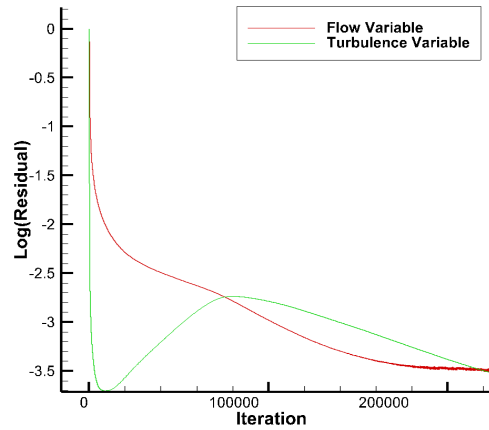
Figure 3.5: Residual history of turbulent case

Figure 3.6, 3.7 show the mean velocity vectors over the flat plate for the laminar and the turbulent flow cases. Both of the solutions agree very well with the theoretical boundary layer profiles as shown in Figure 3.8.
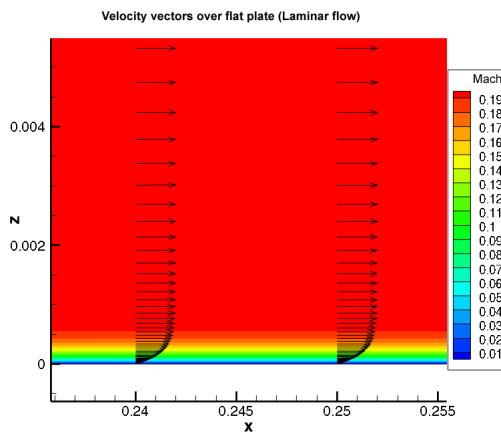
Figure 3.6: Velocity vectors for laminar case
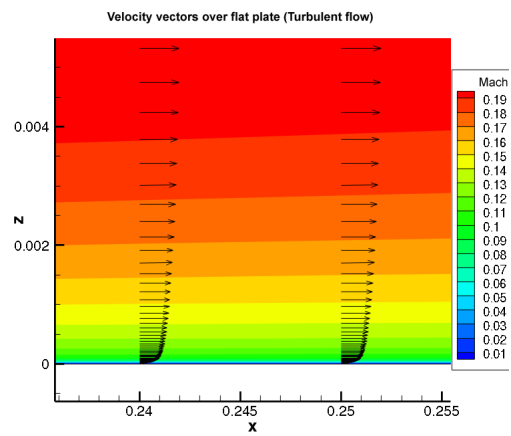
Figure 3.7: Velocity vectors for turbulent case

For a turbulent flow, velocity distribution within the boundary layer can be examined as u^+ y^+ curve in log chart at Figure 3.8. HYP3D simulated the flow in the sub layers of the boundary layer successfully.

The surface skin friction coefficient distribution along the flat plate taken from HYP3D simulation is also compared with those provided by NASA Turbulence

41

modelling resource data[2]. In Figure 3.9. shows these distributions. Slight differences at the trailing edge (X=1) due to boundary condition interactions. Also it should be noted that reference data is the results of a simulation which has a 2 meters long flat plate.
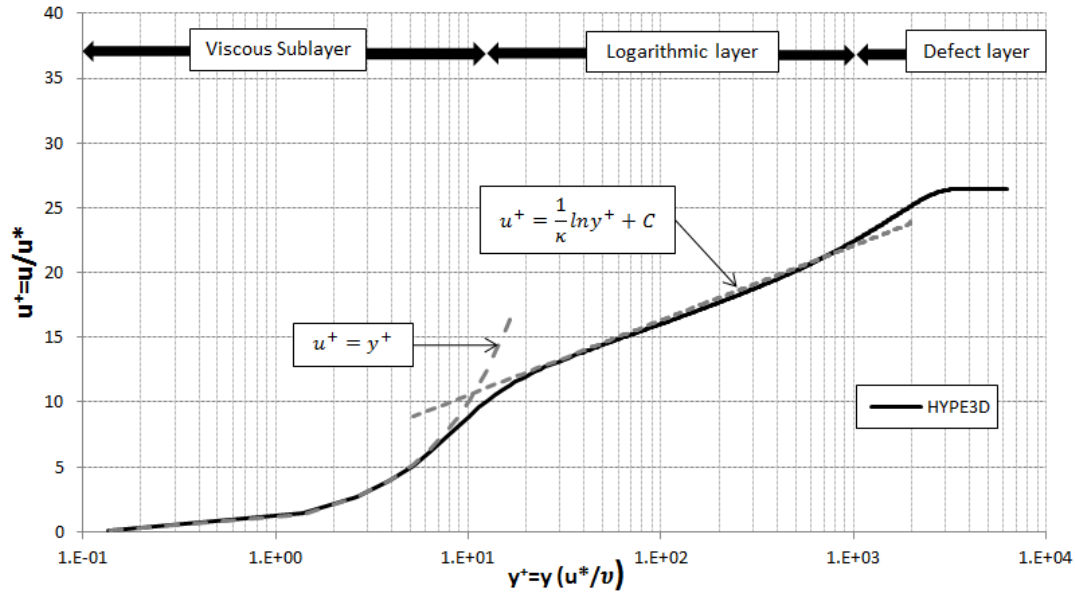
Figure 3.8: Sub-layers of turbulent boundary layer
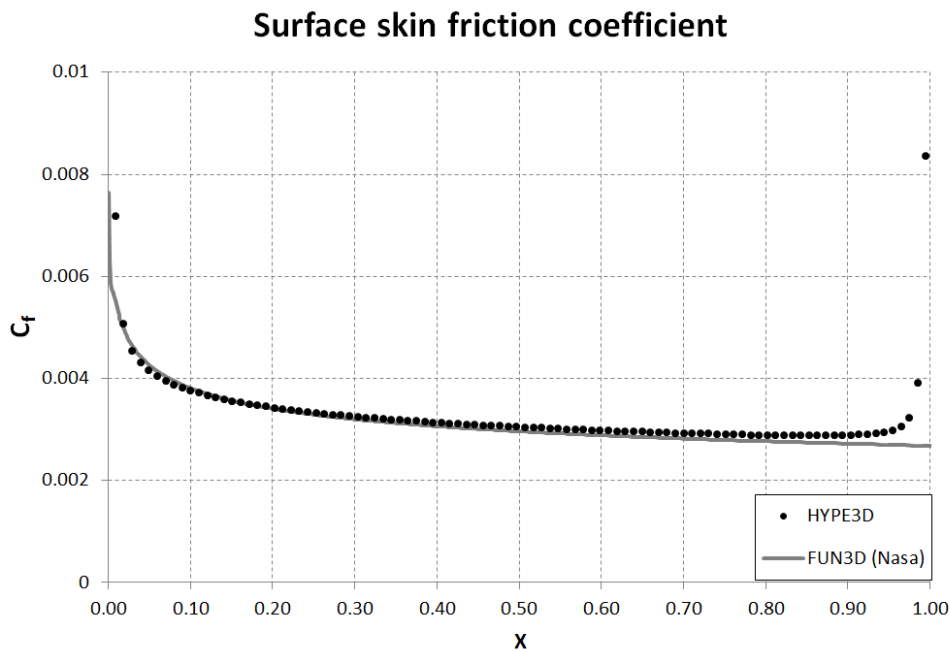
Figure 3.9: Surface skin friction coefficient

42

3.2 Parallel Performance

Speedup and efficiency change with the number of cores used in HYP3D simulations are presented in Figure3.10. Increasing the number of cores in use, decreases the efficiency. For the benchmark case of HYP3D, which is explained in the Section 3.1 in detail, maximum speed-up is achieved for 32 number of cores with 50 % efficiency. This drop in efficiency, is caused by the time lag for the boundary condition communications between the processors. In addition to this, after a point, communication bandwidth between the cores and CPU's becomes the limit of the parallelization performance. This calculations are performed in high performance cluster composed of 1 server with 8 nodes. Each worker node has 4 separate 2.3 Ghz CPU's with 16 cores and 256 GB DDR3 with 1333 MHz memory. It has totally 512 cores and 2TB memory.
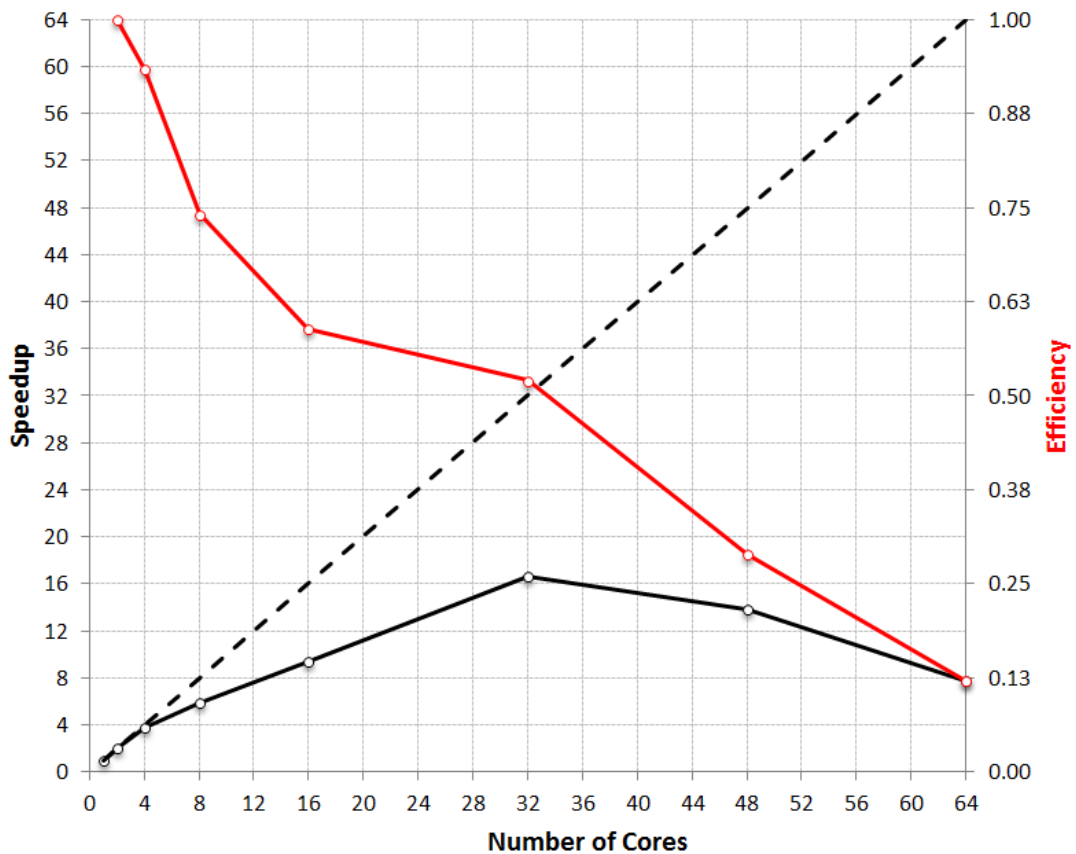
Figure 3.10: Speed-up/Efficiency vs. Number of Cores

3.3 Implementations of Boundary conditions

As stated earlier two approaches are assessed to overcome the failures in the interpolation of flow variables due to the differences in grid and ground surface resolution in WRF and HYP3D solution domains.

For one day simulation boundary layer profiles are created at the outer boundary of HYP3D. Two different cases are investigated. The first one is a case of the WRF ground boundary is lower than that for HYP3D. In the second case HYP3D ground level is at 80 meters above the WRF ground level. Figure 3.11 and 3.12 show boundary layer profiles drawn at 2 locations which are at the outer boundary of HYP3D solution domain.
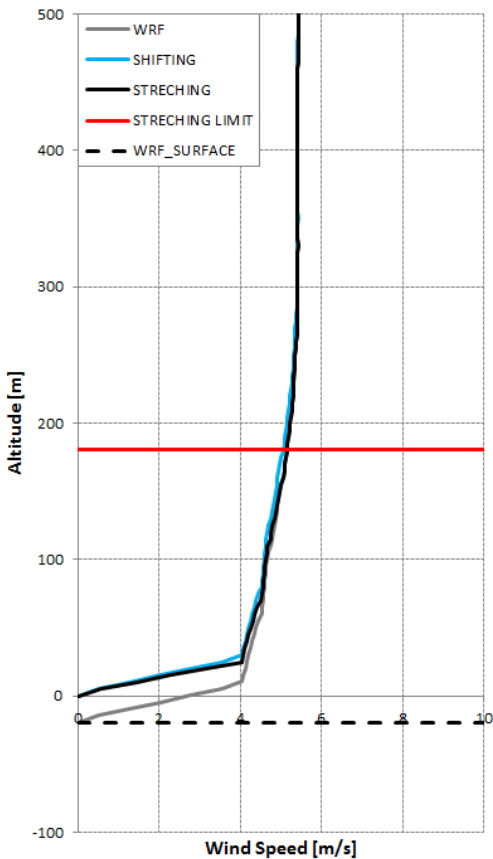
Figure 3.11: Different BLP for Shifting and Stretching Approach (Case 1)
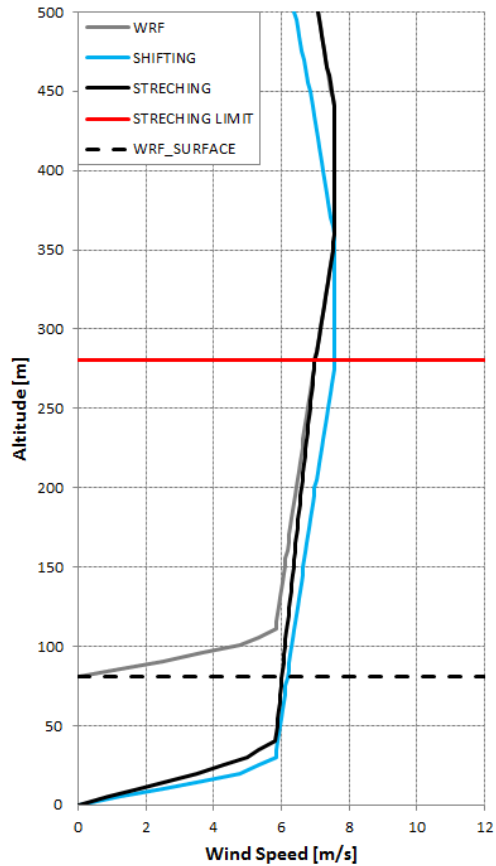
Figure 3.12: Different BLP for Shifting and Stretching Approach(Case 2)

In Figure 3.11 at the selected coordinate, ground level of HYP3D surface is actually higher than the altitude of the corresponding ground surface in WRF solution domain. Therefore shifting of boundary layer profile of WRF performed in the positive altitudinal direction. In contrast, for the case where real altitude of the ground surface is lower than the altitude of the corresponding ground surface in WRF solution domain, shifting of boundary layer profile of WRF performed in the negative attitudinal direction as seen in Figure 3.12. When boundary layer profile at the high altitude is well examined, it can be commented that unrealistic profile is created with the shifting approach. In order to minimize disturbance of flow velocities especially at high altitudes, the stretching approach is used.

3.4 Grid Resolution

In computational grids for CFD solutions, the high resolution terrain topography is generated using the data obtained from ASTER GDEM, which is a product of METI (The Ministry of Economy, Trade, and Industry of Japan) and NASA (The United States National Aeronautics and Space Administration). ASTER GDEM data provide surface elevation with 1.5 arc-sec horizontal resolution($\approx$ 30 meters).

The data obtained from ASTER GDEM, is first converted into Universal Transverse Mercator (UTM) coordinates. The converted data is imported to the GAMBIT software as the points defining a surface in cartesian coordinate system (in meters). The computational grid is then generated with 30 meter horizontal resolution and three different vertical resolutions are shown in Table 3.2. The upper boundary of the solution domain is located at about 2000 meters altitude.

Table 3.2: Shortest grid lengths in vertical direction

Grid	Shortest grid lengths in vert.dir. [m]
WRF	50m
Structured	30m
Structured	15m
Structured	7.5m
Unstructured	30m
Unstructured	20m
Unstructured	15m
Hybrid	30m
Hybrid	10m
Hybrid	5m

The unsteady coupled solution is performed with HYP3D for 24 hour period on three grids with different vertical resolutions. The solution at the location of the met-mast data (71.4 m altitude) is compared with each other in the Figures 3.13,3.14 and3.15. Also at the 200 meters above the ground similar comparisons are performed and showed at the Figures 3.16,3.17 and 3.18.

46
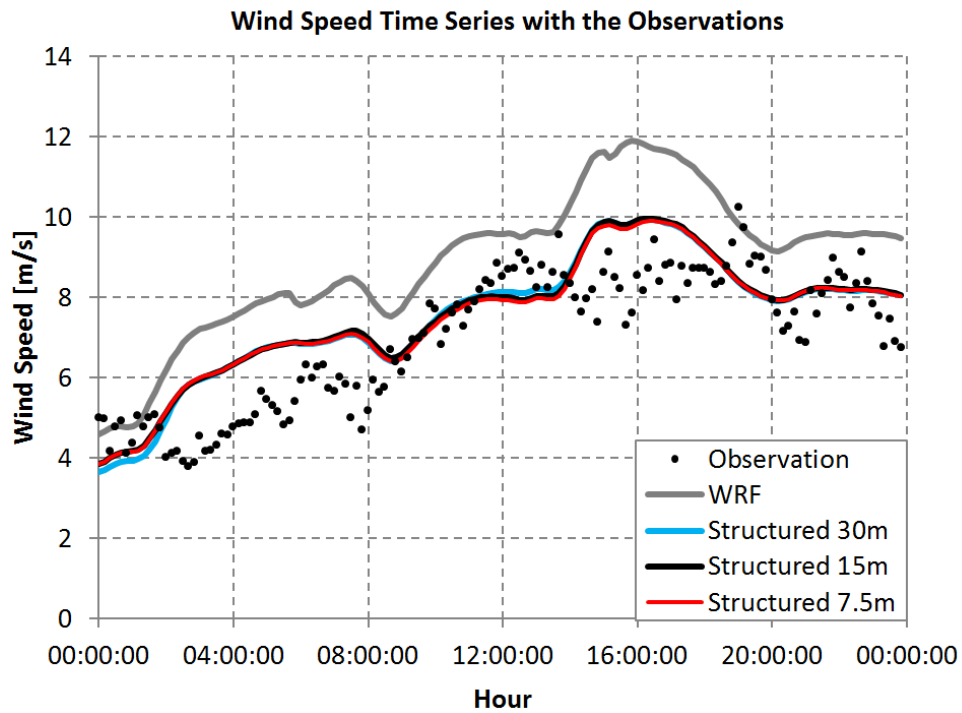
Figure 3.13: Wind speed time series comparison for structured grids
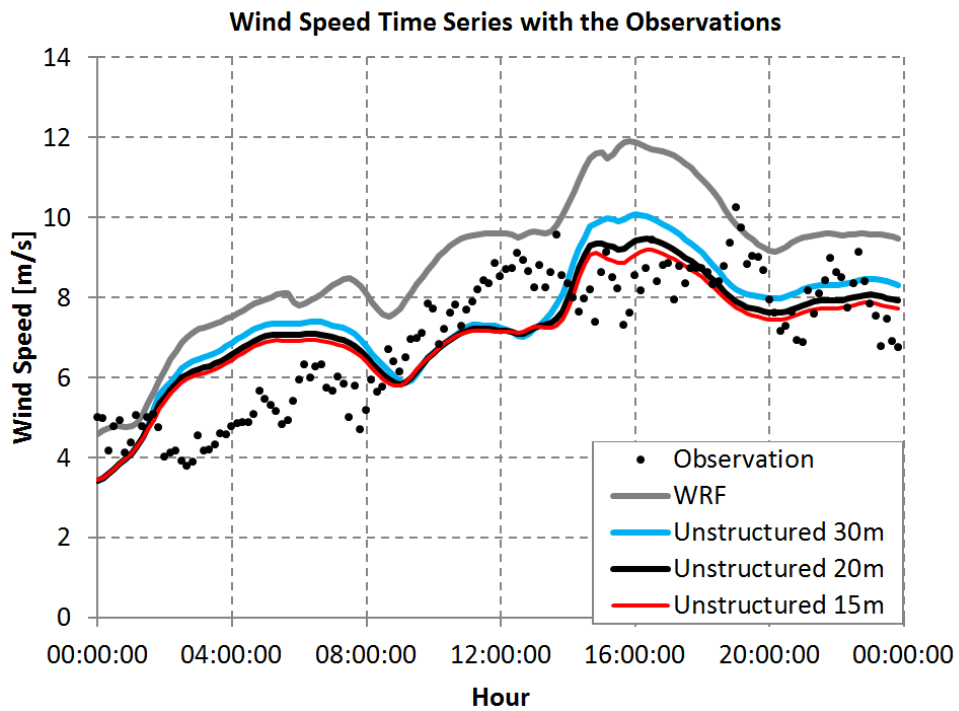
Figure 3.14: Wind speed time series comparison for unstructured grids
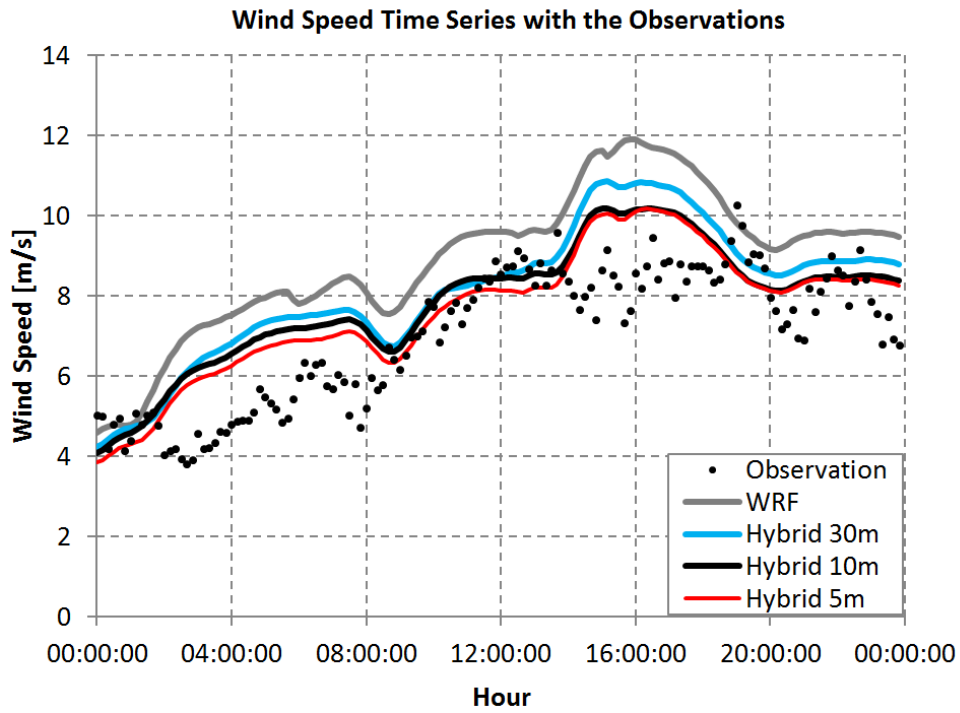
Figure 3.15: Wind speed time series comparison for hybrid grids
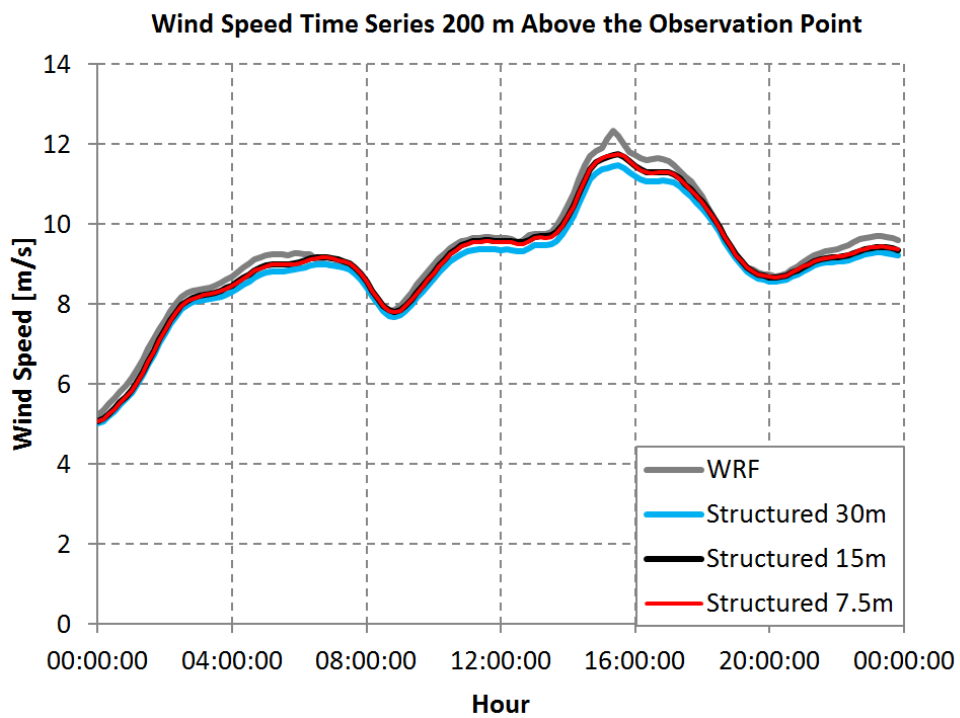
Figure 3.16: Wind speed time series comparison for structured grids at 200m above the observation point
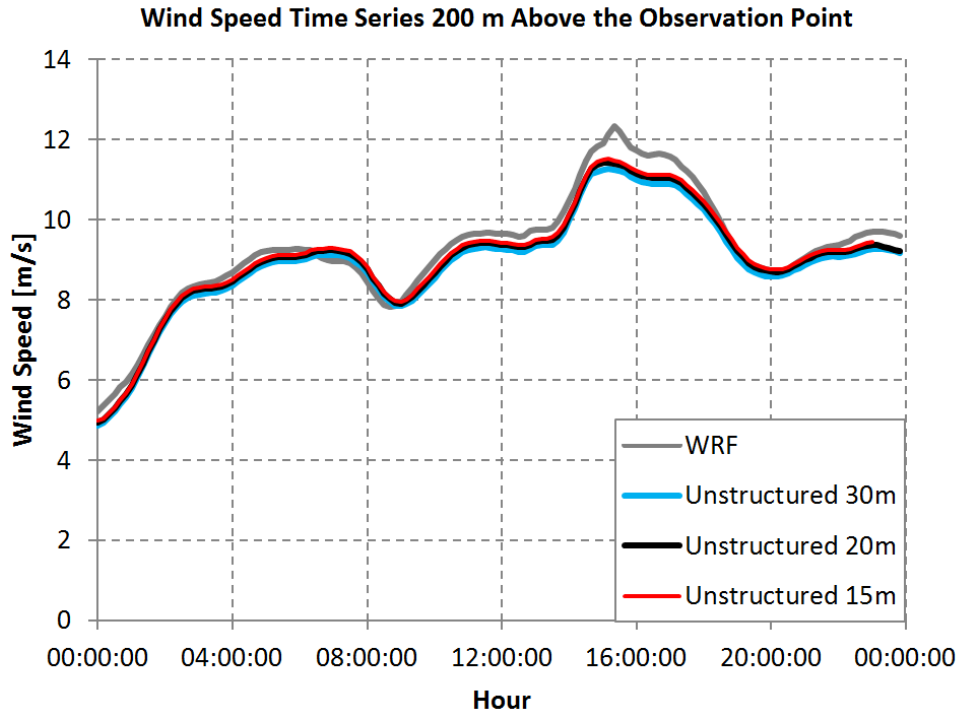
Figure 3.17: Wind speed time series comparison for unstructured grids at 200m above the observation point
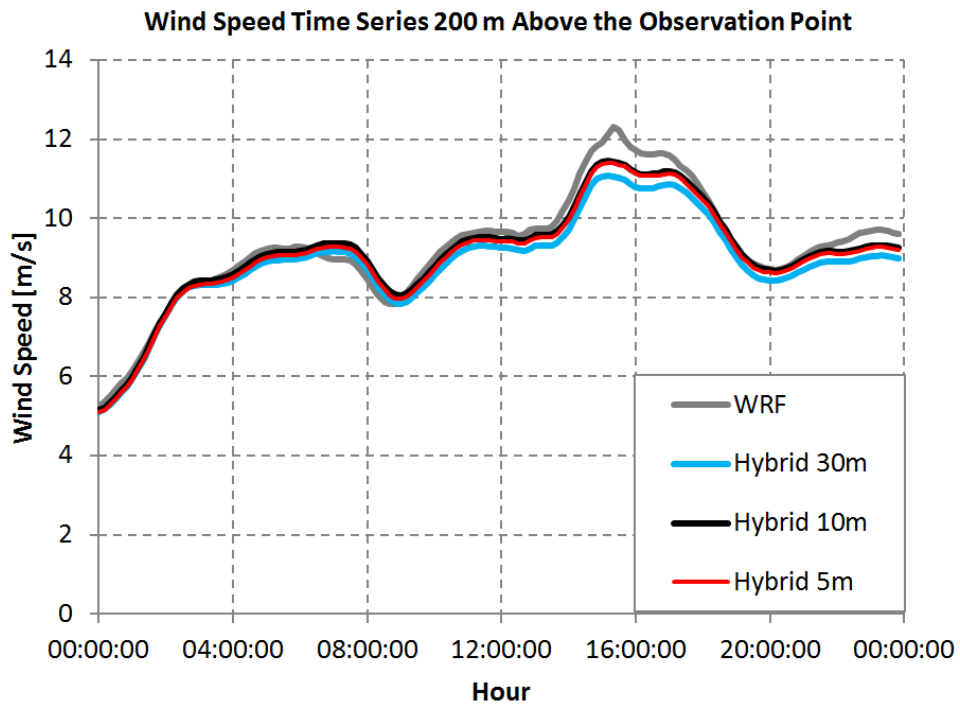
Figure 3.18: Wind speed time series comparison for hybrid grids at 200m above the observation point

49

As seen the grid resolution in the boundary layer increases the predictions better agreed with the observation data. In order to quantify the performance of the predictions, the root mean square of the deviation of the numerical solution from the observation data (RMS-Deviation) shown in Table 3.3. All the HYP3D results seems to be consistent with each other.

Table 3.3: RMS of the deviation of the numerical solution from the observation data

Grid	Surface resolution in z-dir. [m]	RMS-Deviation
WRF	**50m**	**1.858216925**
Structured	30m	1.119359676
Structured	15m	1.11349908
Structured	**7.5m**	**1.097548869**
Unstructured	30m	1.368435204
Unstructured	20m	1.200148459
Unstructured	15m	1.143525082
Hybrid	30m	1.51965739
Hybrid	10m	1.257065786
Hybrid	5m	1.130787133

In Figures 3.16 - 3.18, predictions are compared at a higher altitude 200 m above the observation point. All the flow solutions are in agreement with each other and with the WRF prediction as expected.

Based on the results presented in Table 3.3. the structured grid solution with 7.5 meter surface grid size provides the least deviation from the observation data and it is used in the remaining computations.

3.5 HYP3D-WRF Validation

In this section unsteady atmospheric flow solutions by using HYP3D are carried out over MERSIN/MUT area in a 3 km x 2km region for further validation of the HYP3D solutions against WRF predictions. The predictions are compared at certain points, close and away from the surface as shown in Figure 3.19 and Table 3.4.
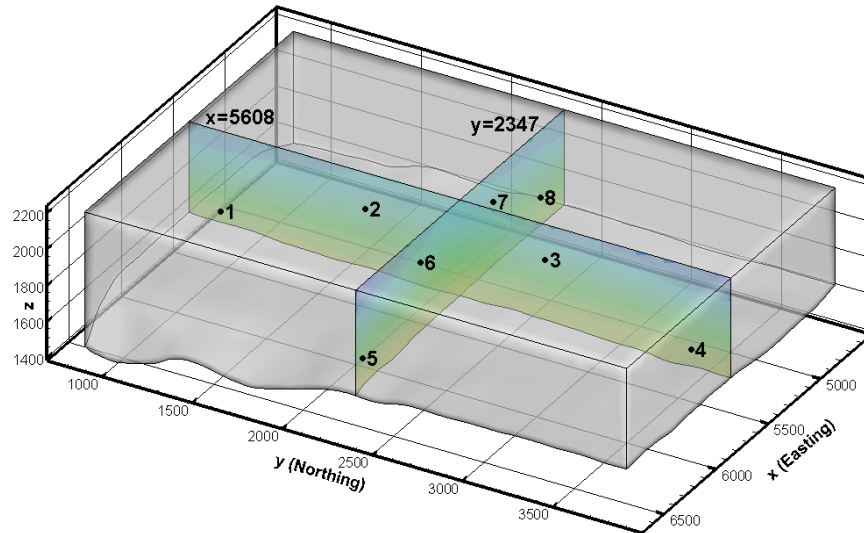
Figure 3.19: Slices in X and Y directions and the locations of comparison points

Table 3.4: Distances from observation point

Point	Easting	Northing	Altitude
1	5608	1047	1741
2	5608	1847	1991
3	5608	2847	1991
4	5608	3647	1741
5	4748	2347	1741
6	5278	2347	1991
7	5938	2347	1991
8	6468	2347	1741

In Figures 3.20 and 3.21 the wind speed difference distributions at mid-sectional cuts, between the WRF and HYP3D predictions are presented in time. In addition, in Figures 3.22 - 3.29, the wind speed variation in time is compared at the specific points given in Figure 3.19.

51
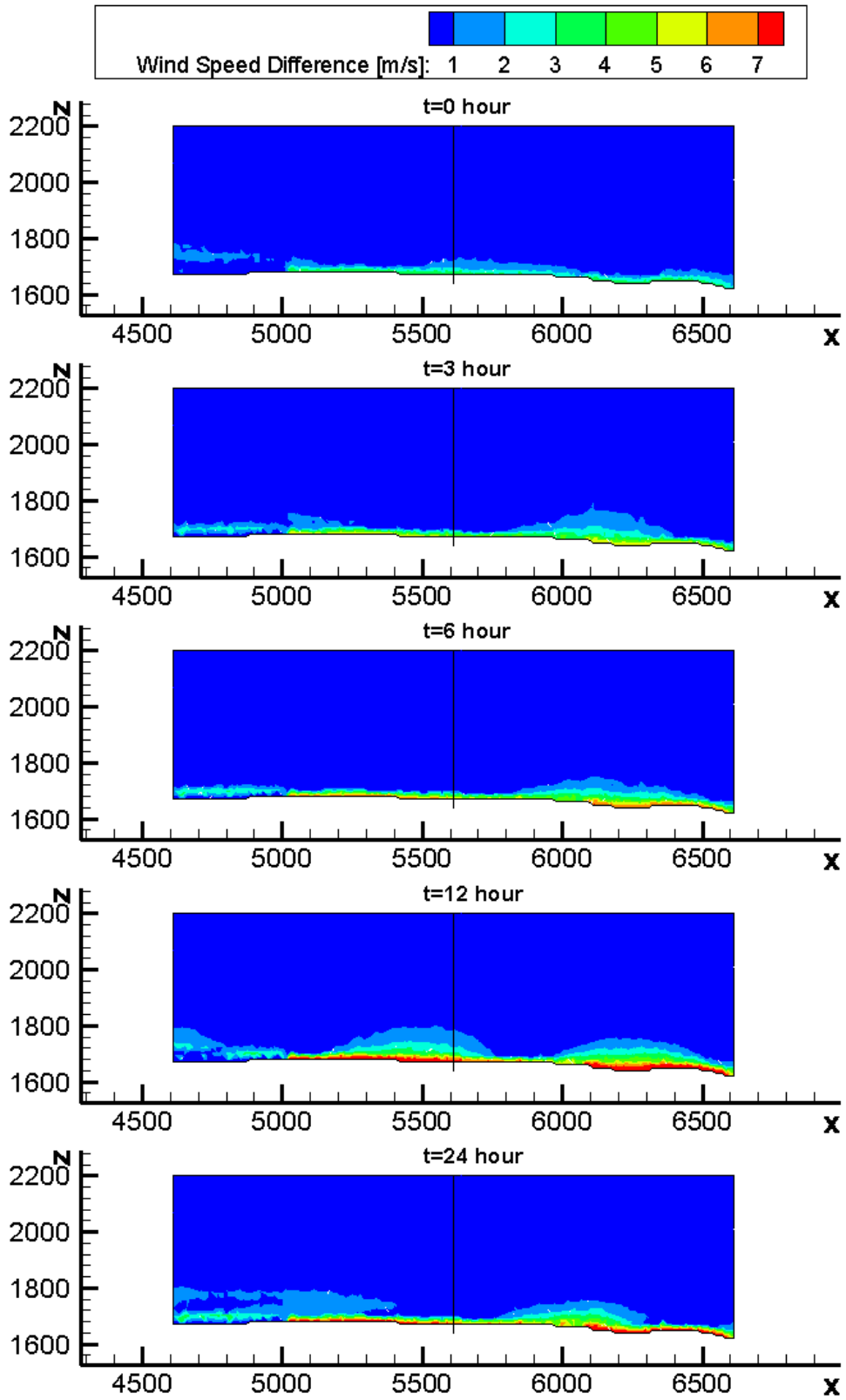
Figure 3.20: Wind speed differences between WRF-HYP3D along Y=2347
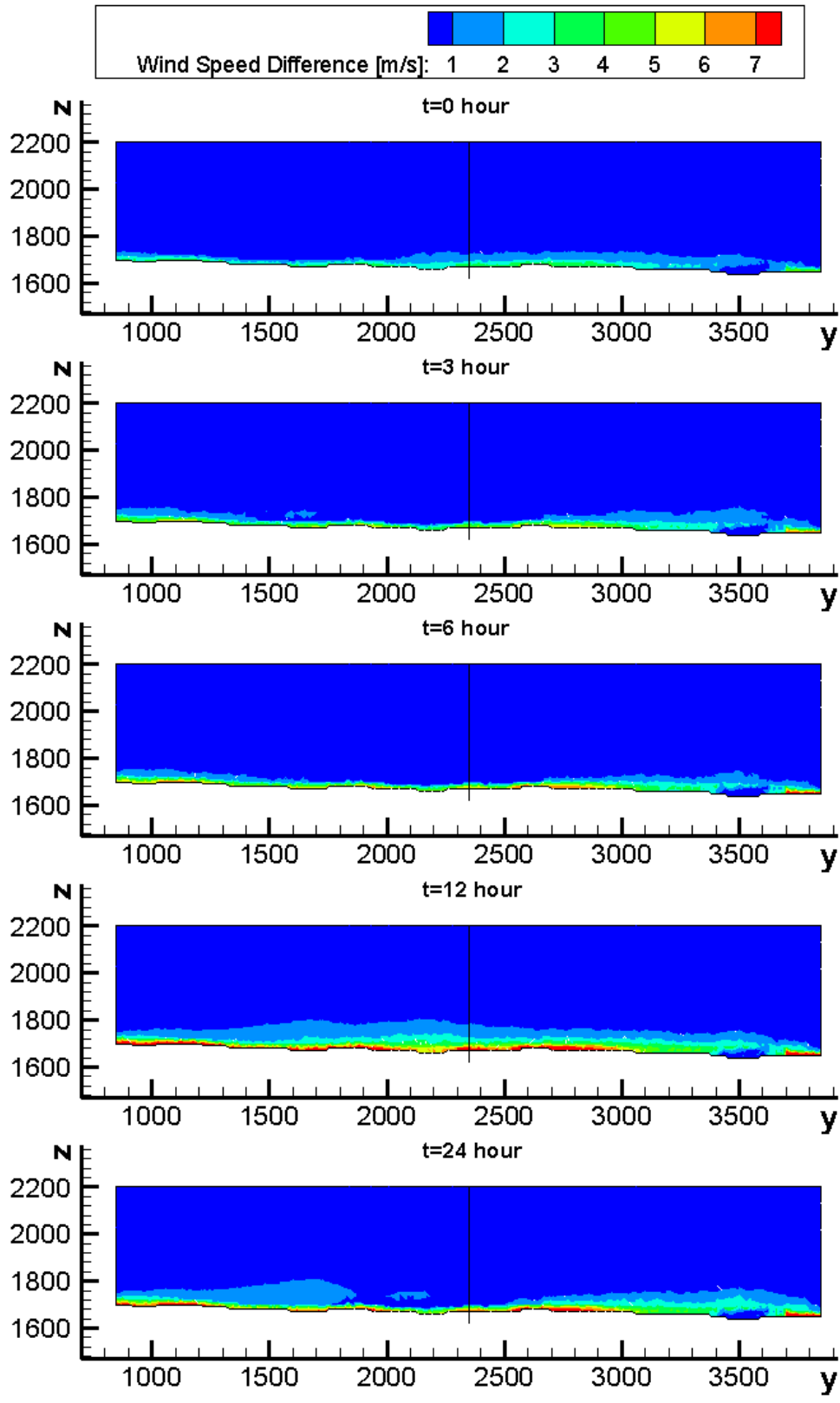
Figure 3.21: Wind speed differences between WRF-HYP3D along X=5608

Based on the results presented above, the agreement between WRF and HYP3D gets better at higher altitudes and the maximum deviation occurs close to the ground as expected.
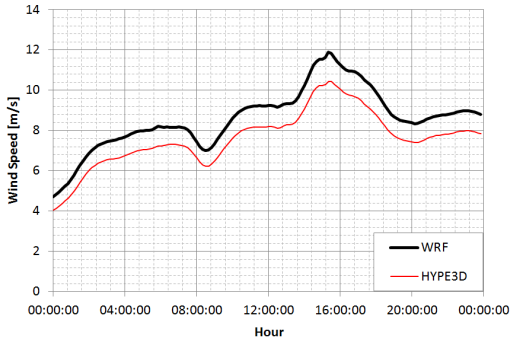
Figure 3.22: Wind speed variation at Point 1
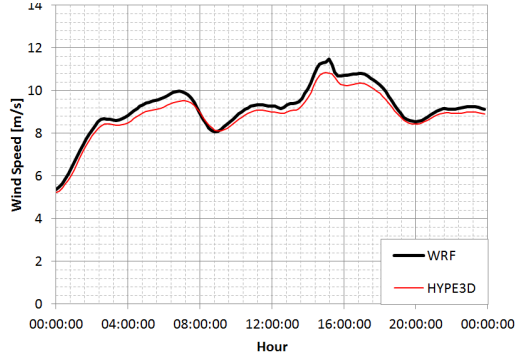
Figure 3.23: Wind speed variation at Point 2
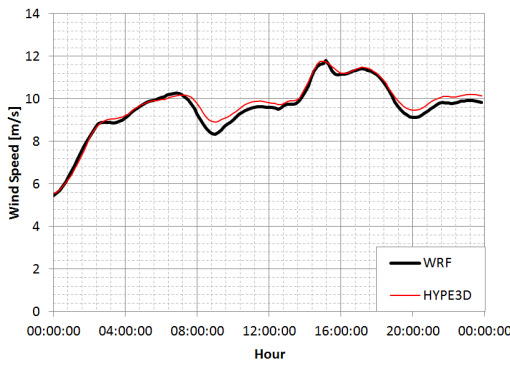
Figure 3.24: Wind speed variation at Point 3
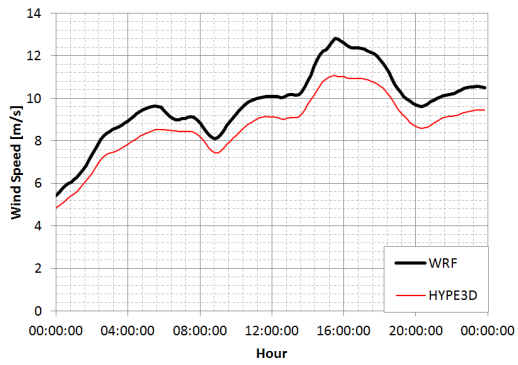
Figure 3.25: Wind speed variation at Point 4
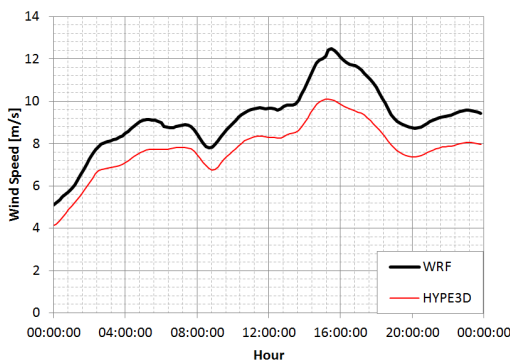
Figure 3.26: Wind speed variation at Point 5
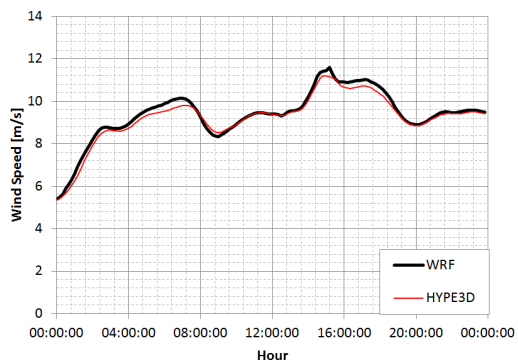
Figure 3.27: Wind speed variation at Point 6
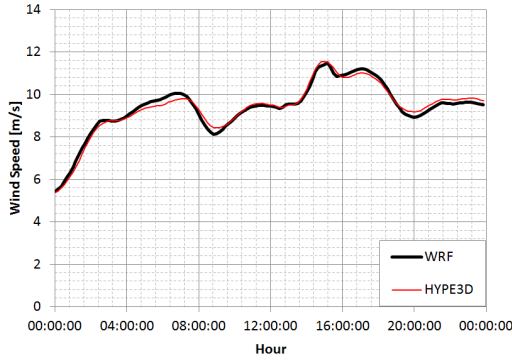
Figure 3.28: Wind speed variation at Point 7
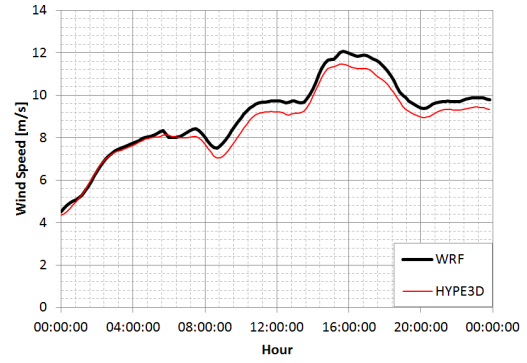
Figure 3.29: Wind speed variation at Point 8

3.6 Annual Wind Assessment Analysis

For an annual wind assessment analysis, unsteady coupled atmospheric flow solutions are performed for one year period for the Mut/Mersin region in Turkey where a wind farm is being constructed and met-mast data for year 2010 are available. The WRF solutions are similarly performed using the data obtained from NCEP (National Centers for Environmental Prediction) Final Analysis (FNL from GFS) (ds083.2 dataset) with 12 monthly solutions. The simulation time is between the date 01.01.2010 and 15.12.2010. The terrain data for the WRF simulations are obtained from UCAR (University Corporation of Atmospheric Research) and simulation is performed with a parent domain of 3 km horizontal resolution and a nest of 1 km resolution where the wind farm is located. The parent and the nested solution domains are of the size 100x79 (horizontal) x 50 (vertical), and 88x67 (horizontal) x 50 (vertical) respectively.

Then, the coupled HYP3D solutions are performed for the same monthly time intervals using the unsteady and the spatially varying boundary conditions extracted from the WRF solution. HYP3D domain is partitioned into 16 subgrids and a monthly solution is obtained in about 10 days on 16 processors.

All results are presented as time series, power density contour, Weibull distribution and wind rose plots.

Variation of the wind speed at the location of the met-mast data (so called virtual met-mast data) is extracted from the solution. The yearly data obtained are compared against observation data for each month in Figures 3.30,3.31,3.32,3.33.

As shown the numerical predictions are, in general, in agreement with the observation data although some deviations occur for some durations along the simulations.
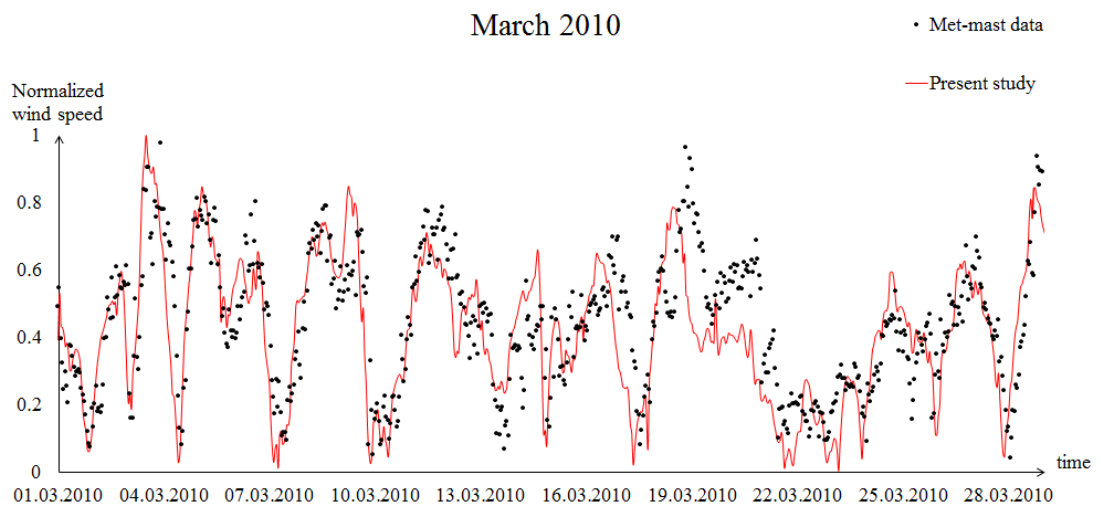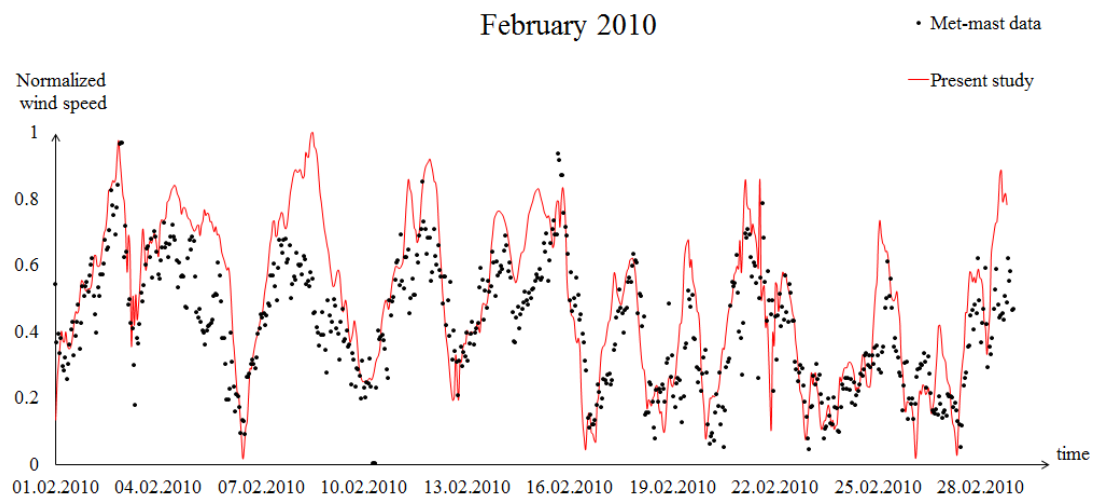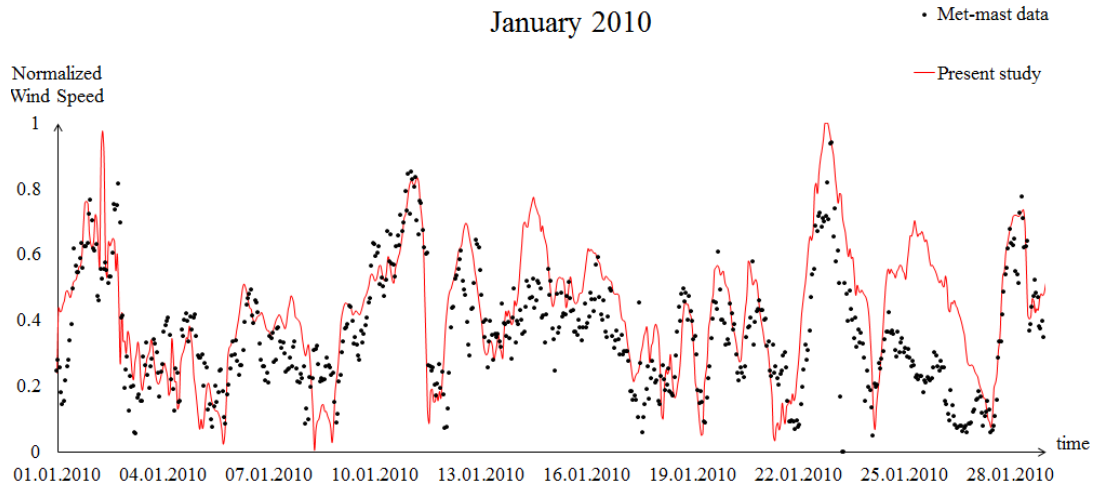
Figure 3.30: Monthly variation of the wind speed (January-March)
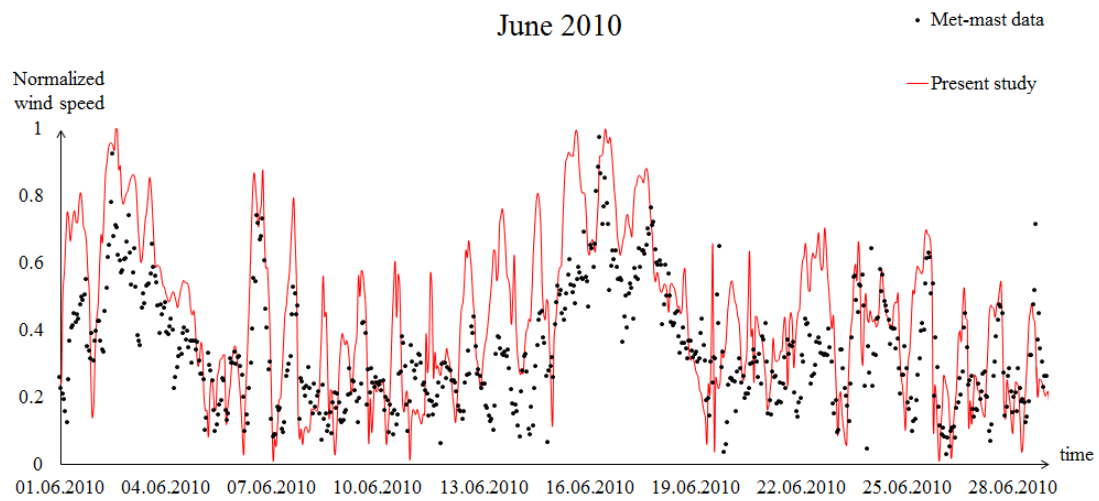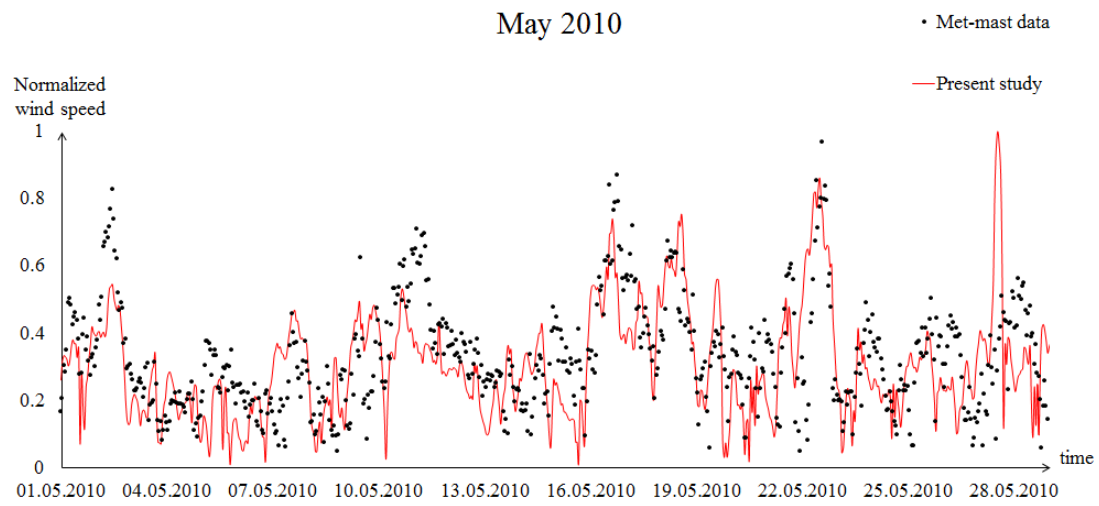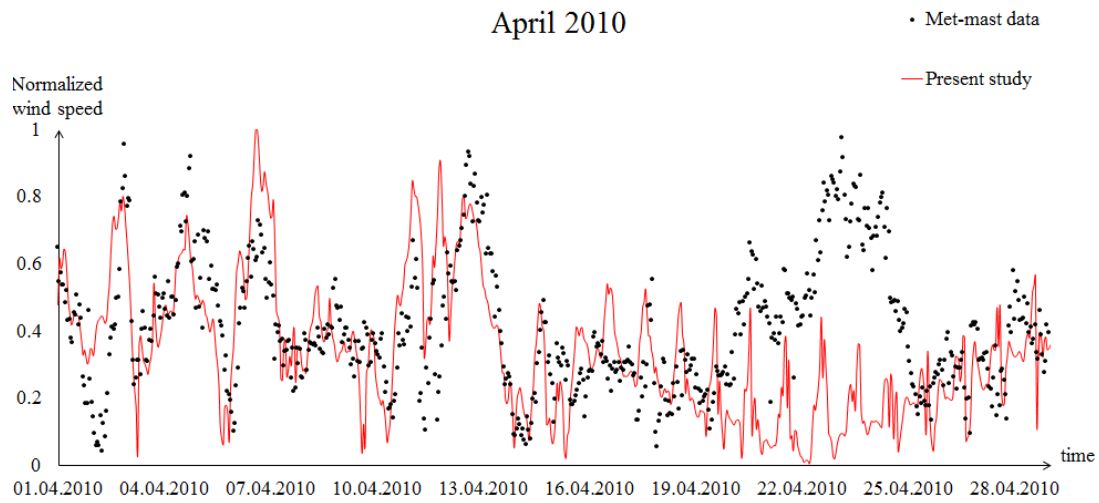
Figure 3.31: Monthly variation of the wind speed (April-June)
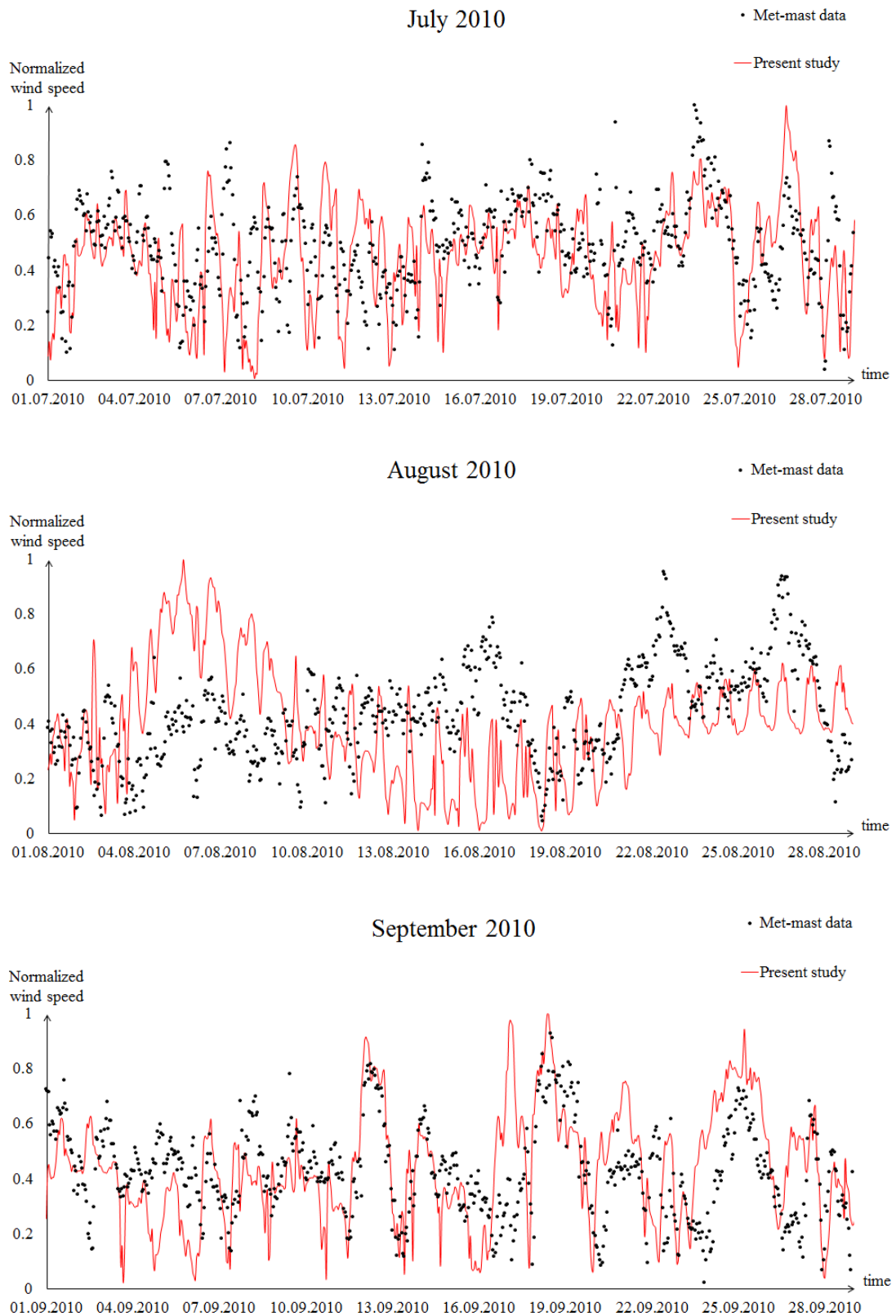
Figure 3.32: Monthly variation of the wind speed (July-September)
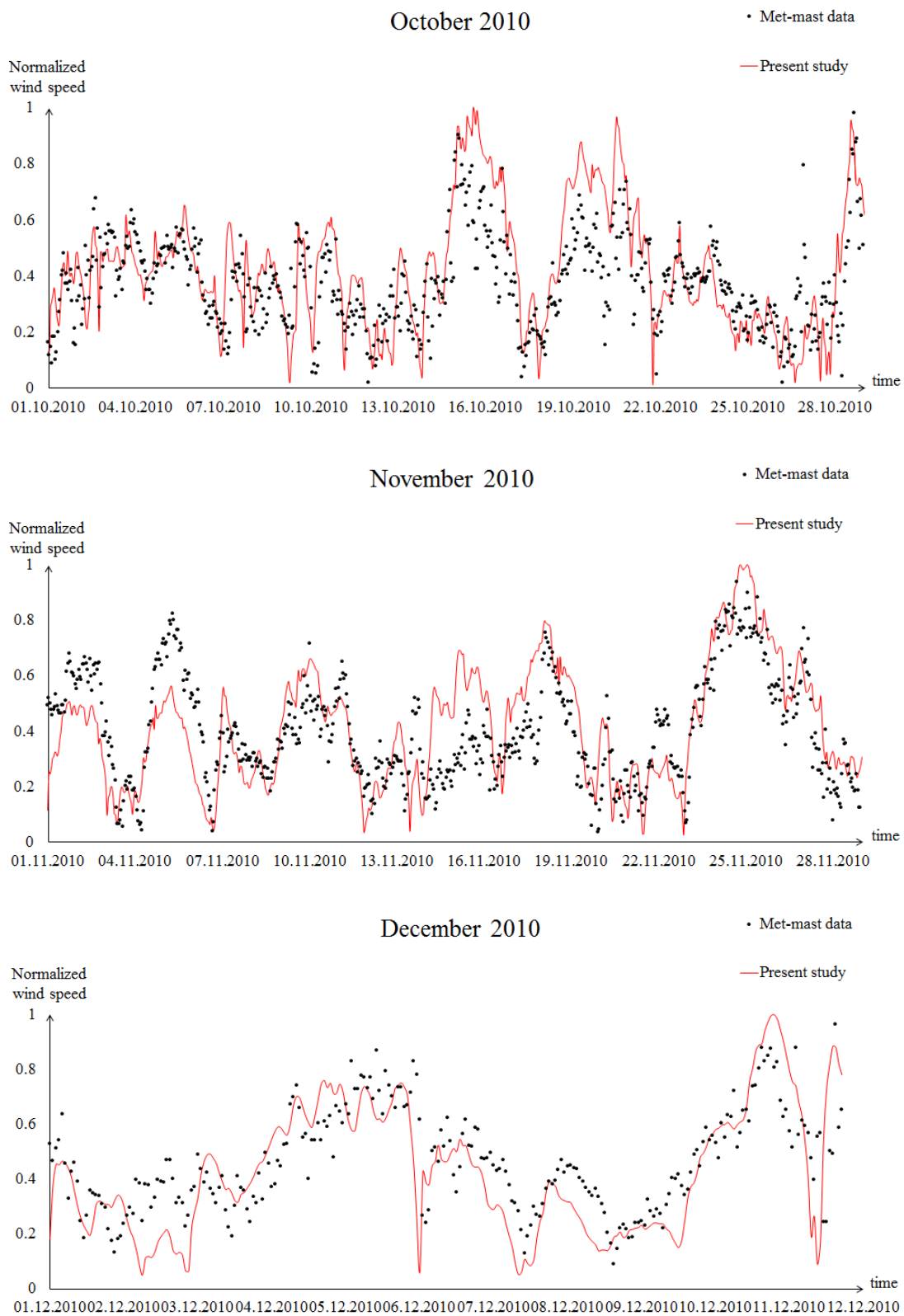
Figure 3.33: Monthly variation of the wind speed (October-December)

3.6.1 Power Density Maps

The atmospheric flow solutions obtained for the year 2010 is then processed to obtain power density maps (Section 2.5) at 80 and 100 meters altitude as shown in Figures 3.34 and 3.35. The North-East corner of the region has the highest wind energy potential. Multiplication of the power density values with a selected turbine blades' swept area, provides the theoretical wind power potential. Taking the betz limit and the turbine efficiency into consideration, instantaneous power production can be estimated roughly by using Figures 3.34 and 3.35.

In Figure 3.36 the power potential difference between 80 meters and 100 meters altitudes is given. It is observed that the north half of the region can provide significantly higher wind energy production at 100 meter altitude than 80 meter altitude. Such an analysis at different altitudes can also be used to providing the best turbine hub height.
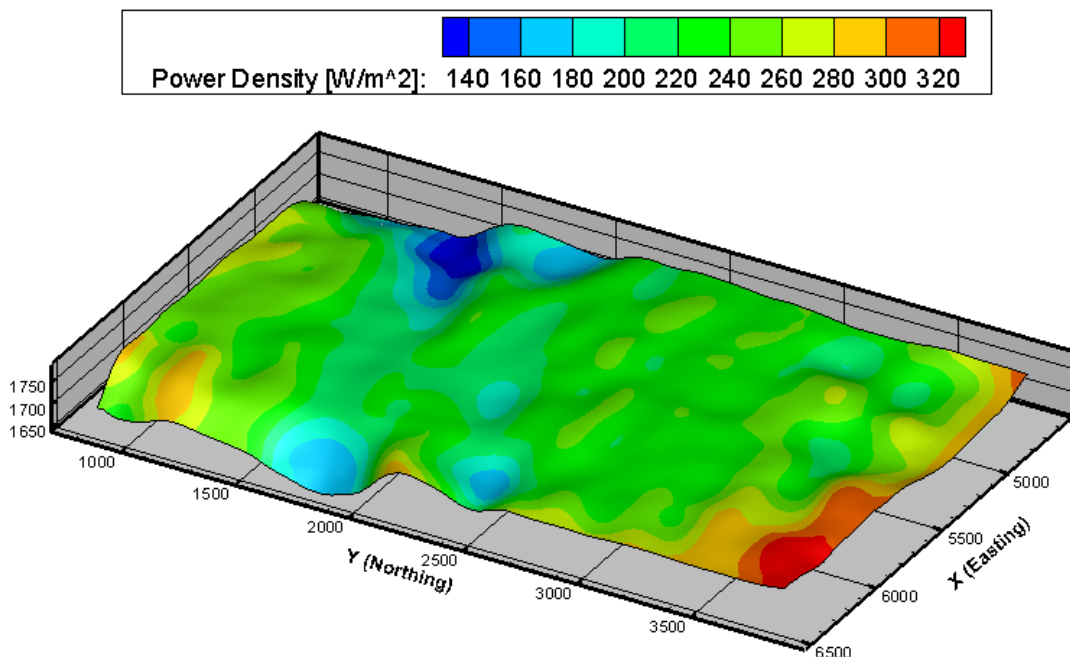
Figure 3.34: Power density distribution at 80m altitude
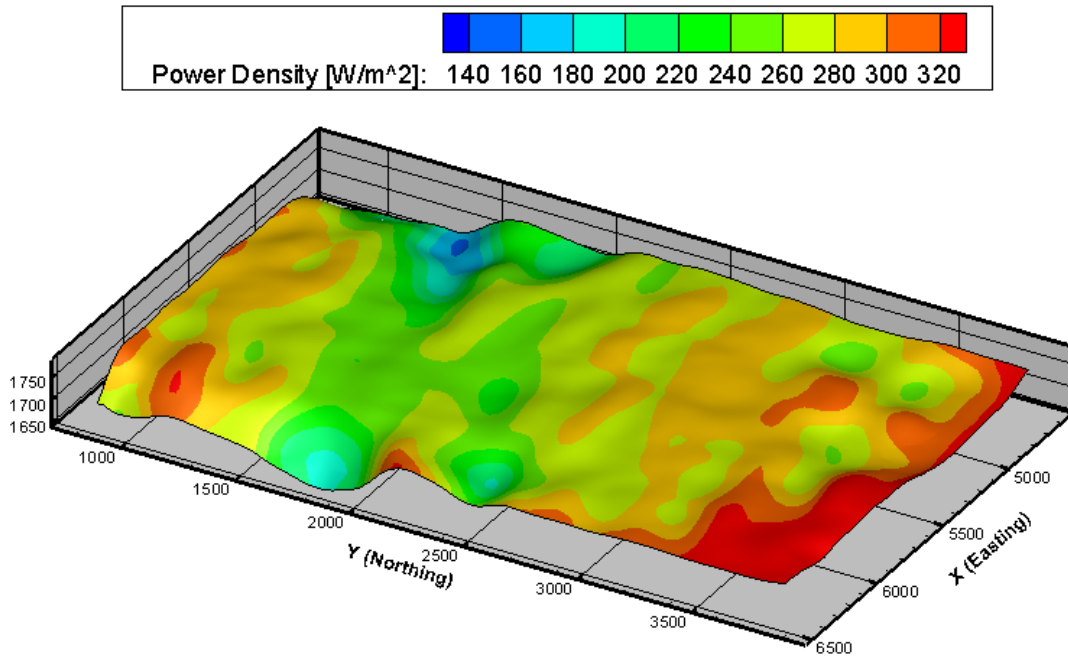
Figure 3.35: Power density distribution at 100m altitude
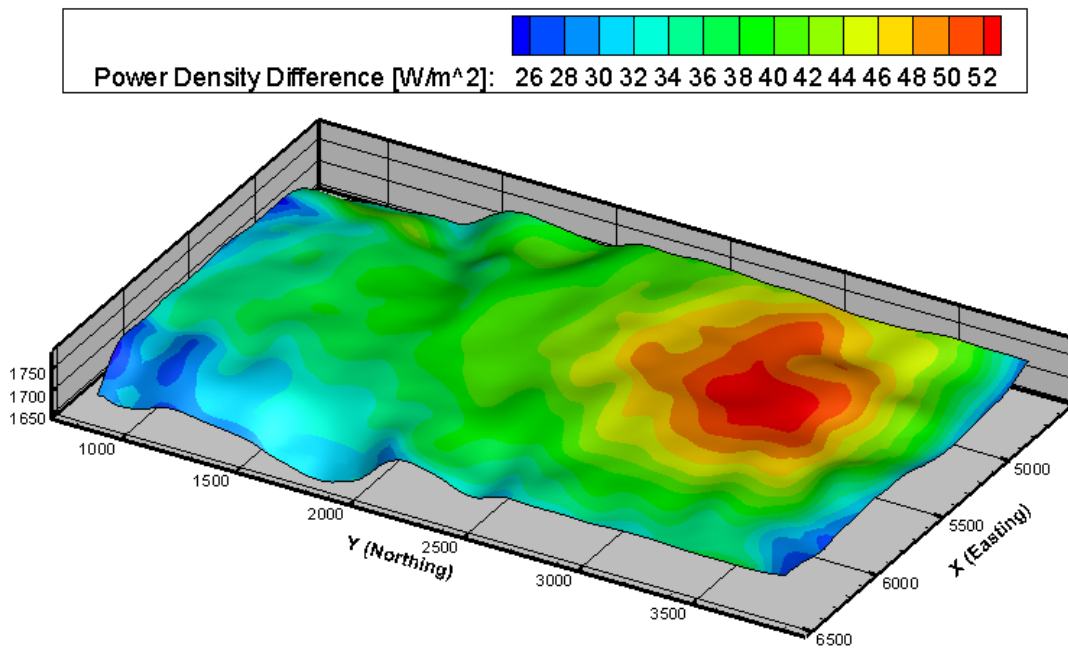
Figure 3.36: Power density distribution difference between 80m and 100m altitude

3.6.2 Weibull Probability Distribution Analysis

Weibull probability function which are defined by shape and scale parameters and the wind rose distributions may be evaluated for any location in the flowfield. Weibull and wind rose distributions provide a valuable statistical information about the wind speed variation. The Weibull and the wind rose distributions are evaluated at the met-mast location using the met-mast data, and the WRF and HYP3D solutions for one year period and are given in Figure 3.37,3.38,3.39. As shown all the solutions are in a general agreement, however HYP3D predictions are in slightly better agreement with the observation data.

Weibull probability function coefficients which are shape (k) and scale (λ) parameters, (Section 2.5.) may be evaluated for every nodes in the flow field by using the 1 year long solution data. λ is related to the most probable average wind speed and; k is indicates the width of the distribution. High values of k indicate a clustered distribution around λ value, whereas low values of k indicate a scattered distribution. The distribution of the the scale and shape parameter at the 80 meters altitude from the ground surface are given In Figures 3.40 and 3.41. In general, for the maximum wind power production at a given location both values should be high.

In order to take these parameters into account a new parameter $k \cdot \lambda^3$ is introduced.(Figure 3.42) Since the wind power is proportional to the cube of wind speed, such a parameter may be a good indicator of the wind energy potential. The $k \cdot \lambda^3$ distribution at 80 meter altitude is given in Figure 3.42. It is observed that in addition to the North-East region, Southern part of the region has high values of $k \cdot \lambda^3$, which should also be considered for a possible site of a wind turbine.
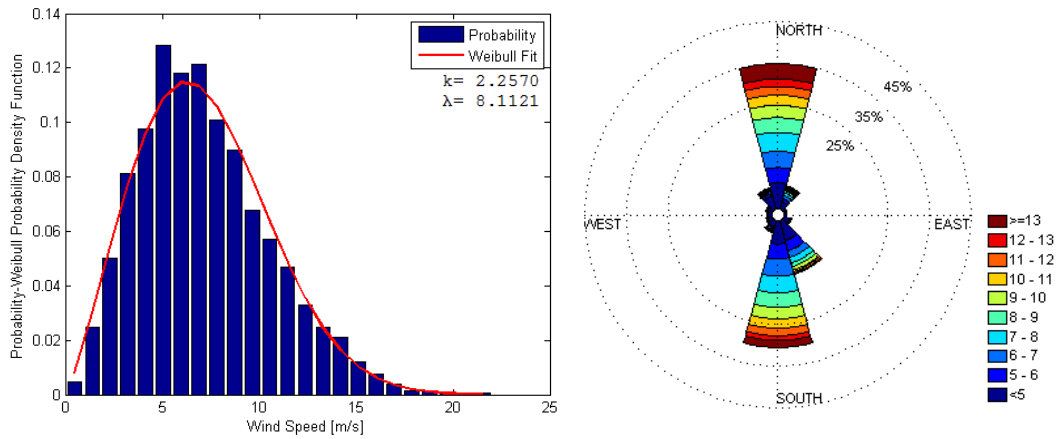
Figure 3.37: Weibull and wind rose distributions for measurements
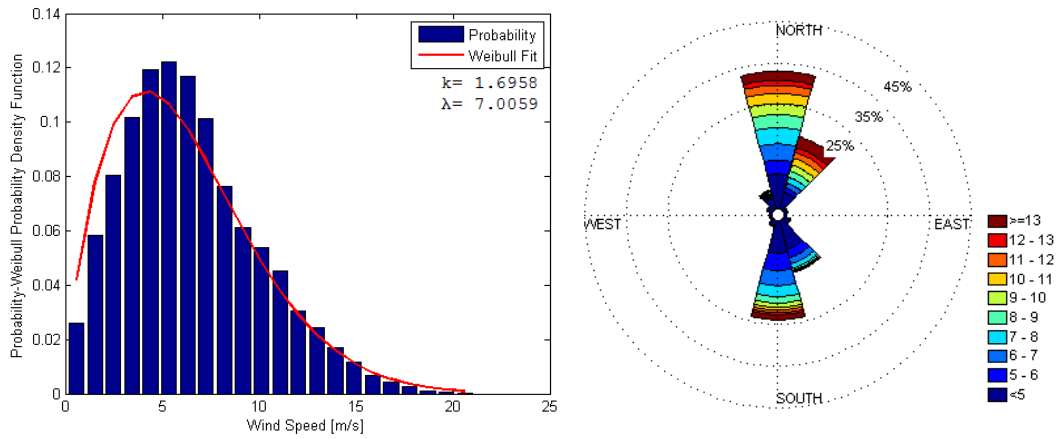
Figure 3.38: Weibull and wind rose distributions for WRF
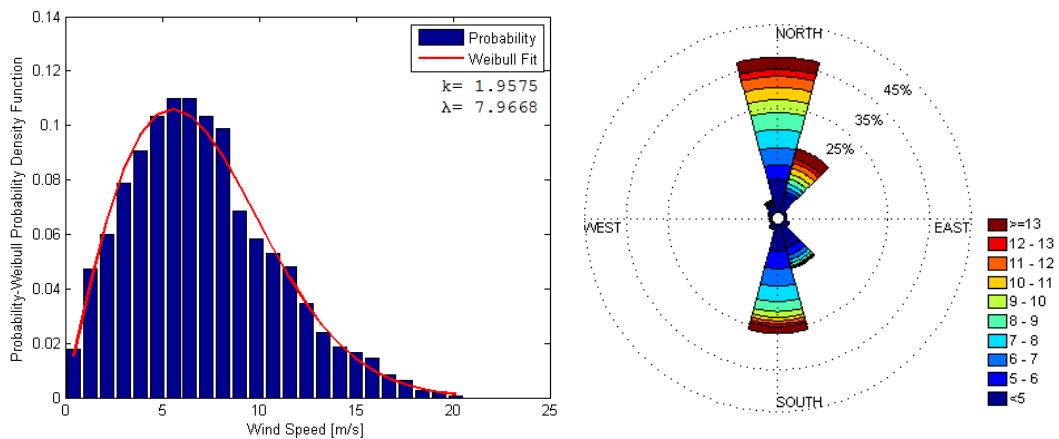
Figure 3.39: Weibull and wind rose distributions for WRF-HYP3D Coupling
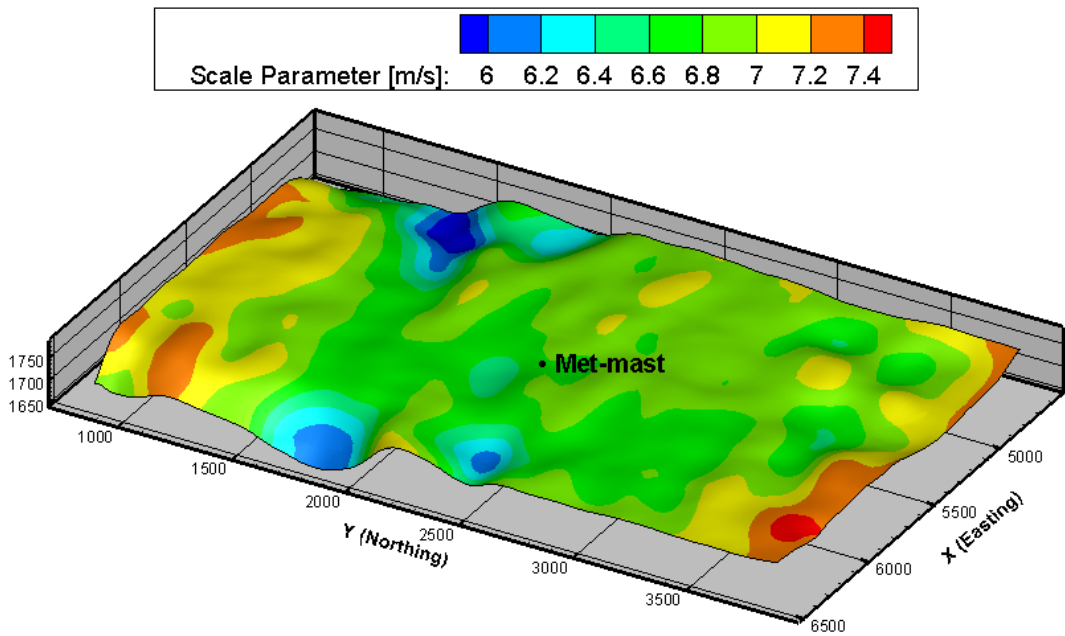
Figure 3.40: Scale parameter distribution at 80m altitude
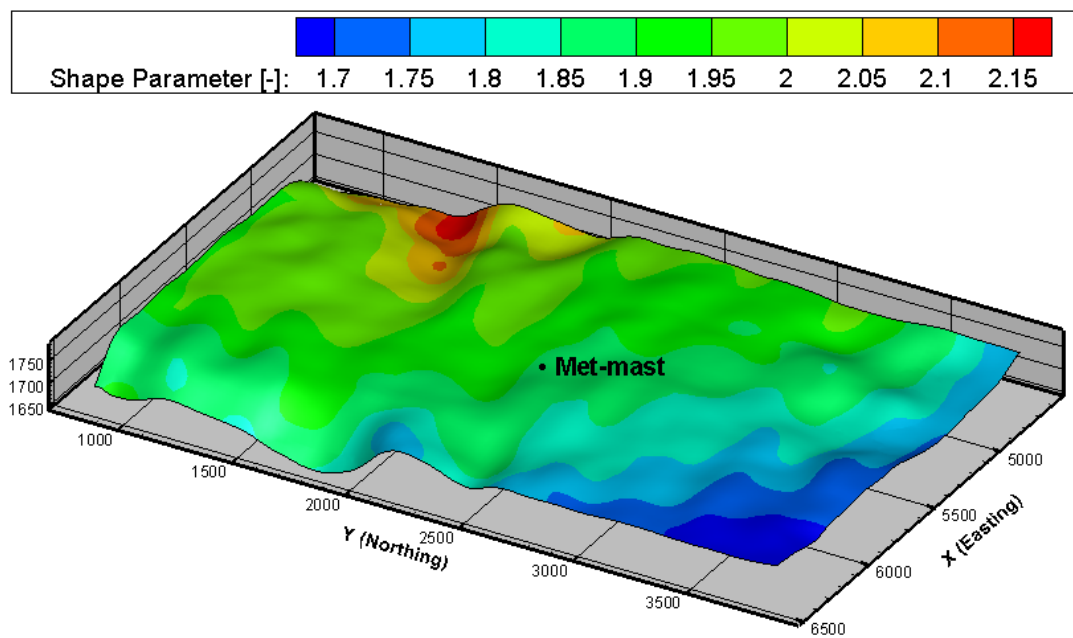
Figure 3.41: Shape parameter distribution at 80m altitude
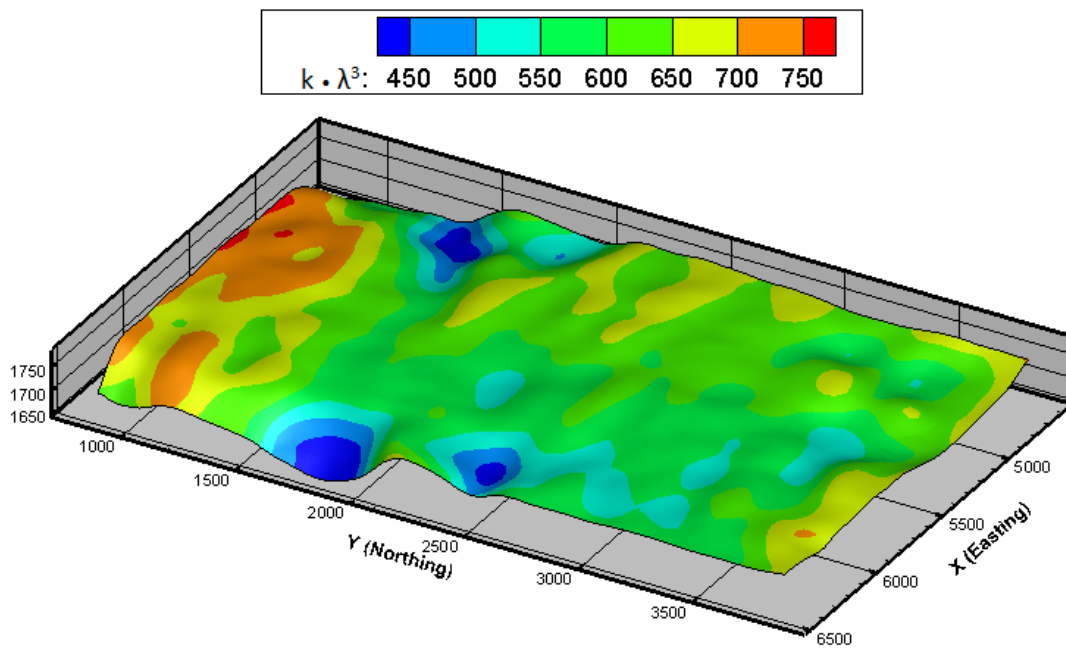
Figure 3.42: Distribution of $k \cdot \lambda^3$ at 80 meter altitude

3.6.3 Annual Energy Production Estimation

The annual energy production estimation for a location at a given altitude can be obtained using Weibull distribution and the power curve of a given wind turbine. In this study two typical 2MW wind turbines are considered. Their power curves are given in Figure 3.43. As shown, "Turbine A" is more efficient at low speeds. The power density distribution at 80 meters altitude is given in Figure 3.44. In addition $k \cdot \lambda^3$ distribution is also given in Figure 3.45. Based on these distributions the maximum annual energy production locations are identified as Point 1 and Point 2. Point 2 is located in a region where the power density is maximum. Whereas Point 1 is located in a region where $k \cdot \lambda^3$ is maximum. The wind speed probabilities, the corresponding Weibull fit curves, Weibull parameters and the wind rose distributions for Point 1 and 2 are shown in Figures 3.46 and 3.47, respectively. Although power density for Point 2 ($341W/m^2$) is higher than that of Point 1 ($266W/m^2$), $k\lambda^3$ value of Point 2 ($928m^3/s^3$) is lower than that of Point 1 ($1040m^3/s^3$).
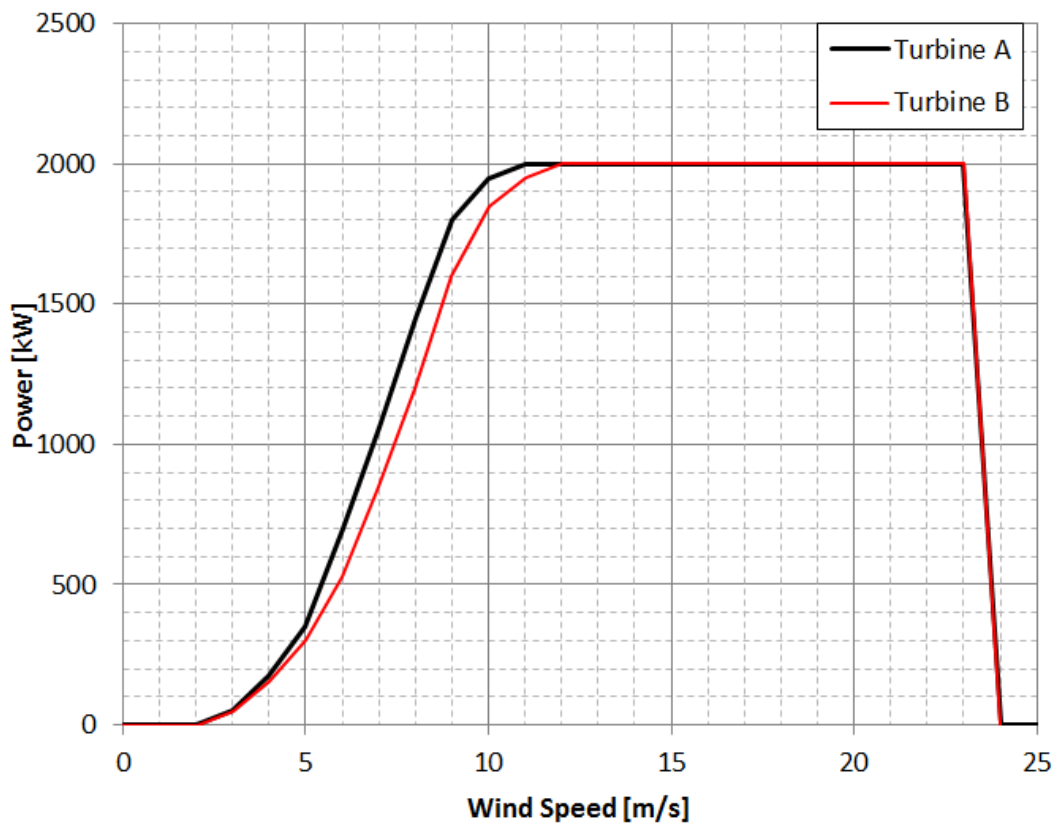
Figure 3.43: Power curves of Turbine A and Turbine B
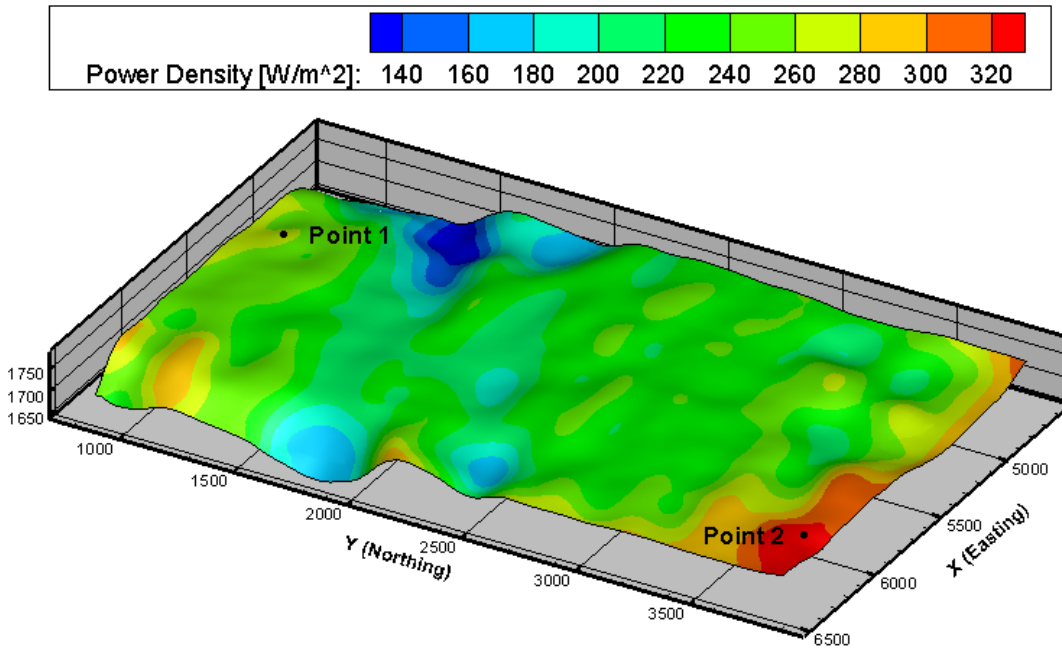
Figure 3.44: Location of selected points on power density distribution
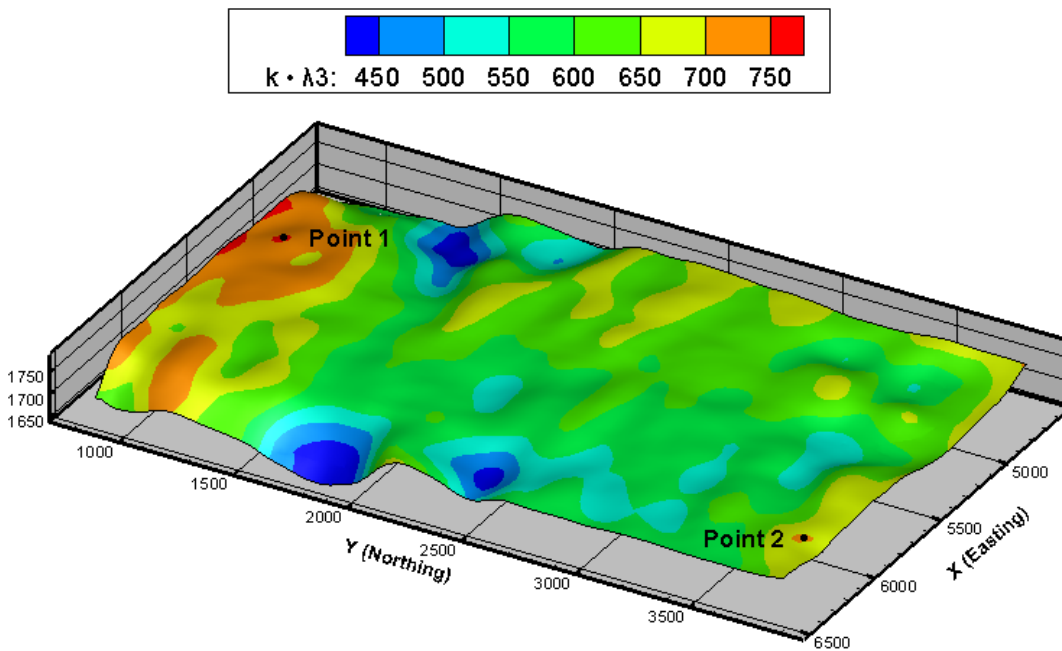
Figure 3.45: Location of selected points on $k\lambda^3$ distribution

Mean power productions and annual energy production estimations (AEP) are evaluated for the "Turbine A" and "Turbine B" at locations 1 and 2 using the wind speed probabilities and the power curves associated with the each turbine. The evaluated values are presented in the Table 3.5. It is observed that, Turbine A produces the maximum power at the both locations. However Turbine B

produces the maximum power at Point 2 where the power density distribution is low but $k \cdot \lambda^3$ value is high.
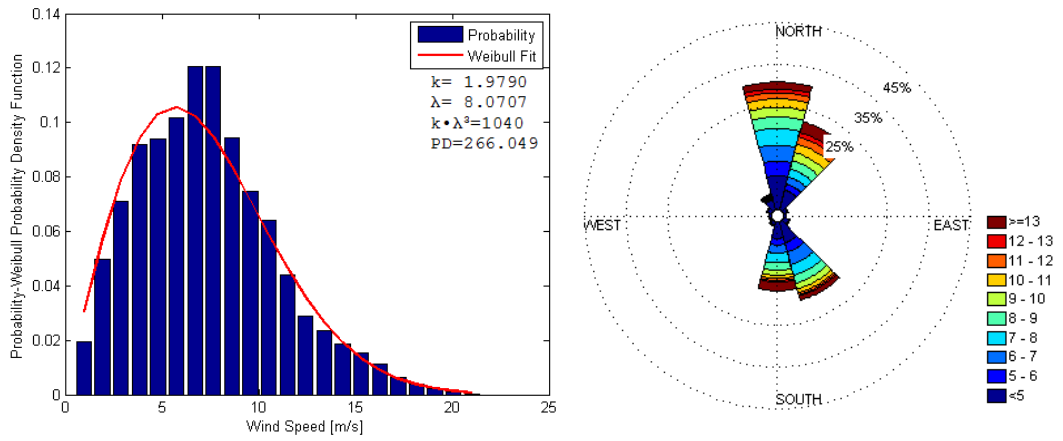
Figure 3.46: Weibull and wind rose distributions for Point 1
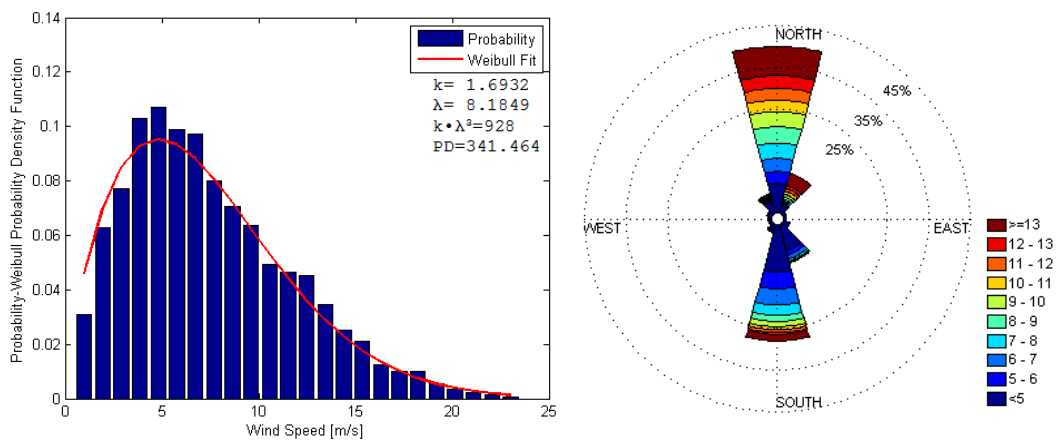
Figure 3.47: Weibull and wind rose distributions for Point 2

Table 3.5: Mean Power of Turbines and Annual Energy Productions (AEP)

Model	Location	Power Density [W/m2]	$k\lambda^3$	Mean Power [KW]	AEP [MWh/y]
Turbine A	**Point 1**	266.049	**1040**	**923.32**	**8088**
	Point 2	341.464	928	907.14	7946
Turbine B	Point 1	266.049	1040	828.84	7260
	Point 2	**341.464**	928	**833.47**	**7301**

These results support the significance of $k \cdot \lambda^3$ in micro-siting of wind turbines. It may also be concluded that power curves of the turbines should be considered for micro-siting. Such a need can be satisfied with the evaluation of the turbine specific annual energy production estimation maps which are presented in Figures 3.48 and 3.49. Based on these distributions the best locations for each turbine can easily be identified.
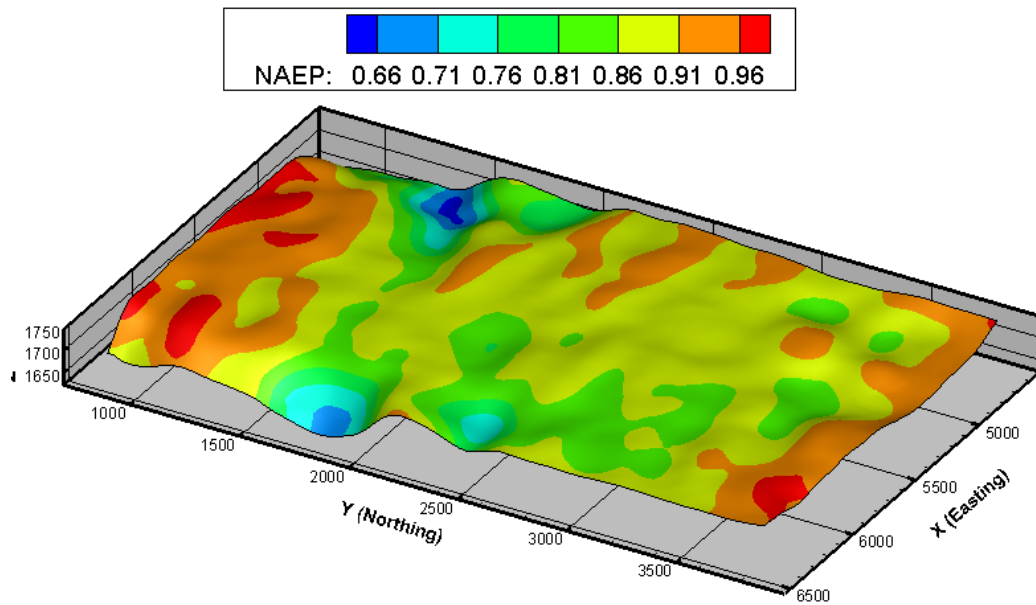
Figure 3.48: Turbine specific Normalized Annual Energy Production for "Turbine A"
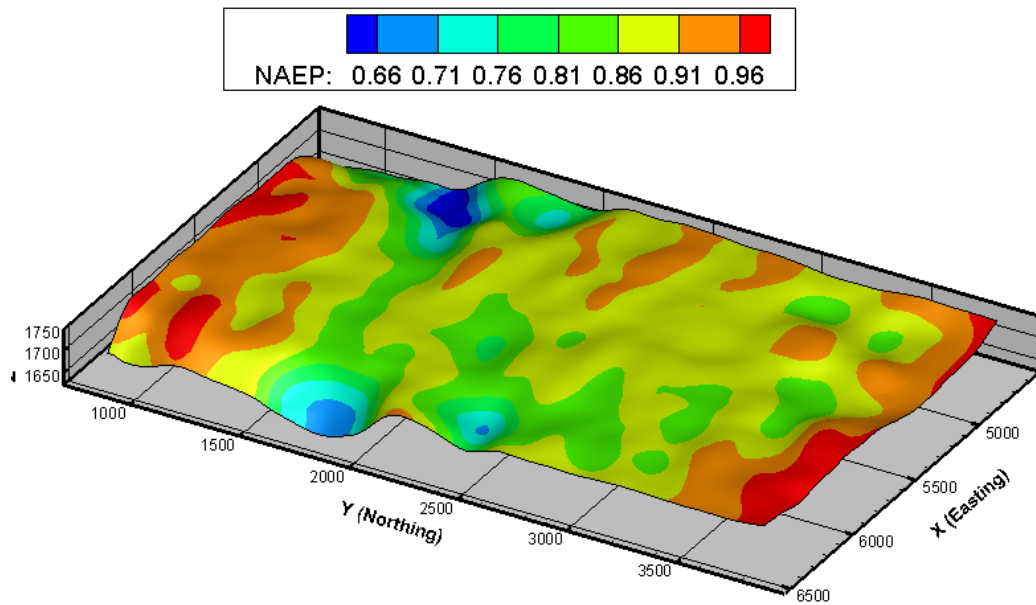
Figure 3.49: Turbine specific Normalized Annual Energy Production for "Turbine B"

CHAPTER 4

CONCLUDING REMARKS

Atmospheric flow solutions for 1 year duration are computed using an in-house, parallelized 3 dimensional Navier-Stokes solver HYP3D coupled with a meso-scale meteorological weather prediction software WRF and the wind power potential of a specific area is assessed. The main steps of the study performed can be summarized as follows;

- For 1 year numerical atmospheric meso scale simulation, initial and boundary conditions of WRF is obtained from the NCEP Final Analysis dataset.

- Solution domain for numerical weather prediction software WRF is created and solved in 12 separate cases. Each case corresponds one of the month of a year and each of them is solved in parallel environment.

- High resolution terrain data is generated by using ASTER GDEM dataset and various structured/unstructured/hybrid grids are created by using GAMBIT.

- Data mining tools which can extract the flow variables in a location in the solution domain is developed.

- Implementation of boundary conditions and data interaction routines between parallel partitions of HYP3D are modified and improved for time and spatially varying boundary condition utilization. Also statistical data collection routines for wind speed and direction are written for the post-process of the simulation.

- Parallel performance assessment with speedup/efficiency plots and validation of Navier stokes solver HYP3D are performed.

- By means of data mining tools developed in the study, boundary conditions of HYP3D for 1 year duration simulation is created from the WRF results.

- Navier-Stokes solver with Spalart-Allmaras turbulence model HYP3D is run for 12 separate cases. Again each case corresponds one of the month of a year and each of them is solved in parallel environment.

- From the WRF and HYP3D results wind speed time series data are extracted with data mining tools. Then all results are compared against observations provided from the real met-mast.

- Power density distributions for different altitudes are obtained and compared with each other.

- Wind Rose and Weibull probability distribution analysis is done for the whole domain and alternative turbine locations are researched.

- Annual energy production estimation is performed for two different turbine models and best locations are searched for these turbines.

- Turbine model based annual energy production maps are presented for the whole region.

Implementing introduced methodologies, several analysis performed for different aspects of the study. HYP3D Navier Stokes solver is first validated with turbulent and laminar flow over a flat plate simulations. Created case is explained in detail and the results are presented. Sub-layers of turbulent boundary layer and surface skin friction coefficient are compared with the theoretical values and their consistency is presented.

Boundary layer profiles for newly introduced shifting and stretching approaches in the thesis study are compared and results are discussed. The superiority of the stretching approach over shifting approach is explained.

Several structured, unstructured and hybrid grids are created and results are compared against WRF results and also the observations. Differences from observations are quantitatively compared in root mean square deviation form and tabulated clearly.

For the selected points and surface cuts along easting and northing directions, the wind speed differences between WRF results and WRF-HYP3D coupling results are presented. It is shown that the highest differences between the results can be seen around the near surface regions and for the higher altitudes, this difference disappears.

1-year simulation results of HYP3D are presented monthly as a comparison with observations. It is shown that the results are quite in agreement with the observation data.

Power density maps for 80 meters and 100 meters altitude from the ground surface are generated and power density difference distribution between these surfaces is depicted. The critical areas are shown in contour plots.

For the Weibull probability distribution, shape and scale parameters at the all nodes in the flowfield is calculated and at a specific height above the ground, distributions of these parameters are plotted. Probabilities of the different wind speed bins, Weibull fit curves and wind roses for the chosen locations are presented. A new indicator which is a combination of Weibull parameters is introduced as $k \cdot \lambda^3$. Using this parameter new hot spots are investigated.

With the help of power curves of two different turbine models, annual energy production estimations are performed for the whole solution domain. Using these distributions most effective areas for a specific turbine are presented.

As a future work, atmospheric stability and different turbulence models may be added to the Navier-Stokes solver. Wake effects of individual turbines, and canopy models of corresponding terrain may be modelled. Long term correlations with the 40-year reanalysis data may be applied to the results.

REFERENCES

[1] Meteorology Glossary, American Meteorological Society. `http://glossary.ametsoc.org/wiki/Monin-obukhov_similarity_theory`. Accessed: 2014-06-25.

[2] NASA, Langley Research Center, turbulence modeling resource. `http://turbmodels.larc.nasa.gov/flatplate_sst.html`. Accessed: 2014-06-30.

[3] Tecplot 360 software. `http://www.tecplot.com/products/tecplot-360/`. Accessed: 2014-06-29.

[4] G. Ahmet, E. Leblebici, and I. H. Tuncer. Terrain fitted turbulent flow solutions coupled with a mesoscale weather prediction model. Visby, Sweden, Sept 18-20, 2013. EAWE 9th PhD Seminar on Wind Energy in Europe.

[5] G. Botta, R. Castagna, M.Borghetti, and D.Mantegna. Wind analysis on complex terrain - the case of acqua spruzza. *Jour. Wind Eng. Ind. Aerodyn*, 39:357–66, 1992.

[6] A. J. Bowen and N. G. Mortensen. Wasp prediction errors due to site orography. Denmark, 2004. Risø National Laboratory.

[7] A. J. Bowen and T. Saba. The evaluation of software for wind turbine siting in hilly terrain. New Delhi, India., 1995. 9th International Conference on Wind Engineering.

[8] B. C. Cochran and R. R. Damiani. Harvesting wind power from tall buildings. Houston, Texas, 2008. WindPower 2008.

[9] R. G. Derickson and J. A. Peterka. Development of a powerful hybrid tool for evaluating wind power in complex terrain: Atmospheric numerical models and wind tunnels. Reno, Nevada, January 2004. 42nd AIAA Aerospace Sciences Meeting and Exhibit.

[10] F. R. Eldridge. *Wind Machines*. The MITRE Energy Resources and Environment Series, Von Nostrand Reinhold Company N.Y. USA, 1980.

[11] P. Gipe. *Wind Power Renewable Energy for Home, Farm, and Business*. Chelsea Green Publishing Company, White River Junction, Vermont,USA,

2004.

[12] D. Heinemann. Wind flow modelling - the bases for resource assessment and wind power forecasting. Oldenburg,Germany. ForWind Center for Wind Energy Research Energy Meteorology Unit, Presentation.

[13] T. Hiester and W. Pennell. *The meteorological aspects of siting large wind turbines.* Report NO: PNL-2522, Pacific Northwest Laboratories, Richland,WA, 1981.

[14] J. R. Holton and G. J. Hakim. *An introduction to dynamic meteorology.* Academic press, 2013.

[15] P. Jackson and J. Hunt. Turbulent wind flow over a low hill. *Q. J. Roy. Meteorol. Soc.*, 101:929–955, 1975.

[16] H.-M. H. Juang. A spectral fully compressible nonhydrostatic mesoscale model in hydrostatic sigma coordinates: Formulation and preliminary results. *Meteorology and Atmospheric Physics*, 50(1-3):75–88, 1992.

[17] G. Karypis and V. Kumar. A fast and highly quality multilevel scheme for partitioning irregular graphs. In *SIAM Journal on Scientific Computing*, volume 20, page 359—392, 1999.

[18] E. Leblebici, G. Ahmet, and I. H. Tuncer. Atmospheric turbulent flow solutions coupled with a mesoscale weather prediction model. Kos Island Greece, 2013. Eccomas special Interest Conference,3rd South-East European Conference on Computational Mechanics.

[19] E. Leblebici, G. Ahmet, and I. H. Tuncer. Unsteady atmospheric turbulent flow solutions coupled with a mesoscale weather prediction model. METU, Ankara, Turkey, Oct. 3-4, 2013. RUZGEM'2013 Conference on Wind Energy Science and Technology.

[20] E. Leblebici, G. Ahmet, and I. H. Tuncer. Atmospheric turbulent flow solutions coupled with a mesoscale weather prediction model. Oldenburg, Germany, Oct.9-11 , 2012. EAWE 4th Scientific Conference; The Science of Making Torque from Wind.

[21] E. Leblebici, G. Ahmet, and I. H. Tuncer. Terrain modeling and atmospheric turbulent flow solutions based on meteorological weather forecast data. METU, Ankara, Turkey, Sep. 14-16, 2011. 6th Ankara International Aerospace Conference.

[22] E. Leblebici, G. Ahmet, and I. H. Tuncer. Wind potential estimations based on unsteady turbulent flow solutions coupled with a mesoscale weather prediction model. METU, Ankara, Turkey, Sept. 11-13, 2013. 7th Ankara

International Aerospace Conference.

[23] D. Lindley, P. Musgrove, J. Warren, and R. Hoskin. Operating experience from four uk wind farms. York, UK, 1993. 15th BWEA Annual Wind Energy Conference.

[24] Y. Liu, T. Warner, Y. Liu, C. Vincent, W. Wu, B. Mahoney, S. Swerdlin, K. Parks, and J. Boehnert. Simultaneous nested modeling from the synoptic scale to the les scale for wind energy applications. *Journal of Wind Engineering and Industrial Aerodynamics*, 99(4):308–319, 2011.

[25] J. F. Manwell, J. G. McGowan, and A. L. Rogers. *Wind Energy Explained Theory, Design and Application*. John Wiley and Sons LTD., Chichester, UK, 1988.

[26] Ömer Emre Orhan and G. Ahmet. A comparative study of virtual and operational met mast data. Copenhagen, Denmark, June. 18-20, 2014. EAWE 5th Scientific Conference; The Science of Making Torque from Wind.

[27] N. G. Mortensen, D. N. Heathfield, L. Myllerup, L. Landberg, and O. Rathmann. Getting started with wasp 9. Roskilde, Denmark, June 2007. Risø National Laboratory.

[28] D. Morton, O. Nudson, D. Bahls, and G. Newby. Pushing wrf to its computational limits. `http://weather.arsc.edu/Events/AWS10/Presentations/MortonBenchmark.pdf`. Accessed: 2014-06-06.

[29] N.A.Phillips. A coordinate system having some special advantages for numerical forecasting. *Journal of Meteorology*, 14:184–185, April 1957.

[30] T. R. Oke. *Boundary layer climates*, volume 5. Psychology Press, 1987.

[31] E. S. Politis and P. K. Chaviaropoulos. Micrositing and classification of wind turbines in complex terrain. Belgium, 2008. WindPower 2008.

[32] S. J. Reid. Modelling of channelled winds. pages 391–6, Warwick, UK, July 1995. BWEA Conference.

[33] A. Sathe and W. Bierbooms. Influence of different wind profiles due to varying atmospheric stability on the fatigue life of wind turbines. In *Journal of Physics: Conference Series*, volume 75, page 012056. IOP Publishing, 2007.

[34] A. M. Sempreviva, I. Troen, and A. Lavagnini. Modelling of wind power potential in sardinia. Rome Italy, October 1986. European Wind Energy Association Conference and Exhibition.

[35] W. C. Skamarock, J. B. Klemp, J. Dudhia, D. O. Gill, D. M. Barker, W. Wang, and J. G. Powers. A description of the advanced research wrf version 2. Technical report, DTIC Document, 2005.

[36] J. F. Walker and N. Jenkins. *Wind Energy Technology.* John Wiley and Sons LTD., Chichester, UK., 1997.

[37] W. Wang, C. Bruyere, M. Duda, J. Dudhia, D. Gill, H. Lin, J. Michalakes, S. Rizvi, X. Zhang, J. Beezley, et al. Arw version 3 modeling system user's guide. mesoscale & miscroscale meteorology division. *National Center for Atmospheric Research (July 2010), http://www. mmm. ucar. edu/wrf/users/docs/user_ guide_ V3/ARWUsersGuideV3. pdf,* 2010.

[38] F. J. Zajaczkowski, S. E. Haupt, and K. J. Schmehl. A preliminary study of assimilating numerical weather prediction data into computational fluid dynamics models for wind prediction. *Journal of Wind Engineering and Industrial Aerodynamics,* 99(4):320–329, 2011.

CURRICULUM VITAE

CONTACT INFORMATION	Department of Aerospace Eng. Middle East Technical University Havacılık ve Uzay Müh.Bölümü ODTÜ Çankaya/ANKARA 06800 Türkiye	*Mobile:* 0505-6020386 *Work:* 0312-2107449 *Fax:* 0312-2104250 *E-mail:* gahmet@ae.metu.edu.tr *Web:* www.gokhanahmet.com

CITIZENSHIP   Republic of Turkey, Turkish Republic of Northern Cyprus

RESEARCH INTERESTS   Wind Assessment, Computational Fluid Dynamics, Wind Energy, Numerical Weather Forecast, Data Assimilation, Parallel Computing

EDUCATION   **Middle East Technical University**, Ankara, TURKEY

Ph.D., Aerospace Engineering, **September 2005 to present**
- Area of Study: *Wind Assessment, Computational Fluid Dynamics*
- Thesis Topic: *Wind Farm Site Selection Using Weather Forecast Software and Navier-Stokes Solver*
- Qualification Exam: *Aerodynamics, Aerothermodynamics and Propulsion*, December 2010
- (CGPA: 3.57/4.00)
- Adviser: Prof.Dr.İsmail H. TUNCER

Eskişehir Osmangazi University, Eskişehir, TURKEY

B.S., Mechanical Engineering, June 2005
- (CGPA: 3.13/4.00)

ACADEMIC APPOINTMENTS   **Graduate Research Assistant   September 2005 to present**
Department of Aerospace Engineering,
Middle East Technical University
- Academic Staff Transfer from Samsun 19 Mayıs Unv.
- Faculty Member Education Program

CONFERENCE PUBLICATIONS   *Nümerik Hava Tahmin Yazılımlarıyla Akuple Edilmiş Yüksek Çözünürlüklü Atmosferik Akış Çözümleri,* E. Leblebici, G. Ahmet and I.H. Tuncer, V. Ulusal Havacılık ve Uzay Konferansı (UHUK), Erciyes Üniversitesi, Kayseri, Turkey, Sept. 8-10, 2014

A Comparative Study of virtual and operational met mast data, Ö.E.Orhan, G. Ahmet and I.H. Tuncer, EAWE 5th Scientific Conference; The Science of Making Torque from Wind, Copenhagen, Denmark, June. 18-20, 2014

Unsteady Atmospheric Turbulent Flow Solutions Coupled With A Mesoscale Weather Prediction Model, E.Leblebici, G.Ahmet and I.H. Tuncer, RUZGEM'2013 Conference on Wind Energy Science and Technology, Ankara, Turkey, Oct. 3-4, 2013

Terrain Fitted Turbulent Flow Solutions Coupled with a Mesoscale Weather Prediction Model, G. Ahmet, E. Leblebici and I.H.Tuncer, EAWE 9th PhD Seminar on Wind Energy in Europe, Visby, Sweden, Sept 18-20, 2013

Wind Potential Estimations Based on Unsteady Turbulent Flow Solutions Coupled with a Mesoscale Weather Prediction Model, E. Leblebici, G. Ahmet and I.H. Tuncer, 7th Ankara International Aerospace Conference, Ankara, Turkey, Sept. 11-13, 2013

Atmospheric turbulent flow solutions coupled with a Mesoscale weather prediction model, E.Leblebici, G.Ahmet and I.H. Tuncer, III. South-East European Conference on Computational Mechanics, SEECCM'2013 (Special Interest Conferences of the ECCOMAS and IACM), Kos Island, Greece, June 12-14, 2013

Atmospheric Turbulent Flow Solutions Coupled with a Mesoscale Weather Prediction Model, E. Leblebici, G. Ahmet, and I.H. Tuncer, EAWE 4th Scientific Conference; The Science of Making Torque from Wind, Oldenburg, Germany, Oct.9-11 , 2012

A Comparative Study of Yield Assessment Using Data from an Operational Wind Farm and The Predictions Obtained Using Wind Atlas Methodology and CFD Calculations, Ö.E.Orhan, G.Ahmet, M.Yıldız and O.Uzol, EAWE 4th Scientific Conference; The Science of Making Torque from Wind, Oldenburg, Germany, Oct.9-11 , 2012

Nümerik Hava Tahmin Yazılımlarıyla Akuple Edilmiş Yüksek Çözünürlüklü Atmosferik Akış Çözümleri, E.Leblebici, G.Ahmet, and I.H.Tuncer, IV. Ulusal Havacilik ve Uzay Konferansi, İstanbul, Turkey, Sep. 12-14, 2012

Assessment and Comparison of an Operational Wind Farm Using Wind Atlas and CFD Methods, Ö.E.Orhan, B. Bayırlar, Ç.Ünalan

and G. Ahmet, 18th International Energy and Environment Fair and Conference, ICCI'12, İstanbul, Turkey, Apr. 25-27, 2012

Terrain Modeling and Atmospheric Turbulent Flow Solutions Based on Meteorological Weather Forecast Data, E. Leblebici, G. Ahmet, and I.H. Tuncer, 6th Ankara International Aerospace Conference, Ankara, Turkey, Sep. 14-16, 2011

Meteorolojik Hava Tahminleri İcin Uyumlu Dik Ayrısım (POD) Yöntemiyle Veri Asimilasyonu, G.Ahmet, S.Kumru, M.Kaya and I.H.Tuncer, III. Ulusal Havacılık ve Uzay Konferansı, Eskisehir, Turkey, Sep. 16-18, 2010

Development and Application of a POD Based Data Assimilation Method for Meteorological Flowfields, M. Kaya, G. Ahmet, S. Kumru and I.H. Tuncer, 5th Ankara International Aerospace Conference, Ankara, Turkey, Aug. 17-19, 2009

<table>
<tr><td>CONFERENCE ADMINISTRATION</td><td>

10th EAWE PhD Seminar on Wind Energy in Europe, Orléans, France **Oct. 28-31, 2014**
- *Scientific Committee Member*
- Paper Reviewer (Subject:Power generation by Wind, Wind-Turbulence, Aerodynamics)

RUZGEM'2013 Conf.on Wind Energy Science & Tech.,Turkey **Oct. 3-4, 2013**
- *Scientific Committee Member*
- Paper Reviewer (Subject:Wind Resource Assessment and Micrositing)

7th**Ankara International Aerospace Conf.**,Turkey **September 11-13, 2013**
- *Local Committee Member*
- Facility arrangement, equipment maintenance and proceeding preparation

6th**Ankara International Aerospace Conf.**,Turkey **September 14-16, 2011**
- *Local Committee Member*
- Facility arrangement, equipment maintenance and proceeding preparation

</td></tr>
</table>

Eccomas Thematic Conference,Antalya,Turkey **May 23-25, 2011**
- *Local Committee Member*
- Session management and proceeding preparation

5th**Ankara International Aerospace Conf.**,Turkey **August 17-19, 2009**
- *Local Committee Member*
- Facility arrangement, equipment maintenance and proceeding preparation

TEACHING
EXPERIENCE

Middle East Technical University, Ankara, TURKEY

Teaching Assistant **September 2007 to present**
Shared responsibility for lectures, homework and project assignments, laboratory studies, and grades.
- ME105 Computer Aided Engineering Graphics
- CENG200 Introduction to Computers and FORTRAN Programming
- AE305 Numerical Methods
- AE495 Wind Energy and Wind Turbine Technology

Summer Practice Supervisor **June 2012 to present**
Project assignments, team work management, laboratory studies.
- AE400 Summer Practice 3

ACADEMIC
EXPERIENCE

Middle East Technical University, Ankara, TURKEY

Project Assistant **February 2013 to May 2013**
- Includes SWOT(Strengths,Weaknesses,Opportunities,Threats analysis in Ankara Development Agency project: "Sectoral Analysis Project on Wind Energy Technologies".

Consultant **December 2012 to present**
- ESKODA Enerji Üretim Pazarlama İthalat ve İhracat Anonim Şirketi
- Consultancy service on wind assessment of two wind farms near ÇANAKKALE and BURSA region in Turkey.

Consultant **December 2012 to present**
- Güney Rüzgarı Elektrik Üretim ve Ticaret Anonim Şirketi

- Consultancy service on wind assessment of a wind farm near MERSİN region in Turkey.

Consultant   **December 2012**

- Boylam Enerji Yatırım Üretim ve Ticaret Anonim Şirketi
- Consultancy service on wind assessment of a wind farm near ÇANAKKALE region in Turkey.

Researcher   **November 2012 to present**

- TÜBİTAK (Turkish Sci. and Tech. Research Council) project: 112M104 "Development of a Navier-Stokes Flow Solver on Topografic Unstructured Grids for Micro Site Selection of Wind Turbines".

Researcher   **July 2007 to July 2010**

- TÜBİTAK (Turkish Sci.and Tech.Research Council) project: 107Y105 "Application and Development of Data Assimilation Models in Parallel Computing Environments for MM5 Program Used in Meteorological Forecasting".

SUMMER
SCHOOLS AND
CERTIFICATES

- Certificate of Achievement *WindSim*, METUWind, Turkey, 2012

- *7th EAWE PhD Seminar on Wind Energy in Europe* and *3rd EAWE PhD Summer School,* DuWind, TU Delft, Netherlands, 2011

- *5. Yüksek Başarımlı Hesaplama ve Paralel Programlama Yaz Okulu,* UYBHM, ITU, Turkey, 2010

TECHNICAL
SKILLS

Programming: Fortran, MATLAB, UNIX shell scripting, GNU make, MPI, OpenMP, Html
Computer Applications: LaTeX, most common productivity packages (for Windows and Linux platforms), Vim, Photoshop, WindSim, Ansys-Fluent, WRF (Weather Research and Forecasting Model), MM5
Computer-Aided Design: CadKey, Gambit, SolidWorks
Operating Systems: Microsoft Windows family, Mac-OS, Linux, and other UNIX variants

MISCELLANEOUS *Marital Status:* Single

Languages: Turkish(native), English

Hobbies: Astronomy, Amateur Theatre, Marine-Reef Aquariums, Snowboarding, RC Airplanes, Darts, Yoga